



**Electrochemical Biosensors Based on Molecularly Imprinted Polymer
Biomimetic Receptors**

Nur Indah Wardani

**A Thesis Submitted in Fulfillment of the Requirements for the Degree of
Doctor of Philosophy in Chemistry (International Program)**

Prince of Songkla University

2023

Copyright of Prince of Songkla University



**Electrochemical Biosensors Based on Molecularly Imprinted Polymer
Biomimetic Receptors**

Nur Indah Wardani

**A Thesis Submitted in Fulfillment of the Requirements for the Degree of
Doctor of Philosophy in Chemistry (International Program)**

Prince of Songkla University

2023

Copyright of Prince of Songkla University

Thesis Title Electrochemical biosensors based on molecularly imprinted polymer biomimetic receptors
Author Miss Nur Indah Wardani
Major Program Chemistry

Major Advisor

.....
 (Prof. Dr. Panote Thavarungkul)

Examining Committees:

.....Chairperson
 (Assoc. Prof. Dr. Weena Siangproh)

Co-advisor

.....
 (Assoc. Prof. Dr. Warakorn Limbut)

.....Committee
 (Prof. Dr. Panote Thavarungkul)

.....Committee
 (Assoc. Prof. Dr. Warakorn Limbut)

.....Committee
 (Asst. Prof. Dr. Apichai Phonchai)

The Graduate School, Prince of Songkla University, has approved this thesis as fulfillment of the requirements for the Doctor of Philosophy Degree in Chemistry

.....
 (Asst. Prof. Dr. Thakerng Wongsirichot)
 Acting Dean of Graduate School

This is to certify that the work here submitted is the result of the candidate's own investigations. Due acknowledgement has been made of any assistance received.

.....Signature
(Prof. Dr. Panote Thavarungkul)
Major Advisor

.....Signature
(Assoc. Prof. Dr. Warakorn Limbut)
Co-Advisor

.....Signature
(Miss Nur Indah Wardani)
Candidate

I hereby certify that this work has not been accepted in substance for any degree and is not being currently submitted in candidature for any degree.

.....Signature

(Miss Nur Indah Wardani)

Candidate

Thesis Title	Electrochemical biosensors based on molecularly imprinted polymer biomimetic receptors
Author	Miss Nur Indah Wardani
Major Program	Chemistry
Academic Year	2022

Abstract

This thesis presents the utilization of molecularly imprinted polymer (MIP) biomimetic receptors as recognition elements in the development of two MIP electrochemical biosensors. One is a MIP cryogel for the direct detection of insulin, performed in a flow system. The other is an electrochemical biosensor with dual MIPs for the simultaneous determination of creatinine and albumin to provide the albumin to creatinine ratio (ACR) value. The insulin sensor was prepared using a gold electrode modified with carboxylated multiwalled carbon nanotubes (f-MWCNTs) to provide a large surface area platform for the high loading of the MIP cryogel and to increase the conductivity of the sensor. The MIP cryogel porous structure provided a large number of the imprinted recognition sites and improved the access of insulin to/from the MIP cavities. In addition, the flow system facilitated the mass transfer and limited the non-specific binding. This MIP cryogel provided a 0.050-1.40 pM linear range and a low limit of detection (LOD) of 33 fM with good stability at room temperature. For the dual MIP sensor, it was prepared on the dual screen-printed carbon electrodes (SPdCEs) modified with f-MWCNTs and redox probes, polymethylene blue (PMB) and ferrocene (Fc). The surface imprinting and electropolymerization were carried out to obtain more controlled imprinted binding sites of the two analytes on the respective electrode. This sensor was able to selectively recognize the two analytes with linear ranges of 5.0-100 ng mL⁻¹ and 100-2500 ng mL⁻¹ for creatinine and 5.0-100 ng mL⁻¹ for albumin with an LOD of 1.5±0.2 ng mL⁻¹ and 1.5±0.3 ng mL⁻¹, respectively. The two MIP electrochemical biosensors exhibited good reusability and the real sample detection results showed comparable performances to the clinically employed standard methods ($P > 0.05$). The good performances of these MIP electrochemical biosensors, i.e., high

sensitivity and selectivity, low limit of detection, and high stability indicate their potential as alternative methods for analysis.

Acknowledgements

The completion of this thesis would be quite impossible without the support and help of many people.

I would like to express the deepest appreciation to my advisor, Prof. Dr. Panote Thavarungkul, my co-advisor, Assoc. Prof. Dr. Warakorn Limbut, for their help, guidance, encouragement, and patience during my study. My sincere thanks for their instructions and scientific spirit that will be a benefit to my future career and my whole life. I would also thank Assoc. Prof. Dr. Proespichaya Kanatharana and Assoc. Prof. Dr. Apon Numnuam for their invaluable help.

I also would like to thank the examination committee members of this thesis for their valuable time and suggestions. My appreciation and thanks also go to the lecturers and staffs of the Chemistry Program and Faculty of Science, Prince of Songkla University, Hat Yai, Thailand for their helps during my PhD study.

I would like to acknowledge the financial support from the Thailand Education Hub for ASEAN Countries (TEH-AC), Office of the Higher Education Commission, Ministry of Education Thailand, Center of Excellence for trace Analysis and Biosensor (TAB-CoE) and Graduate School, Prince of Songkla University.

Sincerely thank to Dr. Jittima Choosang, Dr. Suparat Cotchim, Dr. Sirirat Ouiganon, Titiwan Changsan, Natha Nontipichet, and all Center of Excellence for trace Analysis and Biosensor (TAB-CoE) members, for their support and encouragement, to one and all who, directly or indirectly, have lent their helping hands.

I am extremely grateful to my parents and my family for their support, prayers, caring and preparing me for my future.

Nur Indah Wardani

The Relevance of The Research Work to Thailand

The purpose of this Doctor of Philosophy Thesis in Chemistry (Analytical chemistry) is the development of electrochemical biosensors using molecularly imprinted polymer (MIP) as recognition element. These developed MIP electrochemical biosensors can be applied to measure target analytes in clinical analysis, such as insulin, urine creatinine, and albumin, which can be beneficial as alternative methods for the quantitative analysis of trace target analytes by several governmental and private sectors in Thailand.

Contents

	Page
List of Figures	x
List of Abbreviations	xii
List of Publications	xiii
Reprints were made with permission from the publishers	xiv
1. Introduction	1
1.1 Background and rationale	1
1.2 Objectives	3
2. Biosensor	4
2.1 Molecularly imprinted polymer (MIP) a biomimetic receptor	4
2.2 Transducer	8
3. Electrochemical detection of MIP biosensor	9
4. Detection system	12
5. Analytical performances	14
5.1 Linearity	14
5.2 Limit of detection (LOD) and limit of quantification (LOQ)	14
5.3 Binding isotherm	15
5.4 Selectivity	15
5.5 Reproducibility	16
5.6 Reusability and long-term stability	16
5.7 Real sample analysis	17
5.8 Recovery	17
6. Concluding remarks	17
7. References	18
Appendices	27
Paper I	29
Paper II	55
Vitae	84

List of Figures

Figure		Page
2.1	Schematic diagram of a biosensor with types of biorecognition element and transducer.	4
2.2	Schematic of the molecularly imprinted polymer (MIP) preparation. Polymerization of functional monomer and template (target analyte) followed by removal of the template to obtain the specific binding sites. (Adapted from Scognamiglio et al., 2015 with permission).	5
2.3	Preparation of MIP cryogel using insulin as template, (A) chitosan and acrylamide as functional monomers, crosslinker bis-methyleneacrylamide, accelerator TEMED, and initiator APS through (B) bulk polymerization method followed by cryogelation (freezing and thawing) and template removal. Prior to drop-casting pre-polymer MIP mixture, the electrode was modified with f-MWCNTs (Paper I).	7
2.4	Preparation of albumin MIP and creatinine MIP using surface imprinting through anchoring the albumin and creatinine templates on an electropolymerized layer of poly(<i>ortho</i> -phenylenediamine) (PoPD) followed by electropolymerization of <i>ortho</i> -phenylenediamine (<i>o</i> -PD). Prior to the electropolymerization first PoPD the electrode was modified with f-MWCNTs and redox probe (Paper II).	8
3.1	Electrochemical response of the direct measurement of insulin at concentrations of 0.050-1.40 pM using the MIP biosensor in 1.0 mM phosphate buffer at pH 5.30. Square wave voltammetry was performed at the potential range from 0.60 to 0.90 V, with a 50 mV/s scan rate, a 5.0 mV step potential, a 0.010 mV pulse amplitude, and a 1.0 Hz pulse frequency. (Reprinted from Wardani et al., 2023 copyright with permission from Talanta) (Paper I).	10

List of Figures (Cont.)

Figure		Page
3.2	Signals of the indirect measurement of the simultaneous detection of creatinine and albumin mixtures in the range of 0–2500 ng mL ⁻¹ in 0.050 mol L ⁻¹ PBS (pH 7.40) using the dual MIP electrochemical biosensor. Square wave voltammetry (SWV) was performed with potential range of -0.80 V to +0.40 V, a modulation amplitude of 0.10 V, and a 1.0 Hz pulse frequency (Paper II).	11
3.3	The sensitivity (slope of the calibration plot of 0.050-0.40 pM of insulin in 1.0 phosphate buffer at pH 5.30 and a flow rate of 100 μL min ⁻¹) with different loadings of f-MWCNTs (Supplementary data Paper I).	12
4.1	Schematic of insulin detection in a flow system includes insulin rebinding, electrochemical detection, and regeneration. First step, insulin was flowed to pass through the working electrode for the rebinding and stop the flow for 2 mins to stabilize the rebinding, then resume the flow of the buffer for removing matrix compound. Then, flow was stopped to perform the electrochemical detection (second step). Regeneration was performed by flowing the regeneration solution to the electrode surface and stopped for 15 mins to remove the insulin from the imprinted cavity (third step). (Reprinted from Wardani et al., 2023 copyright with permission from Talanta) (Paper I).	13

List of Abbreviations

ACR	albumin to creatinine ratio
CKD	chronic kidney disease
DNA	deoxyribonucleic acid
EIS	electrochemical impedance spectroscopy
Fc	ferrocene
fM	femtomolar
f-MWCNTs	carboxylated multiwalled carbon nanotubes
K_D	binding dissociation constant
LOD	limit of detection
LOQ	limit of quantification
MIP	molecularly imprinted polymer
MWCNTs	multiwalled carbon nanotubes
NIP	non-imprinted polymer
<i>o</i> -PD	<i>ortho</i> -phenylenediamine
PMB	polymethylene blue
pM	picomolar
PNA	peptide nucleic acid
P <i>o</i> PD	poly- <i>ortho</i> -phenylenediamine
R_{ct}	charge transfer resistance
SD	standard deviation
SPdCEs	dual screen-printed carbon electrodes
SWCNTs	single walled carbon nanotubes
SWV	square wave voltammetry

List of Publications

This thesis contains general summary (introduction, background information, and conclusion) from this Ph.D. work and the following papers which are referred to in the text by their roman numerals.

Paper I **Wardani, N. I.**, Kangkamano, T., Wannapob, R., Kanatharana, P., Thavarungkul, P., Limbut, W. 2023. Electrochemical sensor based on molecularly imprinted cryogel and multiwalled carbon nanotubes for direct insulin detection. *Talanta* 254, 124137.

(Reprinted with permission of Elsevier)


Paper II **Wardani, N. I.**, Kanatharana, P., Thavarungkul, P., Limbut, W. 2023. Molecularly imprinted polymer dual electrochemical sensor for the one-step determination of albuminuria to creatinine ratio (ACR). *Talanta* 265, 124769.

(Reprinted with permission of Elsevier)


Reprints were made with permission from the publishers

Figure 2.2

Reprinted with permission of Elsevier


RightsLink

Home
Help
Live Chat
Nur Indah Wardani



Synthetic biology and biomimetic chemistry as converging technologies fostering a new generation of smart biosensors

Author: Viviana Scognamiglio, Amina Antonacci, Maya D. Lambrea, Simona C. Litescu, Giuseppina Rea

Publication: Biosensors and Bioelectronics

Publisher: Elsevier

Date: 15 December 2015

Copyright © 2015 Elsevier B.V. All rights reserved.

Order Completed

Thank you for your order.

This Agreement between Miss. Nur Indah Wardani ("You") and Elsevier ("Elsevier") consists of your license details and the terms and conditions provided by Elsevier and Copyright Clearance Center.

Your confirmation email will contain your order number for future reference.

License Number	5521191161158	Printable Details
License date	Apr 03, 2023	

Licensed Content	Order Details
Licensed Content Publisher	Type of Use
Elsevier	reuse in a thesis/dissertation
Licensed Content Publication	Portion
Biosensors and Bioelectronics	figures/tables/illustrations
Licensed Content Title	Number of figures/tables/illustrations
Synthetic biology and biomimetic chemistry as converging technologies fostering a new generation of smart biosensors	1
Licensed Content Author	Format
Viviana Scognamiglio, Amina Antonacci, Maya D. Lambrea, Simona C. Litescu, Giuseppina Rea	both print and electronic
Licensed Content Date	Are you the author of this Elsevier article?
Dec 15, 2015	No
Licensed Content Volume	Will you be translating?
74	No
Licensed Content Issue	
n/a	
Licensed Content Pages	
11	

Requestor Location	Tax Details
Requestor Location	Publisher Tax ID
Miss. Nur Indah Wardani Kohong Interdorm Kho Hong Hat Yai, สงขลา 90110 Thailand Attn: Miss. Nur Indah Wardani	GB 494 6272 12

\$ Price	
Total	0.00 USD

Total: 0.00 USD

CLOSE WINDOW
ORDER MORE

Paper I

Reprinted with permission of Elsevier



RightsLink



Home



Help ▾



Live Chat



Sign in



Create Account



Electrochemical sensor based on molecularly imprinted polymer cryogel and multiwalled carbon nanotubes for direct insulin detection

Author:

Nur Indah Wardani, Tawatchai Kangkamano, Rodtichoti Wannapob, Proespichaya Kanatharana, Panote Thavarungkul, Warakorn Limbut

Publication: Talanta

Publisher: Elsevier

Date: 1 March 2023

© 2022 Elsevier B.V. All rights reserved.

Journal Author Rights

Please note that, as the author of this Elsevier article, you retain the right to include it in a thesis or dissertation, provided it is not published commercially. Permission is not required, but please ensure that you reference the journal as the original source. For more information on this and on your other retained rights, please visit: <https://www.elsevier.com/about/our-business/policies/copyright#Author-rights>

BACK

CLOSE WINDOW

Paper II

Reprinted with permission of Elsevier



RightsLink



Home



Help ▾



Live Chat



Sign in



Create Account



Molecularly imprinted polymer dual electrochemical sensor for the one-step determination of albuminuria to creatinine ratio (ACR)

Author:

Nur Indah Wardani, Proespichaya Kanatharana, Panote Thavarungkul, Warakorn Limbut

Publication: Talanta

Publisher: Elsevier

Date: Available online 7 June 2023

© 2023 Published by Elsevier B.V.

Journal Author Rights

Please note that, as the author of this Elsevier article, you retain the right to include it in a thesis or dissertation, provided it is not published commercially. Permission is not required, but please ensure that you reference the journal as the original source. For more information on this and on your other retained rights, please visit: <https://www.elsevier.com/about/our-business/policies/copyright#Author-rights>

BACK

CLOSE WINDOW

1. Introduction

1.1 Background and rationale

In recent years, biosensors have been developed as a promising tool in medicine for early diagnosis of numerous diseases. A biosensor is referred to as a device providing the quantitative and/or qualitative analytical information by incorporating a biorecognition element and a transducer (Karunakaran et al., 2015). The biorecognition element has a significant role in obtaining high selectivity through its specific binding to the target analyte. Biomolecules such as antibodies, enzymes, nucleic acids, and whole cells are biorecognition elements, employed to provide such high specificity. However, they are relatively expensive with poor stability (Iskierko et al., 2016).

To replace biomolecule recognition elements, several synthetic biomimetic receptors such as peptide nucleic acids (PNA), aptamers, and molecularly imprinted polymers (MIPs) are now being considered. They provide a more stable, cost effective, high affinity binding ability similar to the biomolecules (Justino et al., 2015). Among these biomimetic receptors, MIPs are frequently used due to their capability of mimicking biomolecules with complementary recognition sites, shape, and functional groups. Their attractive features are high thermal and chemical stability, low cost and relatively simple preparation (Scognamiglio et al., 2015). They are produced by the polymerization of functional monomers around a template molecule (the target analyte) and its removal at the end of polymerization (Ansari, 2017; Iskierko et al., 2016).

The binding between an analyte and the MIP imprinted cavity is mostly an affinity reaction. The detectable response, by a transducer, is the measure of a physicochemical change after the rebinding of the target analyte to the MIP. The electrochemical, optical, piezoelectric or thermal transducers, convert such a binding into a measurable signal. A biosensor based on electrochemical transduction has more advantages due to its high degree of selectivity and sensitivity, low cost, and quick analysis (Mani et al., 2021). This type of biosensor monitors the analyte as an electrical signal that is produced by the interaction of the analyte and the recognition element at the sensing electrode (Rassaei et al., 2011). By combining the MIP and electrochemical transducer, an effective biosensor with superiority for selective and sensitive detection

is promising. Some recent reports of the MIP based electrochemical biosensors have shown high selectivity and sensitivity to a wide range of small molecules and metal ions (Torkashvand et al., 2017; Zheng et al., 2018). They have also been developed for large molecules and multi analytes detection (Fatoni et al., 2014; Khumngern et al., 2022; Liu et al., 2019; Zhang et al., 2022).

MIP electrochemical biosensor signal can either be based on direct or indirect measurement. For a non electroactive analyte, direct measurement can be obtained through the change of electrical property of the electrode surface such as resistance and capacitance change (Trevizan et al., 2021). For example, a capacitive technique measures the change in dielectric property as a result of the rebinding between the analyte and the MIP (Ertürk & Mattiasson, 2017). This technique is convenient for the detection of non-electroactive analytes such as trypsin (Ertürk et al., 2016), amphetamine (De Rycke et al., 2021; El-Akaad et al., 2021), and imidacloprid (El-Akaad et al., 2020) by observing the decrease of the total capacitance when the binding occurs on the perfect insulating MIP layer. Alternatively, when the rebinding involves an electroactive analyte and is followed by the transfer of electron to the electrode surface, this can be directly detected as a current response that increases with the concentration of the analyte. One of the most widely used detection technique is voltammetry that monitored the current response of the rebinding at an applied potential (Suryanarayanan et al., 2010). For example, the voltametric detection of histamine (Herrera-Chacón et al., 2020) or tyrosine (Herrera-Chacón et al., 2020) using the MIPs by monitoring the oxidation currents after their rebinding. This direct detection using voltammetry technique is investigated for the detection of insulin, an electroactive compound (**Paper I**).

For a non-electroactive analyte, the indirect measurement is commonly performed via an external or internal redox probe with electrochemical impedance spectroscopy (EIS) and voltammetry. With an external redox probe such as $\text{Fe}(\text{CN})_6^{4-}/\text{Fe}(\text{CN})_6^{3-}$ (Khosropour et al., 2023) or $\text{Ru}(\text{NH}_3)_6^{2+}/\text{Ru}(\text{NH}_3)_6^{3+}$ (Peng et al., 2016), the electron transfer between the probe in the solution and the electrode surface was hindered by the rebinding of the analyte to the imprinted cavity, thus either resistance or current response can be recorded (Elfadil et al., 2021). With a conductive

MIP, the change of resistance or current response might not only be from the hindering of the electron transfer of the probe but also possibly from the electrochemical property of the MIP such as the decrease of MIP conductivity due to the diffusion of the probe (Sharma et al., 2019). Also, the diffusion of the probe could influence the MIP-analyte interaction (Mazzotta et al., 2016). It is preferable to obtain the response of the rebinding solely from the internal redox probe such as ferrocene (Fc) (Khumngern et al., 2022) and polymethylene blue (PMB) (Phonklam et al., 2020). Furthermore, the combination of different MIPs and different internal redox probes with distinct oxidation/reduction potentials could be developed for simultaneous multianalyte detection (**Paper II**).

To improve biosensor performance, carbon nanomaterials such as multiwalled carbon nanotubes (MWCNTs), single walled carbon nanotubes (SWCNTS), and graphene that have a large surface area to volume ratio, good conductivity, and biocompatibility are beneficial (Yang et al., 2018). Multiwalled carbon nanotubes (MWCNTs) are often used due to their large surface area, high strength and stability (Dai et al., 2015). Their surface can also be easily functionalized with carboxylic acid groups (f-MWCNTs) resulting in high dispersibility, thus, providing an evenly distributed MWCNTs on the electrode surface (Huang et al., 2019; Ni et al., 2020). Therefore, it is interesting to incorporate f-MWCNTs and MIP for the development of electrochemical biosensors which can be performing in a flow (**Paper I**) or a batch system (**Paper II**).

1.2 Objectives

To develop electrochemical biosensors using MIPs as biomimetic recognition elements for single and simultaneous detection. Two sub-projects were studied as follows.

Sub-project I: Electrochemical sensor based on molecularly imprinted polymer cryogel and multiwalled carbon nanotubes for direct insulin detection (**Paper I**).

Sub-project II: Molecularly imprinted polymer dual electrochemical sensor for the one-step determination of albuminuria to creatinine ratio (ACR) (**Paper II**).

2. Biosensor

A biosensor is a device that employs a biorecognition element and a transducer to provide analytical information (Thévenot et al., 2001). The biorecognition element has an important role in picking out the target analyte and generating the information such as analyte concentration, to be transferred to a transducer (**Figure 2.1**). The transducer, whether it be electrochemical, optical, piezoelectric, or thermal, then converts the information from the interaction between the recognition element and target into a measurable signal (Justino et al., 2010).

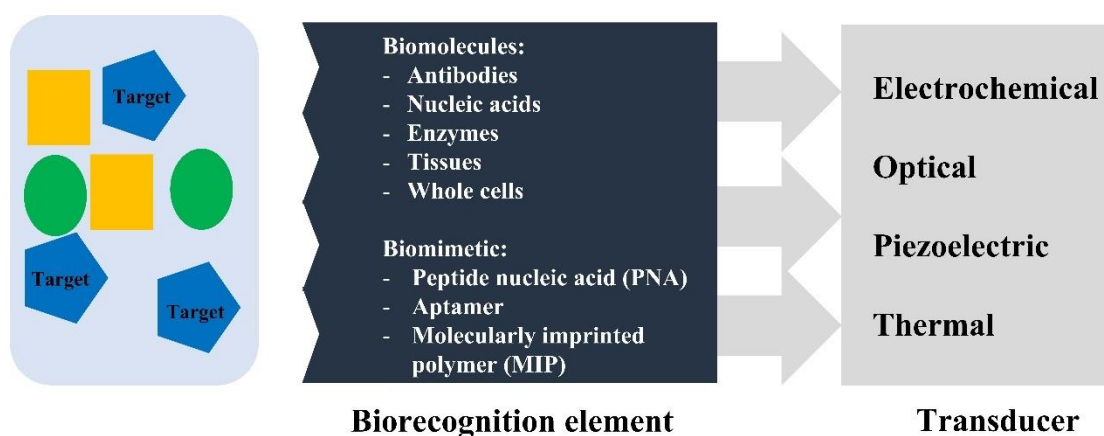


Figure 2.1. Schematic diagram of a biosensor with types of biorecognition element and transducer.

2.1 Molecularly imprinted polymer (MIP) a biomimetic receptor

A biorecognition element or bioreceptor, either a biological or biomimetic molecule, is the part of a biosensor that can provide the selective recognition to the target analyte in the presence of interferences. Biological recognition elements such as enzyme, antibodies, nucleic acids, and whole cells provide selectivity for the target analytes, but they lack stability and have high preparation cost (Iskierko et al., 2016; Justino et al., 2015). These limitations lead to the development of synthetic recognition elements such as peptide nucleic acid (PNA), aptamer, and molecularly imprinted polymers (MIP).

PNA and aptamer are nucleic acids mimic that can provide stable binding to target analytes. PNA provides a more stable binding to a single stranded DNA than DNA itself due to the neutral pseudopeptide backbone (Scognamiglio et al., 2015). As for aptamer, its ability to form a three-dimensional structure has increased its affinity and stability towards the target analyte (Álvarez-Martos et al., 2015). However, PNA and aptamer still require complicated synthesis and high preparation cost.

Molecularly imprinted polymer (MIP) is a polymer synthesized with binding sites which can specifically bind to target analytes. The specific binding sites are obtained from the polymerization of functional monomer around the template (target analyte) through covalent or non-covalent bonding and the removal of template (**Figure 2.2**) (Scognamiglio et al., 2015). Such binding sites are complementary to the target analyte in size, shape, and position of the functional groups, therefore, MIPs are able to mimic variety of analyte receptors with high affinity. As a control of the recognition property, non-imprinted polymer (NIP) is generally synthesized with the same conditions, but without the addition of the target analyte template (Rebelo et al., 2021; Scognamiglio et al., 2015).

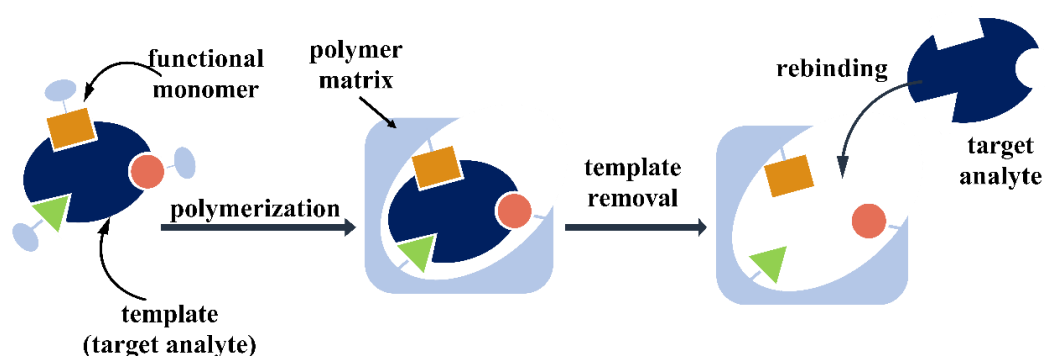


Figure 2.2. Schematic of the molecularly imprinted polymer (MIP) preparation. Polymerization of functional monomer and template (target analyte) followed by removal of the template to obtain the specific binding sites. (Adapted from Scognamiglio et al., 2015 with permission).

Bulk polymerization is the most common and simplest method to obtain the MIP. In this type of imprinting, the template (target analyte) was simply added to

the functional monomer and the imprinted cavities are obtained during the polymerization, distributed all over the bulk. This strategy was used for the preparation of the MIP to selectively recognize insulin, the targeted analyte (**Paper I**). Hence, the insulin molecules are imprinted whole in the polymer matrix. The functional groups of the monomer should be complementary to those of the insulin to provide the selective interaction between the insulin and the MIP. Monomers such as chitosan and acrylamide with their functional groups such as carboxyl, amino, hydroxy, and amide (**Figure 2.3A**), were able to form a stable pre-polymerization complex with insulin with strong reversible binding (Wackerlig & Schirhagl, 2016).

Due to the large size of the insulin, its release and rebinding to the cavity needs further attention to obtain a transducer with a high loading of an MIP layer. An attractive structure suitable for the task is cryogel, a porous material with interconnected micropores that provides a large surface area. Its porosity also enhances the access of analytes to the imprinted cavities as well as their removal (Aslıyüce et al., 2019; Fatoni et al., 2014). This material can be easily fabricated on a transducer via the drop-casting of the pre-polymer mixture followed by freezing and thawing process (Zhang et al., 2019) (**Figure 2.3B**). The MIP and cryogel produced a synergistic improvement of insulin detection achieving a high surface area to volume ratio and improving the remove/binding access of insulin to the imprinted cavities which increase sensor sensitivity and stability (**Paper I**).

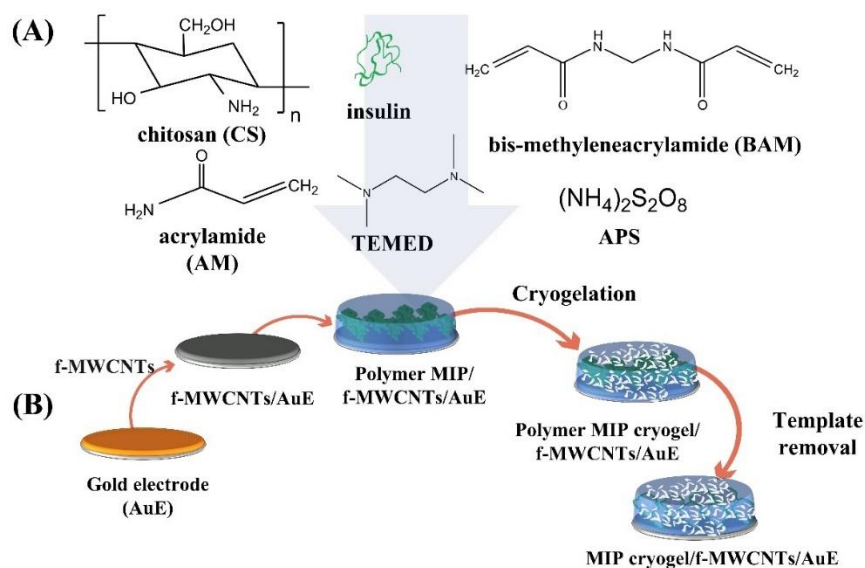


Figure 2.3. Preparation of MIP cryogel using insulin as template, (A) chitosan and acrylamide as functional monomers, crosslinker bis-methyleneacrylamide, accelerator TEMED, and initiator APS through (B) bulk polymerization method followed by cryogelation (freezing and thawing) and template removal. Prior to drop-casting pre-polymer MIP mixture, the electrode was modified with f-MWCNTs (**Paper I**).

Another strategy for the preparation of the MIP is surface imprinting. This procedure provides the templates imprints (albumin and creatinine) very close to the transducer surface (**Figure 2.4**) (**Paper II**). The preliminary anchoring of the target analyte to the transducer surface produce uniformly distributed binding sites (Liu & Dykstra, 2022; Mazzotta et al., 2022). Electropolymerization is a suitable method to prepare surface imprinting MIP on the transducer surface. By varying the number of scan cycles, a suitable thickness of polymer film for albumin and creatinine can be obtained especially with the huge size difference between albumin (66.7 kDa) and creatinine (113.1 Da). A conductive monomer such as *o*-phenylenediamine (*o*-PD), with abundant presence of amine groups (-NH₂) was able to provide a electropolymerized platform for anchoring and binding with albumin and creatinine with good chemical and mechanical stability (Malitesta et al., 2012) (**Paper II**).

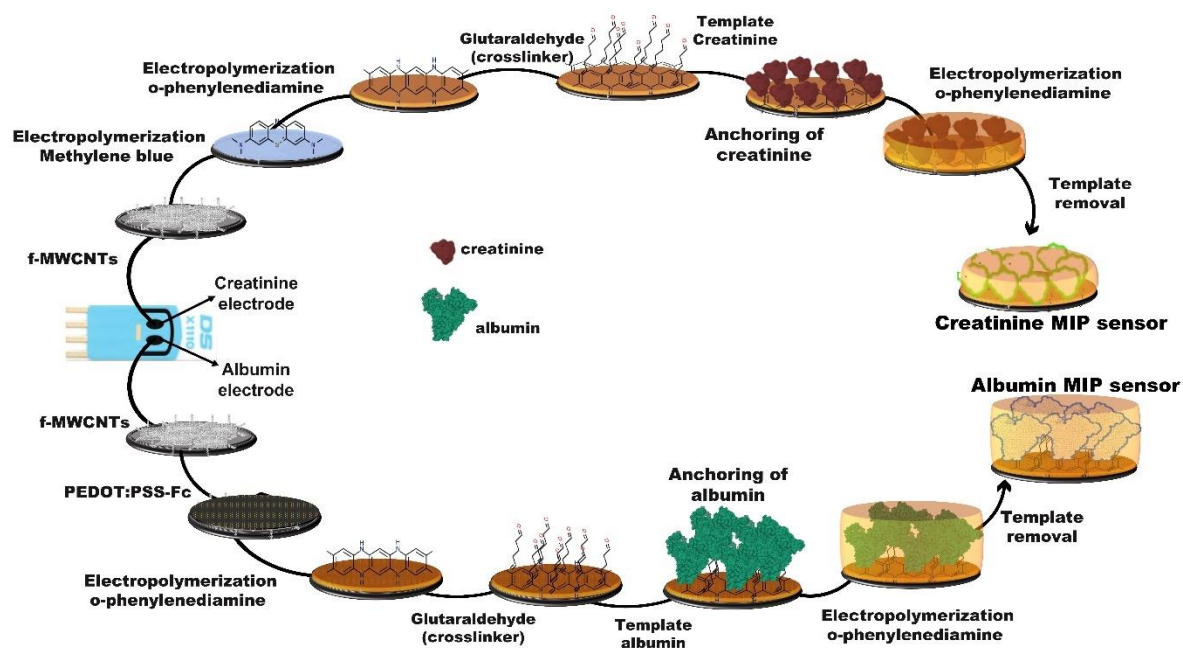


Figure 2.4. Preparation of albumin MIP and creatinine MIP using surface imprinting through anchoring the albumin and creatinine templates on an electropolymerized layer of poly(*ortho*-phenylenediamine) (*PoPD*) followed by electropolymerization of *ortho*-phenylenediamine (*o*-PD). Prior to the electropolymerization first *PoPD* the electrode was modified with f-MWCNTs and redox probe (**Paper II**).

2.2 Transducer

A transducer converts the interaction between the biorecognition element and target analyte into a measurable signal (Justino et al., 2010). Biosensors can be classified according to the type of transducer such as electrochemical, optical, or piezoelectric sensor. Among them, electrochemical transduction provides more advantages due to its high sensitivity and simple to construct (Zhu et al., 2015). Electrochemical signals due to the interaction between target analyte and biorecognition element (receptor) often used in electrochemical biosensors are current, potential, conductivity, or impedance (Antuña-Jiménez et al., 2012).

3. Electrochemical detection of MIP biosensor

The electrical signal of an MIP electrochemical biosensor is a result of the binding of the target analyte to the imprinted cavity. This binding can be evaluated directly from the target analyte or via an electrochemical probe, such as ferri/ferrocyanide, methylene blue or ferrocene (Blanco-López et al., 2004). Electrochemical impedance spectroscopy (EIS) and voltammetric detections are the mostly used approach to monitor such a binding, depending on the property of the analyte.

For electroactive analyte, the rebinding can be monitored by the current response at an applied potential using voltammetry technique. The rebinding of such a target is followed by the transfer of electron to the electrode surface. This can be directly detected as a current response that increases with the analyte concentration (Suryanarayanan et al., 2010). In **Sub-project I (Paper I)**, insulin is a polypeptide with electroactive amino acid such as tyrosine, tryptophan, and cysteine (Berzas Nevado et al., 1999; Marian & Allen, 1977; Zong et al., 2010), thus, its direct detection was observed via square wave voltammetry (SWV), a highly sensitive method due to its capability to minimize the capacitive current (Mirceski et al., 2013). The measured current is resulting from the oxidation of the rebinding insulin molecules within the imprinted cavities (**Figure 3.1**).

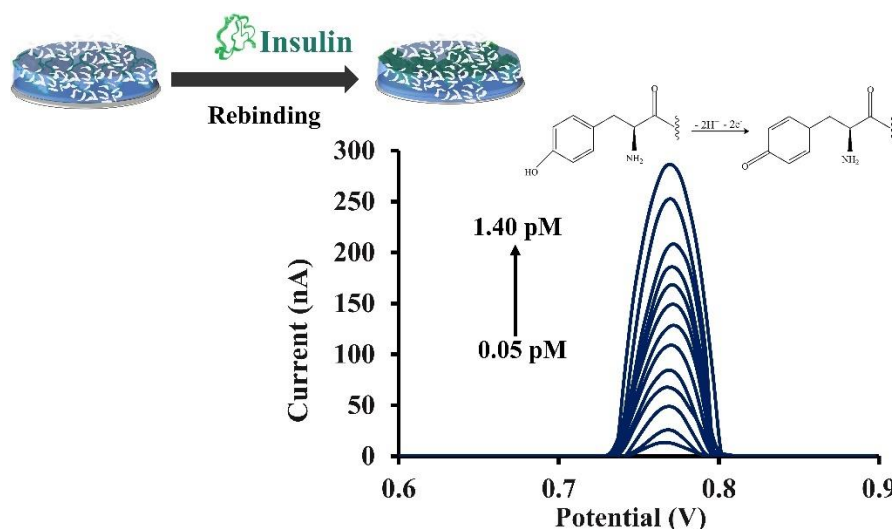


Figure 3.1. Electrochemical response of the direct measurement of insulin at concentrations of 0.050-1.40 pM using the MIP biosensor in 1.0 mM phosphate buffer at pH 5.30. Square wave voltammetry was performed at the potential range from 0.60 to 0.90 V, with a 50 mV/s scan rate, a 5.0 mV step potential, a 0.010 mV pulse amplitude, and a 1.0 Hz pulse frequency. (Reprinted from Wardani et al., 2023 copyright with permission from Talanta) (**Paper I**).

For a non-electroactive analyte, the rebinding might cause a change in the conductivity and/or porosity of the MIP. This change can be monitored by electrochemical impedance spectroscopy (EIS) or voltammetry indirectly with redox probe such as ferri/ferrocyanide, methylene blue, or ferrocene (Elfadil et al., 2021). With the EIS technique, the charge transfer resistance (R_{ct}) increases with its concentration (Cecchini et al., 2017). For the indirect measurement by a voltametric technique, the imprinted cavities of the MIP layer play a role as a charge transfer channel and the redox probe is used as the mediator. As the non-electroactive analyte binds to the imprinted cavity, the electron transfer of the probe is blocked, thus, the current decreases with the analyte concentration (Antuña-Jiménez et al., 2012; Suryanarayanan et al., 2010).

The MIP based electrochemical biosensor has also been developed to simultaneously detect two analytes. The binding of electroactive analytes with distinct oxidation/reduction potential and the MIPs can be detected directly (Liu & Dykstra,

2022). As for the non-electroactive analytes, they need different redox probes to discriminate their signals. **Figure 3.2** shows an example of the simultaneous detection of creatinine and albumin using the dual MIP sensor with polymethylene blue (PMB) and ferrocene (Fc) (**Paper II**). The different oxidation potentials of the two redox probes allow the rebinding of both analytes to be monitored simultaneously in one potential scan by square wave voltammetry (SWV) which enabled sensitive scanning in the potential range of both redox probes (Lovrić, 2010).

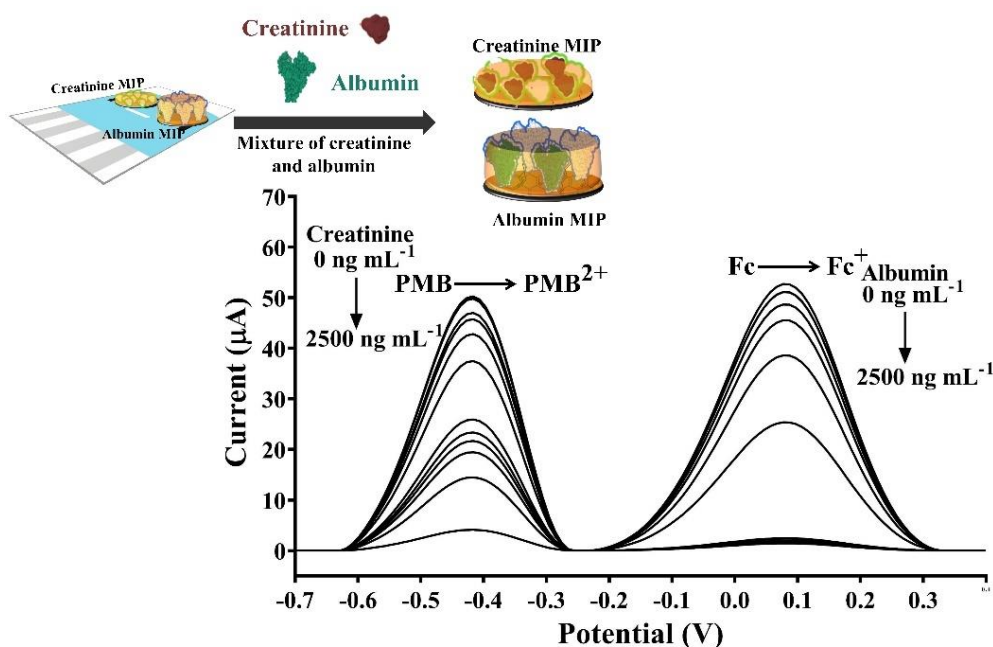


Figure 3.2. Signals of the indirect measurement of the simultaneous detection of creatinine and albumin mixtures in the range of 0–2500 ng mL⁻¹ in 0.050 mol L⁻¹ PBS (pH 7.40) using the dual MIP electrochemical biosensor. Square wave voltammetry (SWV) was performed with potential range of -0.80 V to +0.40 V, a modulation amplitude of 0.10 V, and a 1.0 Hz pulse frequency (**Paper II**).

To increase the electrochemical response, some nanomaterials are commonly integrated with the MIP. Carbon materials such as multiwalled carbon nanotubes (MWCNTs), single walled carbon nanotubes (SWCNTs), and graphene are widely used. Among them, MWCNTs have been an ideal platform for MIP due to their high strength, stability, good conductivity, and large surface areas (Dai et al., 2015).

The increasing surface area of the modified electrode provides a larger platform for the MIP layer. Moreover, their good conductivity can increase the electron transfer between the imprinted cavities and the electrode surface (Yang et al., 2018) that further help achieve a low limit of detection. By functionalizing the MWCNTs with carboxylated acid, their dispersibility is improved, contributing an evenly distributed MWCNTs on the measuring surface (Huang et al., 2019; Ni et al., 2020) (**Papers I-II**). **Figure 3.3** shows an example of insulin detection with different amounts of f-MWCNTs where the sensitivity increased with the amount of f-MWCNTs to 2.00 mg mL⁻¹. The decrease at 2.50 mg mL⁻¹ (**Paper I**) was likely due to the incomplete removal of the larger amount of insulin template.

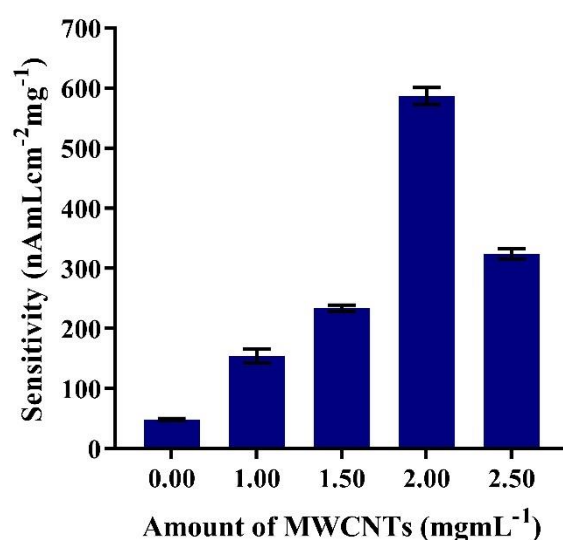


Figure 3.3. The sensitivity (slope of the calibration plot of 0.050-0.40 pM of insulin in 1.0 phosphate buffer at pH 5.30 and a flow rate of 100 $\mu\text{L min}^{-1}$) with different loadings of f-MWCNTs (Supplementary data **Paper I**).

4. Detection system

MIP based electrochemical biosensors have been applied under both flow and batch systems. A flow system consists of a pump, an injection valve, tubing, and a flow cell. The target analyte is injected through an injection valve and passed through by carrier solution to the electrode surface in the flow cell (Kurbanoglu et al.,

2018). A continuous flow stream is beneficial for the MIP electrochemical biosensor since the rebinding, washing, detecting and regenerating of the imprinted cavities, can be carried out continuously (**Figure 4.1**). The flow stream also improves the access of analyte to/out of the imprinted cavities as well as removes the non-specific binding by the surface washing aspect of the flow (Erdőssy et al., 2016) (**Paper I**).

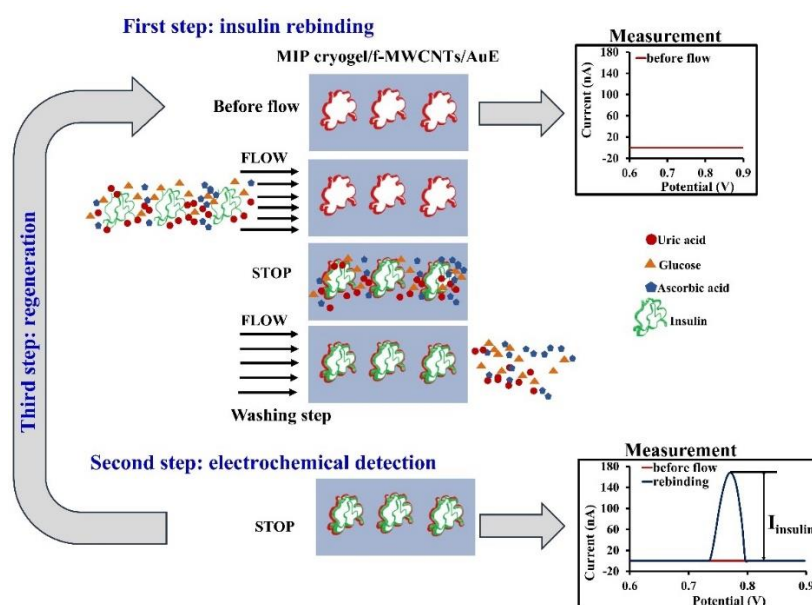


Figure 4.1. Schematic of insulin detection in a flow system includes insulin rebinding, electrochemical detection, and regeneration. First step, insulin was flowed to pass through the working electrode for the rebinding and stop the flow for 2 mins to stabilize the rebinding, then resume the flow of the buffer for removing matrix compound. Then, flow was stopped to perform the electrochemical detection (second step). Regeneration was performed by flowing the regeneration solution to the electrode surface and stopped for 15 mins to remove the insulin from the imprinted cavity (third step). (Reprinted from Wardani et al., 2023 copyright with permission from Talanta) (**Paper I**).

An alternative strategy is a batch system that was employed for the MIP electrochemical detection of **Sub-project II**. In this system there is no need of additional components commonly required by flow system such as tubes, pumping system and injection valves (Quintino & Angnes, 2004). With the analyte solution, a

mixture of albumin and creatinine in a small beaker, the MIP was immersed, and the rebinding of analyte occurred. Followed by the washing step under the stirring condition in supporting electrolyte (phosphate buffer solution). The electrochemical detection step was performed without stirring. This system could also prevent the gradual loss of modified layers, especially the redox probes achieving the high stability of the MIP electrochemical biosensor (**Paper II**).

5. Analytical performances

5.1 Linearity

Linearity of an analytical method is defined as the ability to obtain results proportional to the concentration of analyte in the sample (Taverniers et al., 2004). It can be obtained by performing the calibration curve which can be obtained through measuring a series of analyte concentrations, with replications, before plotting the response, e.g., current (**Paper I**) or current change (**Paper II**), versus the analyte concentration (Thompson et al., 2002). The linearity was determined from the correlation coefficient, r which is normally in the range of $-1 \leq r \leq +1$. In analytical practice, the acceptable linear range can be obtained with the r -value of 0.90-0.99 (Miller & Miller, 2010).

5.2 Limit of detection (LOD) and limit of quantification (LOQ)

The limit of detection (LOD) is the lowest concentration or the quantity that can be detection derived as the smallest signal over the noise level. The value of LOD will determine the ability of the sensor to differentiate the true signal from the noise level but is not necessarily quantified (Justino et al., 2010; Shrivastava & Gupta, 2011). For the limit of quantification (LOQ), the lowest concentration of an analyte should be determined with an acceptable level of repeatability precision and trueness. This work determined the LOD and LOQ values based on the slope of the linear regression. The LOD can be expressed as:

$$LOD = \frac{3S_a}{b}$$

The LOQ can be expressed as:

$$LOQ = \frac{10S_a}{b}$$

Where S_a is the standard deviation and b is the slope of regression in the linear range (Shrivastava & Gupta, 2011).

5.3 Binding isotherm

The affinity of the analyte to the MIP can be evaluated by the binding dissociation constant (K_D). This K_D value was obtained using the Langmuir adsorption isotherm model (Ansell, 2015) based on the equation:

$$I_F = \frac{I_{\max}[F]}{K_D + [F]}$$

where I_F is the current response due to the binding, $[F]$ is the analyte concentration, I_{\max} is the maximum current response at saturated binding, and K_D is the dissociation constant. A low K_D value indicates high binding affinity between the MIP and the analyte. Meanwhile, the less efficient interaction of analyte to the MIP was indicated by the high K_D value (Ansell, 2015) (**Paper I; Paper II**).

5.4 Selectivity

Selectivity is the ability to determine the target analyte in a sample matrix without interference from other components in the sample (Vassman *et al.* 2001). This test was performed by measuring the interfering substances individually and binary mixed with the target analyte at the mid-range of its expected value (Thevenot *et al.* 2001). Common interferences in real sample of human serum and urine such as glucose, ascorbic acid, uric acid, and dopamine could be tested (**Paper I; Paper II**). The current response of the interfering substances individually and binary mixed were compared to the current response of the target analyte. Selectivity towards target

analyte are indicated by the current change of the interfering substances less than 5% and two-way ANOVA for binary mixed (Akhoundian *et al.* 2018) (**Paper I; Paper II**).

5.5 Reproducibility

Reproducibility of the electrode preparation represents the closeness of the agreement between the results of several measurement using the same condition of preparation and operation. In this work, several electrodes were prepared at different times and used to measure a series of the target analyte. The standard deviations (SD) of the responses of the concentrations tested using different electrodes were used to indicate the acceptability of the modified electrode preparation (Taverniers *et al.*, 2004) (**Paper I; Paper II**).

5.6 Reusability and long-term stability

Reusability of the MIP electrochemical biosensor is defined as the recovery of recognition property after binding and regeneration cycle. In **sub-project I**, the reusability was assessed as the operational stability by performing the binding and regenerating cycles continuously with the response after every detection monitored. For the **Sub-project II**, the reusability was examined by repeatedly measuring a series of the target analyte concentrations and its subsequent cycles after the MIP regeneration. The reusability was considered from the number of analyses (**Paper I**) and analysis cycles (**Paper II**) that can be repetitively performed until a percentage of residual activity decreased to below 90% (Thévenot *et al.*, 2001).

In the case of long-term stability, the response of the sensor after a certain period of storage was monitored. Several modified electrodes were prepared at the same time and kept at room temperature. Each electrode represented the storage for a certain week. The sensitivities of the modified electrode for different span of storage time were compared to that of the freshly prepared decreased to below 90% (Thévenot *et al.*, 2001) (**Papers I-II**).

5.7 Real sample analysis

The MIP electrochemical biosensors were applied to determine the target analytes in the real samples, i.e., human serum (**Paper I**) and urine (**Paper II**). The possible matrix effect was firstly investigated by adding different concentration of analyte to the sample. The slope of the calibration curve of the spiked sample is compared with that of the standard analyte. The absence of matrix effect can be observed by the lack significance of both slopes (curve are parallel) (Taverniers et al., 2004). The reliability of the MIP electrochemical biosensor was then determined by statistically comparing the results of the sensor to those of a standard method used in the hospital.

5.8 Recovery

The recovery aims to estimate the true concentration of the target analyte in the real sample confirming the accuracy of the developed MIP electrochemical biosensor. It was calculated as the percentage of the measured of standard analyte and spiked sample solutions, which is depending on the analyte concentration. The % recovery value should be compared to acceptable recovery recommendation (Taverniers et al., 2004). In this work, the recover was calculated as

$$\% \text{ recovery} = \left(\frac{C_1 - C_2}{C_3} \right) \times 100$$

Where, C_1 and C_2 are the measured concentration of spiked sample and spiked blank, respectively. C_3 is the known concentration of the standard target analyte (Miller & Miller, 2010).

6. Concluding remarks

The applications of the molecularly imprinted polymers (MIPs) as biomimetic recognition elements of the electrochemical biosensors were demonstrated in this work. In **Sub-project I**, the MIP cryogel was successfully recognizing the insulin with high selectivity over a wide range of interferences. The combination of carboxylated multiwalled carbon nanotubes (f-MWCNTs), cryogel, and flow system

had further improved the selectivity and sensitivity of the MIP electrochemical biosensor. Thus, a low limit of detection, very good recoveries, high operational and storage stability were achieved, showing a potential of the developed system for the quantification of insulin in human serum from type 1 and type 2 diabetic patients. In **Sub-project II**, the use of MIP for simultaneous determination of creatinine and albumin was successfully developed on a dual screen-printed carbon electrodes (SPdCEs) with f-MWCNTs as a platform. Each MIP was able to sensitively and selectively recognized creatinine and albumin via polymethylene blue (PMB) and ferrocene (Fc) as redox probe without interferences between the two analytes and other interfering species in human urine. Hence, the albumin to creatinine ratio (ACR) value was obtained using this dual MIP sensor with very good recovery, showed good potential for the monitoring of chronic kidney diseases (CKD) patients. The MIPs from both sub-projects exhibited good performances of biomimetic recognition elements such as high selectivity and long-term storage stability at room temperature. Their high affinity binding to the target analytes enabled both single and simultaneous electrochemical biosensor detection.

7. References

- Álvarez-Martos, I., Campos, R., & Ferapontova, E. E. (2015). Surface state of the dopamine RNA aptamer affects specific recognition and binding of dopamine by the aptamer-modified electrodes [10.1039/C5AN00480B]. *Analyst*, 140(12), 4089-4096. <https://doi.org/10.1039/C5AN00480B>
- Ansari, S. (2017). Combination of molecularly imprinted polymers and carbon nanomaterials as a versatile biosensing tool in sample analysis: Recent applications and challenges. *TrAC Trends in Analytical Chemistry*, 93, 134-151. <https://doi.org/https://doi.org/10.1016/j.trac.2017.05.015>
- Ansell, R. J. (2015). Characterization of the Binding Properties of Molecularly Imprinted Polymers. In B. Mattiasson & L. Ye (Eds.), *Molecularly Imprinted Polymers in Biotechnology* (Vol. 150, pp. 51-93). Springer Int Publishing Ag. https://doi.org/10.1007/10_2015_316

- Antuña-Jiménez, D., Díaz-Díaz, G., Blanco-López, M. C., Lobo-Castañón, M. J., Miranda-Ordieres, A. J., & Tuñón-Blanco, P. (2012). Chapter 1 - Molecularly Imprinted Electrochemical Sensors: Past, Present, and Future. In S. Li, Y. Ge, S. A. Piletsky, & J. Lunec (Eds.), *Molecularly Imprinted Sensors* (pp. 1-34). Elsevier. <https://doi.org/10.1016/B978-0-444-56331-6.00001-3>
- Aslyüce, S., Mattiasson, B., & Denizli, A. (2019). Combined protein A imprinting and cryogelation for production of spherical affinity material. *Biomedical Chromatography*, 33(10), e4605. <https://doi.org/10.1002/bmc.4605>
- Bard, A. J., & Faulkner, L. R. (2000). *Electrochemical Methods: Fundamentals and Applications, 2nd Edition*. John Wiley & Sons, Incorporated. <https://books.google.co.th/books?id=hQocAAAAQBAJ>
- Berzas Nevado, J. J., Rodriguez Flores, J., & Castañeda Peñalvo, G. (1999). Adsorptive stripping square-wave voltammetric behavior of insulin. *Fresenius' Journal of Analytical Chemistry*, 364(8), 753-757. <https://doi.org/10.1007/s002160051427>
- Blanco-López, M. C., Lobo-Castañón, M. J., Miranda-Ordieres, A. J., & Tuñón-Blanco, P. (2004). Electrochemical sensors based on molecularly imprinted polymers. *TrAC Trends in Analytical Chemistry*, 23(1), 36-48. [https://doi.org/10.1016/S0165-9936\(04\)00102-5](https://doi.org/10.1016/S0165-9936(04)00102-5)
- Cecchini, A., Raffa, V., Canfarotta, F., Signore, G., Piletsky, S., MacDonald, M. P., & Cuschieri, A. (2017). In vivo recognition of human vascular endothelial growth factor by molecularly imprinted polymers. *Nano Lett.*, 17, 2307.
- Dai, H., Xiao, D., He, H., Li, H., Yuan, D., & Zhang, C. (2015). Synthesis and analytical applications of molecularly imprinted polymers on the surface of carbon nanotubes: a review. *Microchimica Acta*, 182(5), 893-908. <https://doi.org/10.1007/s00604-014-1376-5>
- De Rycke, E., Trynda, A., Jaworowicz, M., Dubruel, P., De Saeger, S., & Beloglazova, N. (2021). Capacitive sensing of an amphetamine drug precursor in aqueous samples: Application of novel molecularly imprinted polymers for benzyl methyl ketone detection. *Biosensors and Bioelectronics*, 172, 112773. <https://doi.org/10.1016/j.bios.2020.112773>

- El-Akaad, S., De Saeger, S., & Beloglazova, N. (2021). Molecularly imprinted polymer based capacitive sensing of a specific Leuckart marker 4-methyl-5-phenylpyrimidine in wastewater. *Sensors and Actuators B: Chemical*, 343, 130116. <https://doi.org/10.1016/j.snb.2021.130116>
- El-Akaad, S., Mohamed, M. A., Abdelwahab, N. S., Abdelaleem, E. A., De Saeger, S., & Beloglazova, N. (2020). Capacitive sensor based on molecularly imprinted polymers for detection of the insecticide imidacloprid in water. *Scientific Reports*, 10(1), 14479. <https://doi.org/10.1038/s41598-020-71325-y>
- Elfadil, D., Lamaoui, A., Della Pelle, F., Amine, A., & Compagnone, D. (2021). Molecularly Imprinted Polymers Combined with Electrochemical Sensors for Food Contaminants Analysis. *Molecules*, 26(15).
- Entezari, M., Safari, M., Hekmati, M., Hekmat, S., & Azin, A. (2014). Modification of carboxylated multiwall nanotubes with benzotriazole derivatives and study of their anticancer activities. *Medicinal Chemistry Research*, 23(1), 487-495. <https://doi.org/10.1007/s00044-013-0668-3>
- Erdössy, J., Horváth, V., Yarman, A., Scheller, F. W., & Gyurcsányi, R. E. (2016). Electrosynthesized molecularly imprinted polymers for protein recognition. *TrAC Trends in Analytical Chemistry*, 79, 179-190. <https://doi.org/10.1016/j.trac.2015.12.018>
- Ertürk, G., Hedström, M., & Mattiasson, B. (2016). A sensitive and real-time assay of trypsin by using molecular imprinting-based capacitive biosensor. *Biosensors and Bioelectronics*, 86, 557-565. <https://doi.org/10.1016/j.bios.2016.07.046>
- Ertürk, G., & Mattiasson, B. (2017). Capacitive Biosensors and Molecularly Imprinted Electrodes. *Sensors*, 17(2).
- Fatoni, A., Numnuam, A., Kanatharana, P., Limbut, W., & Thavarungkul, P. (2014). A novel molecularly imprinted chitosan-acrylamide, graphene, ferrocene composite cryogel biosensor used to detect microalbumin [10.1039/C4AN01000K]. *Analyst*, 139(23), 6160-6167. <https://doi.org/10.1039/C4AN01000K>

- Herrera-Chacón, A., Dinç-Zor, Ş., & del Valle, M. (2020). Integrating molecularly imprinted polymer beads in graphite-epoxy electrodes for the voltammetric biosensing of histamine in wines. *Talanta*, 208, 120348. <https://doi.org/https://doi.org/10.1016/j.talanta.2019.120348>
- Huang, F., Zhu, B., Zhang, H., Gao, Y., Ding, C., Tan, H., & Li, J. (2019). A glassy carbon electrode modified with molecularly imprinted poly(aniline boronic acid) coated onto carbon nanotubes for potentiometric sensing of sialic acid. *Microchimica Acta*, 186(5), 270. <https://doi.org/10.1007/s00604-019-3387-8>
- Iskierko, Z., Sharma, P. S., Bartold, K., Pietrzyk-Le, A., Noworyta, K., & Kutner, W. (2016). Molecularly imprinted polymers for separating and sensing of macromolecular compounds and microorganisms. *Biotechnology Advances*, 34(1), 30-46. <https://doi.org/https://doi.org/10.1016/j.biotechadv.2015.12.002>
- Justino, C. I. L., Freitas, A. C., Pereira, R., Duarte, A. C., & Rocha Santos, T. A. P. (2015). Recent developments in recognition elements for chemical sensors and biosensors. *TrAC Trends in Analytical Chemistry*, 68, 2-17. <https://doi.org/https://doi.org/10.1016/j.trac.2015.03.006>
- Justino, C. I. L., Rocha-Santos, T. A., & Duarte, A. C. (2010). Review of analytical figures of merit of sensors and biosensors in clinical applications. *TrAC Trends in Analytical Chemistry*, 29(10), 1172-1183.
- Karunakaran, C., Rajkumar, R., & Bhargava, K. (2015). Chapter 1 - Introduction to Biosensors. In C. Karunakaran, K. Bhargava, & R. Benjamin (Eds.), *Biosensors and Bioelectronics*(pp.1-68).Elsevier. <https://doi.org/https://doi.org/10.1016/B978-0-12-803100-1.00001-3>
- Khosropour, H., Saboohi, M., Keramat, M., Rezaei, B., & Ensafi, A. A. (2023). Electrochemical molecularly imprinted polymer sensor for ultrasensitive indoxacarb detection by tin disulfide quantum dots/carbon nitride/multiwalled carbon nanotubes as a nanocomposite. *Sensors and Actuators B: Chemical*, 385, 133652. <https://doi.org/https://doi.org/10.1016/j.snb.2023.133652>
- Khumngern, S., Thavarungkul, P., Kanatharana, P., Bejrananda, T., & Numnuam, A. (2022). Molecularly imprinted electrochemical sensor based on poly(o-phenylenediamine-co-o-aminophenol)incorporated with poly(styrenesulfonate)

doped poly(3,4-ethylenedioxythiophene) ferrocene composite modified screen-printed carbon electrode for highly sensitive and selective detection of prostate cancer biomarker. *Microchemical Journal*, 177, 107311.

<https://doi.org/https://doi.org/10.1016/j.microc.2022.107311>

Krejci, J., Sajdlova, Z., Nedela, V., Flodrova, E., Sejnohova, R., Vranova, H., & Plicka, R. (2014). Effective Surface Area of Electrochemical Sensors. *Journal of The Electrochemical Society*, 161(6), B147. <https://doi.org/10.1149/2.091406jes>

Kurbanoglu, S., Unal, M. A., & Ozkan, S. A. (2018). Recent developments on electrochemical flow injection in pharmaceuticals and biologically important compounds. *Electrochimica Acta*, 287, 135-148.

<https://doi.org/https://doi.org/10.1016/j.electacta.2018.04.217>

Liu, J., Wang, Y., Liu, X., Yuan, Q., Zhang, Y., & Li, Y. (2019). Novel molecularly imprinted polymer (MIP) multiple sensors for endogenous redox couples determination and their applications in lung cancer diagnosis. *Talanta*, 199, 573-580. <https://doi.org/https://doi.org/10.1016/j.talanta.2019.03.018>

Liu, Y., & Dykstra, G. (2022). Recent progress on electrochemical (bio)sensors based on aptamer-molecularly imprinted polymer dual recognition. *Sensors and Actuators Reports*, 4, 100112.

<https://doi.org/https://doi.org/10.1016/j.snr.2022.100112>

Lovrić, M. (2010). Square-Wave Voltammetry. In F. Scholz, A. M. Bond, R. G. Compton, D. A. Fiedler, G. Inzelt, H. Kahlert, Š. Komorsky-Lovrić, H. Lohse, M. Lovrić, F. Marken, A. Neudeck, U. Retter, F. Scholz, & Z. Stojek (Eds.), *Electroanalytical Methods: Guide to Experiments and Applications* (pp. 121-145). Springer Berlin Heidelberg. https://doi.org/10.1007/978-3-642-02915-8_6

Malitesta, C., Mazzotta, E., Picca, R. A., Poma, A., Chianella, I., & Piletsky, S. A. (2012). MIP sensors – the electrochemical approach. *Analytical and Bioanalytical Chemistry*, 402(5), 1827-1846. <https://doi.org/10.1007/s00216-011-5405-5>

Mani, V., Beduk, T., Khushaim, W., Ceylan, A. E., Timur, S., Wolfbeis, O. S., & Salama, K. N. (2021). Electrochemical sensors targeting salivary biomarkers:

- A comprehensive review. *TrAC Trends in Analytical Chemistry*, 135, 116164. <https://doi.org/https://doi.org/10.1016/j.trac.2020.116164>
- Marian, T. S., & Allen, J. B. (1977). The electrochemistry of proteins and related substances: Part II. Insulin. *Journal of Electroanalytical Chemistry and Interfacial Electrochemistry*, 85(1), 173-183. [https://doi.org/https://doi.org/10.1016/S0022-0728\(77\)80162-9](https://doi.org/https://doi.org/10.1016/S0022-0728(77)80162-9)
- Mazzotta, E., Di Giulio, T., & Malitesta, C. (2022). Electrochemical sensing of macromolecules based on molecularly imprinted polymers: challenges, successful strategies, and opportunities. *Analytical and Bioanalytical Chemistry*, 414(18), 5165-5200. <https://doi.org/10.1007/s00216-022-03981-0>
- Mazzotta, E., Turco, A., Chianella, I., Guerreiro, A., Piletsky, S. A., & Malitesta, C. (2016). Solid-phase synthesis of electroactive nanoparticles of molecularly imprinted polymers. A novel platform for indirect electrochemical sensing applications. *Sensors and Actuators B: Chemical*, 229, 174-180. <https://doi.org/https://doi.org/10.1016/j.snb.2016.01.126>
- Miller, J. N., & Miller, J. C. (2010). *Statistics and Chemometrics for Analytical Chemistry 6th Edition* (6th Edition ed.). Pearson Education Limited.
- Mirceski, V., Gulaboski, R., Lovric, M., Bogeski, I., Kappl, R., & Hoth, M. (2013). Square-Wave Voltammetry: A Review on the Recent Progress [<https://doi.org/10.1002/elan.201300369>]. *Electroanalysis*, 25(11), 2411-2422. <https://doi.org/https://doi.org/10.1002/elan.201300369>
- Ni, M., Xu, Y., Wang, C., Zhao, P., Yang, P., Chen, C., Zheng, K., Wang, H., Sun, X., Li, C., Xie, Y., & Fei, J. (2020). A novel thermo-controlled acetaminophen electrochemical sensor based on carboxylated multi-walled carbon nanotubes and thermosensitive polymer. *Diamond and Related Materials*, 107, 107877. <https://doi.org/https://doi.org/10.1016/j.diamond.2020.107877>
- Peng, L., Yarman, A., Jetzschmann, K. J., Jeoung, J.-H., Schad, D., Dobbek, H., Wollenberger, U., & Scheller, F. W. (2016). Molecularly Imprinted Electropolymer for a Hexameric Heme Protein with Direct Electron Transfer and Peroxide Electrocatalysis. *Sensors*, 16(3).

- Phonklam, K., Wannapob, R., Sriwimol, W., Thavarungkul, P., & Phairatana, T. (2020). A novel molecularly imprinted polymer PMB/MWCNTs sensor for highly-sensitive cardiac troponin T detection. *Sensors and Actuators B: Chemical*, 308, 127630.
<https://doi.org/https://doi.org/10.1016/j.snb.2019.127630>
- Quintino, M. S. M., & Angnes, L. (2004). Batch Injection Analysis: An Almost Unexplored Powerful Tool [<https://doi.org/10.1002/elan.200302878>]. *Electroanalysis*, 16(7), 513-523.
<https://doi.org/https://doi.org/10.1002/elan.200302878>
- Rassaei, L., Marken, F., Sillanpää, M., Amiri, M., Cirtiu, C. M., & Sillanpää, M. (2011). Nanoparticles in electrochemical sensors for environmental monitoring. *TrAC Trends in Analytical Chemistry*, 30(11), 1704-1715.
<https://doi.org/https://doi.org/10.1016/j.trac.2011.05.009>
- Rebelo, P., Costa-Rama, E., Seguro, I., Pacheco, J. G., Nouws, H. P. A., Cordeiro, M. N. D. S., & Delerue-Matos, C. (2021). Molecularly imprinted polymer-based electrochemical sensors for environmental analysis. *Biosensors and Bioelectronics*, 172, 112719.
<https://doi.org/https://doi.org/10.1016/j.bios.2020.112719>
- Scognamiglio, V., Antonacci, A., Lambreva, M. D., Litescu, S. C., & Rea, G. (2015). Synthetic biology and biomimetic chemistry as converging technologies fostering a new generation of smart biosensors. *Biosens Bioelectron*, 74, 1076-1086. <https://doi.org/10.1016/j.bios.2015.07.078>
- Shao, W., Mai, J., & Wei, Z. (2022). Nonenzymatic Lactic Acid Detection Using Cobalt Polyphthalocyanine/Carboxylated Multiwalled Carbon Nanotube Nanocomposites Modified Sensor. *Chemosensors*, 10(2).
<https://doi.org/10.3390/chemosensors10020083>
- Sharma, P. S., Garcia-Cruz, A., Cieplak, M., Noworyta, K. R., & Kutner, W. (2019). ‘Gate effect’ in molecularly imprinted polymers: the current state of understanding. *Current Opinion in Electrochemistry*, 16, 50-56.
<https://doi.org/https://doi.org/10.1016/j.coelec.2019.04.020>

- Shrivastava, A., & Gupta, V. B. (2011). Methods for the determination of limit of detection and limit of quantitation of the analytical methods. *Chronicles of Young Scientists*, 2, 21-25.
- Sisolakova, I., Hovancova, J., Orinakova, R., Orinak, A., Trnkova, L., Garcia, D. R., & Radonak, J. (2019). Influence of a polymer membrane on the electrochemical determination of insulin in nanomodified screen printed carbon electrodes [Article]. *Bioelectrochemistry*, 130, 11, Article 107326. <https://doi.org/10.1016/j.bioelechem.2019.06.011>
- Suryanarayanan, V., Wu, C.-T., & Ho, K.-C. (2010). Molecularly Imprinted Electrochemical Sensors. *Electroanalysis*, 22(16), 1795-1811. <https://doi.org/https://doi.org/10.1002/elan.200900616>
- Taverniers, I., De Loose, M., & Van Bockstaele, E. (2004). Trends in quality in the analytical laboratory. II. Analytical method validation and quality assurance. *TrAC Trends in Analytical Chemistry*, 23(8), 535-552. <https://doi.org/https://doi.org/10.1016/j.trac.2004.04.001>
- Thévenot, D. R., Toth, K., Durst, R. A., & Wilson, G. S. (2001). Electrochemical biosensors: recommended definitions and classification | International Union of Pure and Applied Chemistry: Physical Chemistry Division, Commission I.7 (Biophysical Chemistry); Analytical Chemistry Division, Commission V.5 (Electroanalytical Chemistry). 1. *Biosensors and Bioelectronics*, 16(1), 121-131. [https://doi.org/https://doi.org/10.1016/S0956-5663\(01\)00115-4](https://doi.org/https://doi.org/10.1016/S0956-5663(01)00115-4)
- Thompson, M., Ellison, S. L. R., & Wood, R. (2002). Harmonized guidelines for single-laboratory validation of methods of analysis (IUPAC Technical Report). 74(5), 835-855. <https://doi.org/doi:10.1351/pac200274050835> (Pure and Applied Chemistry)
- Torkashvand, M., Gholivand, M. B., & Azizi, R. (2017). Synthesis, characterization and application of a novel ion-imprinted polymer based voltammetric sensor for selective extraction and trace determination of cobalt (II) ions. *Sensors and Actuators B: Chemical*, 243, 283-291. <https://doi.org/https://doi.org/10.1016/j.snb.2016.11.094>

- Trevizan, H. F., Olean-Oliveira, A., Cardoso, C. X., & Teixeira, M. F. S. (2021). Development of a molecularly imprinted polymer for uric acid sensing based on a conductive azopolymer: Unusual approaches using electrochemical impedance/capacitance spectroscopy without a soluble redox probe. *Sensors and Actuators B: Chemical*, 343, 130141. <https://doi.org/https://doi.org/10.1016/j.snb.2021.130141>
- Wackerlig, J., & Schirhagl, R. (2016). Applications of Molecularly Imprinted Polymer Nanoparticles and Their Advances toward Industrial Use: A Review. *Analytical Chemistry*, 88(1), 250-261. <https://doi.org/10.1021/acs.analchem.5b03804>
- Yang, B., Fu, C., Li, J., & Xu, G. (2018). Frontiers in highly sensitive molecularly imprinted electrochemical sensors: Challenges and strategies. *TrAC Trends in Analytical Chemistry*, 105, 52-67. <https://doi.org/https://doi.org/10.1016/j.trac.2018.04.011>
- Zhang, H. Y., Liu, C. J., Chen, L., & Dai, B. (2019). Control of ice crystal growth and its effect on porous structure of chitosan cryogels [Article]. *Chemical Engineering Science*, 201, 50-57. <https://doi.org/10.1016/j.ces.2019.02.026>
- Zhang, M. G., Mullens, C., & Gorski, W. (2005). Insulin oxidation and determination at carbon electrodes [Article]. *Analytical Chemistry*, 77(19), 6396-6401. <https://doi.org/10.1021/ac0508752>
- Zhang, T., Xuan, X., Li, M., Li, C., Li, P., & Li, H. (2022). Molecularly imprinted Ni-polyacrylamide-based electrochemical sensor for the simultaneous detection of dopamine and adenine. *Analytica Chimica Acta*, 1202, 339689. <https://doi.org/https://doi.org/10.1016/j.aca.2022.339689>
- Zheng, W., Zhao, M., Liu, W., Yu, S., Niu, L., Li, G., Li, H., & Liu, W. (2018). Electrochemical sensor based on molecularly imprinted polymer/reduced graphene oxide composite for simultaneous determination of uric acid and tyrosine. *Journal of Electroanalytical Chemistry*, 813, 75-82. <https://doi.org/https://doi.org/10.1016/j.jelechem.2018.02.022>
- Zhu, C., Yang, G., Li, H., Du, D., & Lin, Y. (2015). Electrochemical Sensors and Biosensors Based on Nanomaterials and Nanostructures. *Analytical Chemistry*, 87(1), 230-249. <https://doi.org/10.1021/ac5039863>

Zong, W., Liu, R., Sun, F., Wang, M., Zhang, P., Liu, Y., & Tian, Y. (2010). Cyclic voltammetry: a new strategy for the evaluation of oxidative damage to bovine insulin. *Protein Sci*, *19*(2), 263-268. <https://doi.org/10.1002/pro.313>

Appendices

PAPER I**Electrochemical sensor based on molecularly imprinted polymer cryogel and multiwalled carbon nanotubes for direct insulin detection**

Wardani, N. I., Kankamano, T., Wannapob, R., Kanatharana, P., Thavarungkul, P.,
Limbut, W.

*Reprinted from Talanta (2023) 254, 124137
with permission of Elsevier*



Electrochemical sensor based on molecularly imprinted polymer cryogel and multiwalled carbon nanotubes for direct insulin detection

Nur Indah Wardani^{a,b,c}, Tawatchai Kangkama^{a,b,c,d}, Rodtichoti Wannapob^{a,b,c},
Proespichaya Kanatharana^{a,b,c}, Panote Thavarungkul^{a,b,c}, Warakorn Limbut^{a,b,e,*}

^a Center of Excellence for Trace Analysis and Biosensor, Prince of Songkla University, Hat Yai, Songkhla, 90110, Thailand

^b Center of Excellence for Innovation in Chemistry, Faculty of Science, Prince of Songkla University, Hat Yai, Songkhla, 90110, Thailand

^c Division of Physical Science, Faculty of Science, Prince of Songkla University, Hat Yai, Songkhla, 90110, Thailand

^d Department of Chemistry, Faculty of Science, Thaksin University (Phathalung Campus), Papayom, Phathalung, 93110, Thailand

^e Division of Health and Applied Sciences, Faculty of Science, Prince of Songkla University, Hat Yai, Songkhla, 90110, Thailand

ARTICLE INFO

Keywords:

Insulin oxidation
Diagnosis of type 1 and 2 diabetes
Electrochemical sensor
Molecularly imprinted polymer cryogel
Flow system

ABSTRACT

Insulin is the polypeptide hormone that regulates blood glucose levels. It is used as an indicator of both types of diabetes. An electrochemical insulin sensor was developed using a gold electrode modified with carboxylated multiwalled carbon nanotubes (f-MWCNTs) and molecularly imprinted polymer (MIP) cryogel. The MIP provided specific recognition sites for insulin, while the macropores of the cryogel promoted the mass transfer of insulin to the recognition sites. The f-MWCNTs increased the effective surface area and conductivity of the sensor and also reduced the potential required to oxidize insulin. Insulin oxidation was directly measured in a flow system using square wave voltammetry. This MIP cryogel/f-MWCNTs sensor provided a linear range of 0.050–1.40 pM with a very low limit of detection (LOD) of 33 fM. The sensor exhibited high selectivity and long-term stability over 10 weeks of dry storage at room temperature. The results of insulin determination in human serum using the sensor compared well with the results of the Elecsys insulin assay. The developed MIP sensor offers a promising alternative for the diagnosis and treatment of diabetes.

1. Introduction

Insulin is the only polypeptide hormone that regulates and controls blood glucose levels [1]. Insulin deficiency and insulin resistance, respectively, cause type 1 and type 2 diabetes mellitus, and therefore blood glucose levels are used to diagnose and monitor these conditions. However, personal behaviors such as exercise and diet can affect an individual's blood glucose levels and result in a false diagnosis and incorrect medication [2–4]. Accurate, early diagnosis can be made by detecting insulin rather than blood glucose, leading to better control of both types of diabetes mellitus. The most commonly used techniques for detecting insulin are immunoassays [5–8], chromatographic [9–11] and electrochemical [12–14] techniques, and optical methods [15,16].

Electrochemical detection is an interesting approach that can provide a low detection limit and short analysis time, using less expensive instruments [17]. The direct electrochemical detection of insulin is facilitated by insulin amino acids such as tyrosine, tryptophan, and cystine, which are electro-active. However, slow electron transfer

kinetics, high oxidation potentials, and electrode surface fouling have been observed when using an unmodified electrode [18–20]. Anti-fouling properties and wider linear ranges can be achieved by modifying electrodes with electrocatalytic materials such as metal (Ni, Cu, Co) or metal oxide (NiO, RuO, CoO) nanoparticles but nevertheless, high levels of glucose, uric acid, and ascorbic acid can interfere with responses [21–24]. The performance of electrocatalytic nanoparticles can be improved if they are supported by multiwalled carbon nanotubes (MWCNTs), which can enlarge the electrode surface area, create more active sites for insulin oxidation, and decrease the overpotential of insulin [25,26]. The stabilization of nanoparticles with carboxylated multiwalled carbon nanotubes (f-MWCNTs) leads to more effective loading of nanoparticles, which can contribute to increased electrocatalytic activity towards insulin [27–29]. Nevertheless, high levels of glucose, uric acid, and ascorbic acid in serum samples can interfere with responses due to the electroactivity of nanoparticles towards these compounds. Hence, to achieve highly selective direct insulin detection, different combinations of f-MWCNTs and insulin recognition element

* Corresponding author. Division of Health and Applied Sciences, Faculty of Science, Prince of Songkla University, Hat Yai, Songkhla 90110, Thailand.
E-mail address: warakorn.l@psu.ac.th (W. Limbut).

<https://doi.org/10.1016/j.talanta.2022.124137>

Received 13 July 2022; Received in revised form 21 November 2022; Accepted 24 November 2022

Available online 26 November 2022

0039-9140/© 2022 Elsevier B.V. All rights reserved.

must be investigated.

Despite the improvements that have already been made in the field, there is still a need for the further development of direct electrochemical insulin sensors since a very low limit of detection (LOD) is required. An LOD in the picomolar range is the most suitable to detect the normal level of insulin in blood, which is 12–150 pM [30] and the receptor should be highly selective to avoid detection interference. A lower LOD may be achieved by increasing the surface area of the electrocatalytic interface so that more reaction can occur. A good candidate for this task is a porous polymeric cryogel. This material can be easily fabricated on an electrode surface via a freezing and thawing process [31]. Cryogel can be fabricated to incorporate a molecularly imprinted polymer (MIP) with binding sites specific to the target analyte. The interconnected micropores of cryogel provide a high surface area to volume ratio which can increase sensor sensitivity and stability [32–34]. The porous structure of cryogel will enable the accumulation of insulin at a large number of imprinted sites on the electrode surface. The porous structure of cryogel could also improve the mass transfer of analytes such as proteins to the imprinted cavities of the MIP and make their removal easier [35]. Thus, a suitable MIP and cryogel should produce a synergistic improvement of insulin detection.

MIPs are created by polymerizing a functional monomer with the target analyte as a template for the formation of molecular imprints. After the template molecules are removed, they leave imprinted sites with the same shape and dimensions as the template molecules, and a complementary chemical functionality [36]. Because the imprinted sites are capable of specifically and sensitively rebinding the target analyte, MIPs have been widely developed for a variety of small molecules and biomolecules, including proteins [37,38]. Some MIP electrochemical sensors for insulin detection have achieved picomolar detection limits by using a ferrocyanide/ferricyanide ($[\text{Fe}(\text{CN})_6^{3-/4-}]$) redox probe [39,40]. An MIP can also be prepared from two monomers. This approach diversifies the available functional groups and the strengthened interactions between the MIP and the template have improved selectivity [41–43]. Homogenous MIPs that improved the binding and affinity between imprinted cavities and the template were produced by the co-polymerization of chitosan, a polysaccharide with abundant hydroxyl and amino groups, and acrylamide, which provided amide groups, chemical stability, and hydrophilicity [41,44]. These improvements effectively accumulated the target analyte and, at the same time, eliminated interferences. Acrylamide also acted as a structural functional monomer that stabilized the MIP by forming internal cross-linked structures [41].

The performance of the proposed MIP sensor could be further increased by integrating it with a flow system. This approach offers several advantages over batch electrochemical detection since it limits impurities and cleans the electrode surface [45]. The combination of MIP sensor and a flow system has been used in sample preparation, resulting in improved interaction between analyte and MIP interface via the variation of flow rate [46]. This is especially beneficial for MIP electrochemical detection since selectivity can be improved by choosing a flow stream that limits non-specific binding. In addition, MIP rebinding, washing, detection and regeneration of the imprinted cavities, can be carried out continuously in a stable, selective, and sensitive system. A continuous flow stream was reported to have increased sensitivity by resolving the problem of restricted diffusion of macromolecular insulin [47] to imprinted cavities.

Herein, we report a novel MIP sensor that directly detects insulin. The sensor combines the attractive features of MIP cryogel with a flow system that enables continuous analysis. The sensor platform of carboxylated multiwalled carbon nanotubes (f-MWCNTs) and a cryogel incorporating an MIP of dual-functional monomers creates a large number of imprinted recognition sites that help achieve a low detection limit. The f-MWCNTs, drop-casted onto a gold electrode, enable a higher loading of more evenly distributed MIP cryogel and increase the conductivity of the sensor. The incorporation of the sensor into a flow

system provides additional benefits for the direct electrochemical determination of insulin captured within the imprinted cavities of the MIP. The fabrication steps and operational condition of the sensor were optimized. The analytical performances of the sensor were evaluated using standard solutions and blood serum samples.

2. Experimental

2.1. Reagents and materials

Chitosan from shrimp shells (low viscosity, <200 mPa s) was from Sigma-Aldrich (Louis, USA). Human insulin, acrylamide (AM), *N,N'*-methylene bisacrylamide (BAM), human serum albumin (HSA), L-ascorbic acid, creatinine, uric acid and dopamine were from Sigma-Aldrich, (Steinheim, Germany). Carcinoembryonic antigen (CEA) and alpha fetoprotein (AFP) were from Dako (Denmark). Ammonium peroxodisulfate (APS) and *N,N,N',N'*-Tetramethylethylenediamine (TEMED) were from Merck (Darmstadt, Germany). Sodium dihydrogen *o*-phosphate and disodium hydrogen *o*-phosphate were from Ajax Finechem (Sydney, Australia). MWCNTs (purity $\geq 95\%$, average diameter 60–100 nm, length 2–5 μm) were from Shenzhen Nano-Techbnologies Port Co., Ltd. (Shenzhen, China). MWCNTs were carboxylated (f-MWCNTs) with a 3:1 (v/v) mixture of concentrated H_2SO_4 and HNO_3 , filtered, and stored in a vacuum desiccator before use. Other chemicals used were of analytical quality.

2.2. Apparatus

To evaluate the electrode modification steps, electrochemical impedance spectroscopy (EIS), cyclic voltammetry (CV), and square wave voltammetry (SWV) were performed using an Autolab Type III controlled by a potentiostat-galvanostat with NOVA 2.1 software (Metrohm Autolab B.V., The Netherlands). The impedance spectra were fitted to a Randles equivalent circuit using the FRA module of the NOVA software to obtain the charge transfer resistance (R_{ct}). f-MWCNTs were characterized by Fourier-transform infrared (FT-IR) spectroscopy (VERTEX 70, Bruker, Germany) using the KBr pellet technique (see Section 3.1). Scanning electron microscopy (SEM) was used to study the surface morphology of electrodes (SEM, Quanta 400, FEI, Japan). Insulin was detected electrochemically in a flow system using SWV on an Autolab Type III.

2.3. Electrode modification

A gold electrode (AuE) (3.0 mm diameter, 99.99% purity) was polished with alumina slurries (5.0, 1.0, and 0.30 μm , respectively), rinsed with deionized water, and sonicated in absolute ethanol and deionized water for 2 min before being electrochemically cleaned in 0.50 M sulfuric acid for 30 cycles (0.0–1.6 V vs. Ag/AgCl, 100 mV s^{-1}). f-MWCNTs were suspended in 50% ethanol (see Section 3.3.2). Then, 7.5 μL of the suspension were drop-casted onto the surface of the electrode and allowed to dry for 3 h at room temperature (f-MWCNTs/AuE). The cryogel pre-polymer mixture of 2.5 mL of chitosan (4% w/v in 1% (v/v) acetic acid), 540 mg of AM and 60 mg of BAM (cross linker) was sonicated for 30 min before being adjusted to 5.0 mL with 1.0 mM phosphate buffer at pH 5.30. Ten microliters of this pre-polymer mixture were combined with 5.0 μL of 1.0 μM insulin, 1.0 μL of 50% (w/v) APS and 0.10 μL of TEMED. Then, 4.0 μL of the mixture were drop-casted onto the f-MWCNTs/AuE and frozen at -10°C for at least 5 h. The frozen electrode was thawed at 4°C for 15 min, during which time the ice melted, leaving behind a porous network. The thawed electrode was rinsed with deionized water, and the insulin template was removed by soaking in acetic acid-ethanol at 9:1 (v/v) for 2 h. The fabrication of the MIP cryogel/f-MWCNTs/AuE was complete. The same procedure was used to create a non-imprinted polymer (NIP) cryogel/f-MWCNTs/AuE without the insulin template. When not in use, the electrode was

stored dry in a closed tube at room temperature.

2.4. Electrochemical measurements

The MIP cryogel/f-MWCNTs/AuE, a custom-built Ag/AgCl reference electrode and a stainless-steel tube auxiliary electrode were inserted into a custom-built flow cell (10 μL) and connected to the potentiostat (Fig. 1A). The insulin detection cycle comprised three steps: insulin

rebinding, electrochemical detection, and regeneration (Fig. 1B). For the insulin rebinding step, a 0.50 mL insulin sample in 1.0 mM phosphate buffer at pH 5.30 (the carrier buffer at optimized pH, see Section 3.3.4) was injected through a six-port injection valve (Valco Instrument, USA) into a $100 \mu\text{L min}^{-1}$ continuous flow of buffer. The sample injection was followed by a continuous flow of buffer for 3 min to ensure that the whole volume of sample passed through the working electrode. The flow was stopped for 2 min to stabilize the rebinding, then resumed for

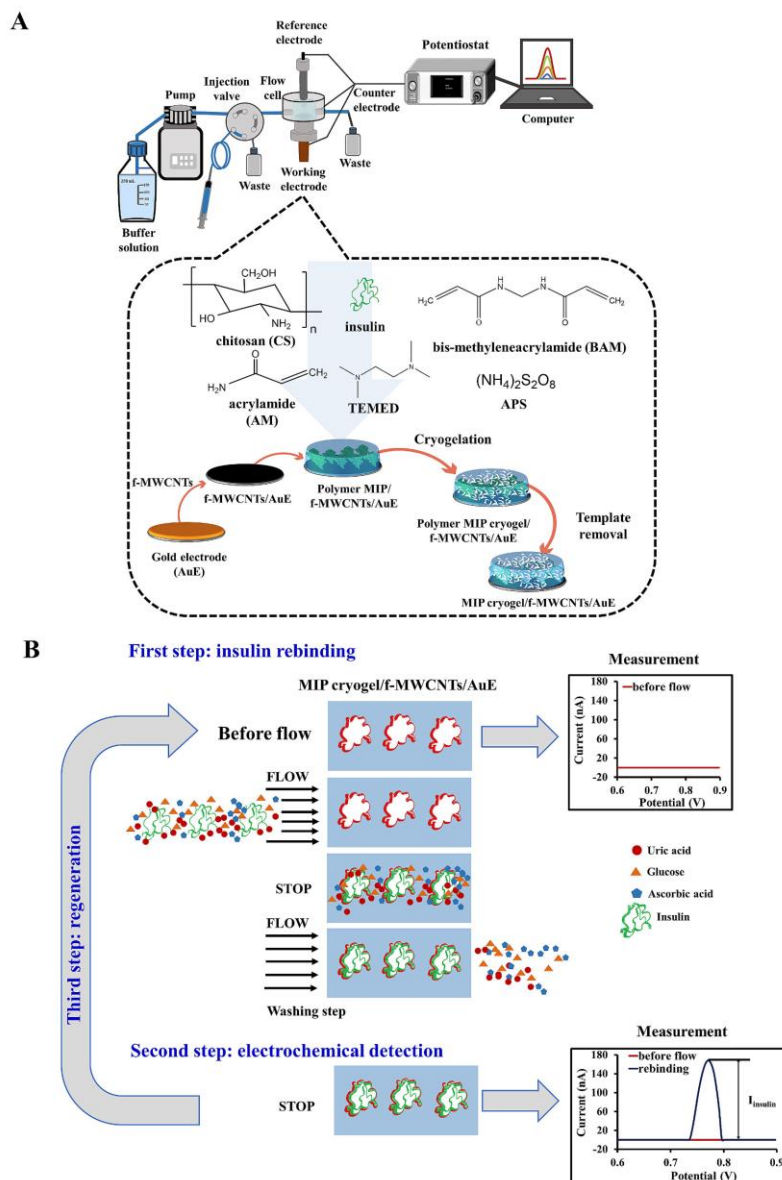


Fig. 1. The preparation of the MIP cryogel/f-MWCNTs modified gold electrode and its use as a working electrode in a flow system (A). Three steps of the insulin detection cycle: insulin rebinding, electrochemical detection, and regeneration (B). (For interpretation of the references to colour in this figure legend, the reader is referred to the Web version of this article.)

another 3 min to remove matrix compounds that may have bound non-specifically to the surface.

To determine the oxidation current of insulin bound to the MIP, the flow was stopped for 10 min while SWV was performed between 0.60 and 0.90 V at a 50 mV/s scan rate with a step potential, pulse amplitude, and pulse frequency of 5.0 mV, 0.010 mV, and 1.0 Hz, respectively. The regeneration solution (0.50 mL of 10% SDS in 20% acrylic acid, see Section 3.3.3) was then injected into the system, which was paused for 10 min to remove bound insulin from the electrode. A continuous flow of buffer was then passed for 15 min to remove insulin from the system. The absence of an insulin oxidation current indicated complete regeneration (Fig. 1B).

2.5. Optimization

The amount of f-MWCNTs and template removal solution used in the electrode modification were optimized. In the operational procedure, the regeneration solution, buffer pH, and flow rate were optimized. A series of standard insulin solutions ($n = 3$) were tested ($n = 3$) at a flow rate of $100 \mu\text{L min}^{-1}$, using a carrier of 1.0 mM phosphate buffer at pH 5.30. The optimal condition was determined by a short analysis time and a high sensitivity, calculated from the slope of the calibration plot.

2.6. Selectivity

The investigation of possible interferences in human serum included the proteins human serum albumin, carcinoembryonic antigen, alpha fetoprotein, and the electroactive compounds glucose, creatinine, uric acid, ascorbic acid, and dopamine. They were tested individually and in binary mixtures with insulin at their normal physiological levels. The electroactive compounds were also tested at much higher levels. The current responses were compared to those of insulin alone. All measurements were carried out in triplicate.

2.7. Reproducibility and stability

The reproducibility of the electrode preparation was examined by determining a series of insulin standards ($n = 3$) with six modified electrodes and comparing the obtained standard deviations and sensitivities. Operational stability was examined by repeatedly measuring insulin at the middle of the linear range [48] in the optimum condition. Long-term stability was evaluated by testing a modified electrode once a week with a series of insulin standards. Storage stability was evaluated using modified electrodes that were prepared at the same time. The responses at each modified electrode to a series of standard insulins were tested after different storage times and compared to those of a freshly prepared electrode. When not in use, each electrode was kept dry in a closed tube at room temperature.

2.8. Real sample analysis

Blood serum samples were obtained from Songklanagarind Hospital, Hat Yai, Thailand. The sample collection and handling protocol were approved by the Human Research Ethics Committee of the Faculty of Medicine, Prince of Songkla University. The matrix effect was first evaluated to obtain an appropriate dilution factor. Slopes from standard insulin solutions and spiked samples were compared and analyzed by two-way ANOVA at the 95% confidence level ($P > 0.05$). For determination with the modified electrode, real samples were prepared at a suitable dilution factor (using 1.0 mM phosphate buffer pH 5.30) that showed no matrix interference. Serum insulin concentration was measured concurrently in the same serum samples using the proposed sensor and the Elecsys insulin assay (Roche Diagnostics, Mannheim, Germany). The paired Student's *t*-test (two-tailed) was used to compare the results from the proposed sensor and the Elecsys insulin assay used by the hospital at a significance level of 0.05. The Elecsys insulin assay is

an electrochemiluminescence immunoassay. In a brief, the Elecsys insulin assay employs a sandwich immunoassay method with two monoclonal antibodies and ruthenium complex as a label. Incubation of insulin from the sample, a biotinylated monoclonal insulin-specific antibody, and a monoclonal insulin-specific antibody labeled with ruthenium complex causes the formation of a sandwich complex. The complex is bound to the solid phase by the reaction of biotin and streptavidin after the addition of streptavidin-coated microparticles. The reaction mixture is aspirated into the measuring cell, where the magnetically captured microparticles are captured on the electrode surface. When a voltage is applied to the electrode, chemiluminescent emission occurs, which is measured by a photomultiplier.

3. Results and discussion

3.1. Characterization of the MIP cryogel/f-MWCNTs/AuE

The surface morphology of variously modified electrodes was examined by SEM. The f-MWCNTs/AuE displayed a filamentous surface structure of f-MWCNTs (Fig. 2A). This evenly distributed feature could contribute to the better dispersion of the carboxylated MWCNTs in ethanol (Supplementary data Fig. S1). The surface of the cryogel/f-MWCNTs/AuE exhibited an interconnected network of macropores (Fig. 2B), in contrast to the smoother non-cryogel modified electrode surface (Fig. 2C). The interconnected pores of the cryogel could increase the mass transfer of insulin to interact with imprinted cavities. The surface of the MIP cryogel/f-MWCNTs/AuE was smooth before the removal of the insulin template (Fig. 2D) but rough afterwards (Fig. 2E). The surface roughness was likely due to the unoccupied imprinted cavities. After the rebinding of insulin, the occupation of the cavities produced a smooth surface (Fig. 2F), similar to the one before template removal (Fig. 2D). In comparison, the NIP cryogel/f-MWCNTs/AuE exhibited the same smooth surfaces before (Fig. 2G) and after template removal (Fig. 2H) and after the rebinding of insulin (Fig. 2I). These changes in morphology confirmed the formation of MIP on the modified electrode.

After each step in the modification procedure, the electrode was characterized in 5.0 mM $[\text{Fe}(\text{CN})_6]^{4-3-}$ by CV and EIS (Supplementary data Fig. S2). The cyclic voltammogram of the bare AuE showed a pair of well-defined redox waves (Supplementary data Fig. S2A). The f-MWCNTs/AuE produced higher redox peaks and increased background current due to the larger surface area and high conductivity of f-MWCNTs. The redox peaks produced by the MIP/f-MWCNTs/AuE before template removal were lower due to the blocking of electron transfer from by the non-conducting MIP layer. After removing the template, there was a significant increase in peak current attributed to the exposed imprinted cavities. The MIP/f-MWCNTs/AuE was then cycled in 1.0 μM insulin in phosphate buffer at pH 5.30. The current again decreased due to the rebinding of insulin, which blocked electron transfer.

The success of the modification steps was confirmed further by fitting the data to a Randles equivalent circuit (Supplementary data Fig. S2B). The arc of the plot can be used to calculate electron transfer resistance (R_{ct}), which corresponds to the resistance of the electrode surface against electrons from the redox probe [49]. The EIS response at the bare AuE produced a semicircular arc in the impedance spectrum that represented an R_{ct} of $90 \pm 4 \Omega$. Due to its large surface area and high conductivity, the f-MWCNTs/AuE produced a smaller arc equivalent to an R_{ct} of $17 \pm 2 \Omega$. The MIP/f-MWCNTs/AuE produced an arc that indicated a higher R_{ct} of $171 \pm 8 \Omega$, which was due to the hindrance of electron transfer by the non-conducting MIP. When the template was removed, exposing the imprinted cavities, the R_{ct} of the system dropped to $45 \pm 3 \Omega$. The presence of insulin caused a slight increase in R_{ct} to $70 \pm 2 \Omega$, which indicated that the target molecule had rebound to the imprinted cavities, blocking electron transfer to the electrode surface.

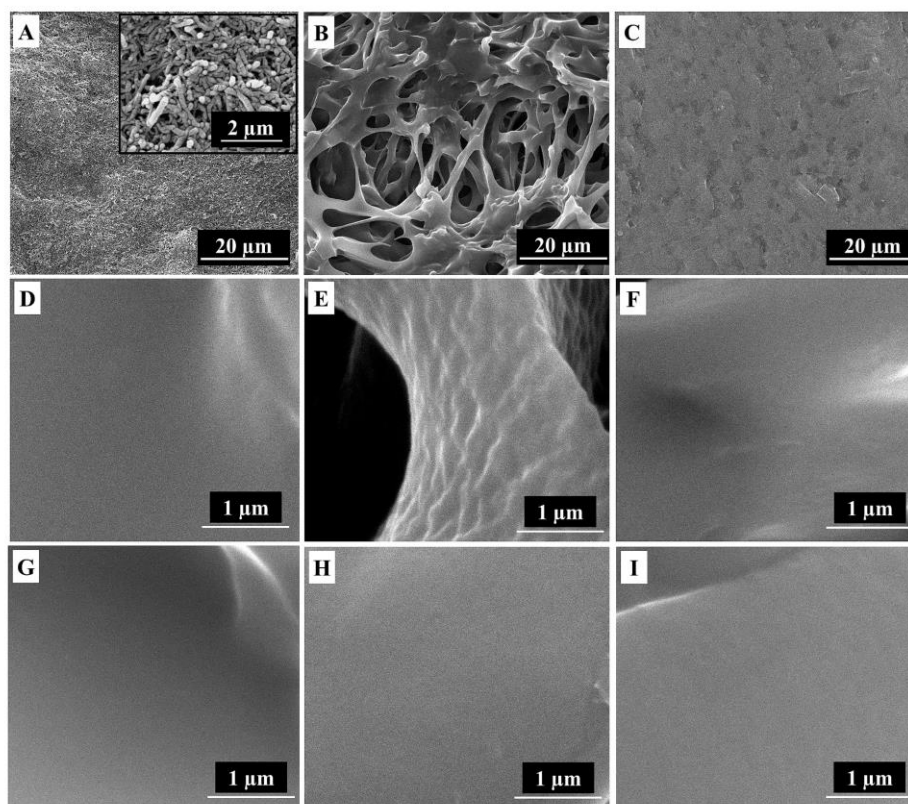


Fig. 2. SEM images show the surfaces of the (A) f-MWCNTs/AuE (inset at 20,000x magnification), (B) cryogel polymer/f-MWCNTs/AuE, (C) non cryogel polymer/f-MWCNTs/AuE, and at higher magnification of (D) MIP cryogel/f-MWCNTs/AuE before template removal, (E) after template removal, (F) after rebinding of 1.0 μM insulin, (G) the NIP cryogel/f-MWCNTs/AuE, (H) after treatment with removal solution and (I) after rebinding of 1.0 μM insulin.

3.2. Electrochemical behavior of insulin on the MIP cryogel/f-MWCNTs/AuE

Insulin consists of 51 amino acids, including tyrosine, with electroactive properties that have been reported to enable the electrochemical oxidation of insulin [18–20] (Supplementary data Fig. S3A). The electrochemical characteristics of 1.0 μM insulin were investigated before and after removal of the insulin template. CV and SWV were performed in phosphate buffer at pH 5.30, using a flow rate of 100 $\mu\text{L min}^{-1}$ over the MIP cryogel/f-MWCNTs/AuE. Before template removal, an irreversible oxidation peak of insulin was observed at approximately 0.76 V. The oxidation peak was not present after template removal, but re-appeared after insulin rebinding (Supplementary data Figs. S3B and C). A regeneration step was then performed to remove bound insulin in preparation for the next detection. Six binding-regeneration cycles were performed with 0.20, 0.30, and 0.40 pM insulin solutions to determine the reversibility of insulin oxidation at the MIP cryogel/f-MWCNTs/AuE. The relative standard deviation (%RSD) of the oxidation currents were 7.9%, 3.5%, and 2.9%, respectively (Supplementary data Fig. S3D). These values show a low random error in measurement that is well within the acceptable limit of 21–30% for 0.1–1.0 pM [50] and indicate the reversibility of the reaction at the electrode and therefore the high possibility of reuse.

3.3. Optimization of experimental conditions

3.3.1. Template removal

The imprinting of specific cavities requires the template to be removed without changing the structure of the polymer. Six solvents were investigated to identify the solvent that most effectively removed the insulin template from the MIP: SDS-acetic acid (SDS-AcOH), HCl, SDS-HCl, HCl-H₂O₂, AcOH, and AcOH-ethanol at 9:1 (v/v). After an incubation period of 4 h, the MIP cryogel/f-MWCNTs/AuEs were used to determine insulin standards by SWV in 1.0 mM phosphate buffer solution at pH 5.30, using a flow rate of 100 $\mu\text{L min}^{-1}$. Only the electrode that was prepared with AcOH-ethanol did not produce an oxidation response of insulin (Supplementary data Fig. S4A). This is likely because AcOH and ethanol work together to denature insulin by lowering pH and disrupting intramolecular bonding [47,51]. Therefore, only AcOH-ethanol completely removed the template molecule. The removal time was then optimized for AcOH-ethanol. The template molecules were completely removed after 2 h, indicated by the absence of an oxidation current. SEM observation confirmed that the polymer structure was preserved (Supplementary data Figs. S4B and C). The template was therefore removed from the MIP with a 9:1 (v/v) mixture of AcOH-ethanol for 2 h.

3.3.2. Amount of f-MWCNTs

The AuE was modified with f-MWCNTs to increase conductivity and obtain more imprinted cavities [26]. The oxidation potential of 1.0 μM insulin was less positive on the MIP cryogel/f-MWCNTs/AuE (0.76 V) than on the MIP cryogel/AuE (0.81 V) (Supplementary data Fig. S5A). This result indicated the superior electrocatalytic activity of the f-MWCNTs towards insulin [26]. The effect of the loading of f-MWCNTs on insulin detection was studied at 0.00 mg mL^{-1} , 1.00 mg mL^{-1} , 1.50 mg mL^{-1} , 2.00 mg mL^{-1} , and 2.50 mg mL^{-1} . Increments of f-MWCNTs provided a larger surface area (Supplementary data Fig. S5B and Table S1) for the deposition of the MIP cryogel layer, and thus more area of MIP. Because the MIP layer is non-conductive, increases in the area of MIP were indicated by increases in the R_{ct} of the system. The R_{ct} value increased from $19 \pm 5 \Omega$ at an f-MWCNTs loading of 0.00 mg mL^{-1} to $190 \pm 4 \Omega$ at a loading of 2.50 mg mL^{-1} (Supplementary data Fig. S5C).

The f-MWCNTs loading was then optimized by testing the rebinding of insulin. The sensitivity of insulin detection increased with increments of f-MWCNTs loading up to 2.00 mg mL^{-1} and decreased at 2.50 mg mL^{-1} (Supplementary data Fig. S5D). This decrease likely occurred because in this condition the MIP cryogel layer had adsorbed a large amount of insulin template that could not be completely removed in 2 h. As can be seen from EIS spectra produced in 5.0 mM $[\text{Fe}(\text{CN})_6]^{4-/3-}$, up to 5 h was required to completely remove the template (Supplementary data Fig. S5E). Hence, a loading of 2.00 mg mL^{-1} f-MWCNTs was selected for further experiments because it provided high sensitivity with a shorter template removal time.

3.3.3. Type of regeneration solution

In the flow system, the binding and regenerating cycles had to run continuously. The efficiency of the regeneration solution was evaluated from the current response after rebound insulin was removed. Five solutions were tested for their regeneration capability: HCl, AcOH, 10% SDS in 10% AcOH, 10% SDS in 10% acrylic acid, and 10% SDS in 20% acrylic acid. The combinations of SDS-AcOH and SDS-acrylic acid had significant effects. These two combinations were effective probably because the pH of the mixtures was much lower than the pI of insulin. This would disrupt the binding and the interaction between SDS and insulin would further help to denature insulin [51,52]. The 10% SDS in 20% acrylic acid solution completely removed insulin in 10 min (Supplementary data Fig. S6A) and was chosen for further study.

3.3.4. pH of buffer solution

The interaction between insulin and the imprinted cavities could be affected by the pH of supporting electrolyte. The detection of insulin was investigated using 1.0 mM phosphate buffer at pH 4.00–6.00. The highest sensitivity was obtained at pH 5.30 (Supplementary data Fig. S6B), where insulin exists in a neutral condition (pI 5.30–5.35) [53] that maintains its structural stability. It is possible that at a lower or higher pH, protonated/deprotonated insulin existed as charged molecules and electrostatic repulsion between insulin and the functional groups of the imprinted cavities inhibited rebinding and hence sensitivity. On the other hand, in a buffer at pH 5.30, neutral insulin will be adsorbed onto the electrode surface via hydrogen bonding (Fig. 3). Similar to the bonding that was proposed for ovalbumin by Dan R et al. [41], a stable form was favorable for rebinding due to the better interaction between protein and imprinted cavities. Therefore, phosphate buffer at pH 5.30 was selected as the supporting electrolyte for insulin detection.

3.3.5. Flow rate

Flow rate is an important parameter because it determines the duration of binding between insulin and imprinted cavities. The effects of flow rates of 50, 100, 150, and 200 $\mu\text{L min}^{-1}$ were studied, where the sensitivity of insulin detection indicated the optimum insulin binding. As expected, sensitivity decreased with increased flow rate (Supplementary data Fig. S6C) due to the shorter contact time [54]. The highest

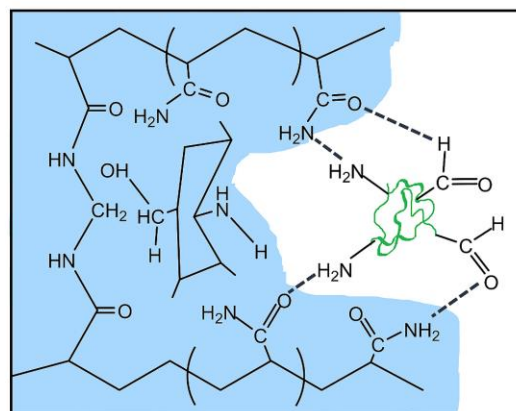


Fig. 3. The proposed mechanism for the hydrogen bonding of insulin on the MIP cryogel/f-MWCNTs/AuE [41].

sensitivity was obtained at a flow rate of 50 $\mu\text{L min}^{-1}$, but the analysis time (insulin detection cycle in Fig. 1B) was the longest at 70 min. Therefore, the flow rate of 100 $\mu\text{L min}^{-1}$ was chosen for further measurement because it still provided a high sensitivity but with a shorter analysis time of 55 min.

3.4. Analytical performances

3.4.1. Linear range and limit of detection (LOD)

The linear range and LOD of the MIP cryogel/f-MWCNTs/AuE toward insulin were determined by SWV in the optimal condition. The performances of an MIP non-cryogel sensor and an NIP cryogel sensor were investigated for comparison. Square wave voltammograms showed that the MIP cryogel sensor produced the best current response (Fig. 4A). The sensitivity of the MIP cryogel system was much higher than the sensitivity of the MIP non-cryogel sensor (Fig. 4B), due to its porous structure, which allowed greater mass transfer of insulin to imprinted cavities. Although the NIP sensor had no insulin imprinted sites, it also produced a linear response, but with a much lower sensitivity. The most likely explanation for the response at the NIP sensor is nonspecific insulin binding. Since insulin is electro-active, a current was produced. Although non-specific binding will affect the sensor, this effect can be removed by washing the sensor longer (see Section 3.5).

The MIP cryogel sensor had a linear range between 0.050 and 1.40 μM and its LOD ($3SD/s$) was 33 fM , where SD is the standard deviation of the intercept and s is the slope of linear regression [55]. These values are more than sufficient for the detection of insulin in human serum in the normal range (12–150 pM) [30].

3.4.2. Binding isotherm

The binding affinity of insulin to the MIP and NIP cryogel sensors was investigated from 0.050 to 3.00 pM , using SWV, and was evaluated using the Langmuir isotherm curve. The dissociation constant (K_D) of the Langmuir isotherm model [56] was calculated using equation (1).

$$I_F = \frac{I_{\max}[F]}{K_D + [F]} \quad [1]$$

where I_F is the current response with the bound insulin, F is the concentration of the insulin (M), I_{\max} is the maximum current response when insulin binding sites are saturated, and K_D is the dissociation constant. The K_D values of the MIP and NIP cryogel sensors were determined based on the slopes of the linear regions of the respective

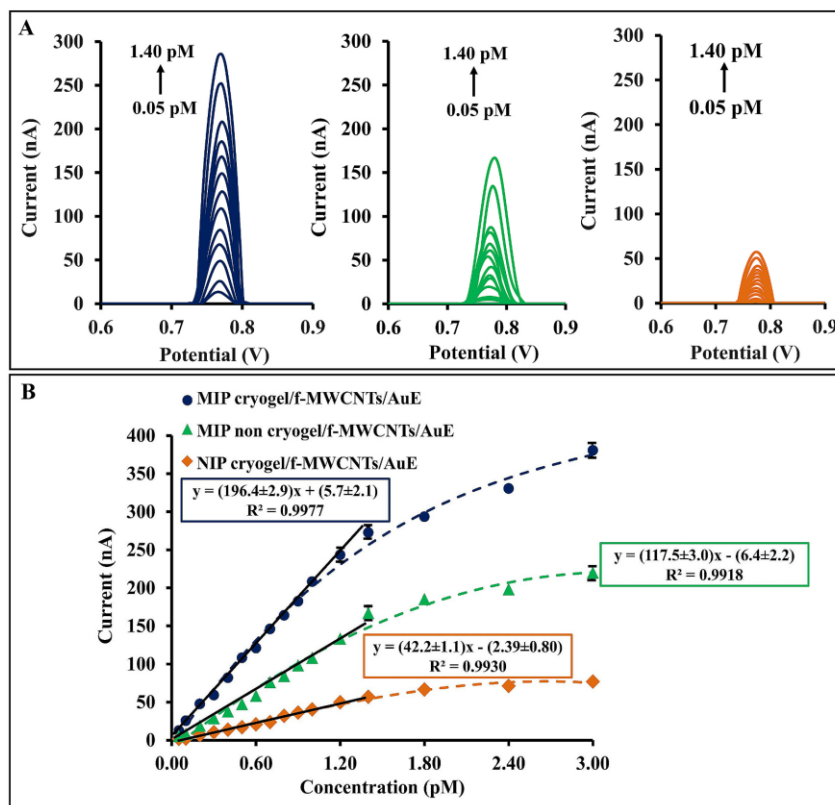


Fig. 4. (A) Square wave voltammograms of (blue line) MIP cryogel sensor, (green line) MIP non-cryogel sensor and (orange line) NIP cryogel sensor from 0.050 to 1.40 pM insulin in 1.0 mM phosphate buffer at pH 5.30. The flow injection condition was a sample loop of 500 μL and a flow rate of 100 $\mu\text{L min}^{-1}$. (B) The current response of the MIP cryogel sensor, MIP non-cryogel sensor, and NIP cryogel sensor towards 0.010–3.00 pM insulin in 1.0 mM phosphate buffer at pH 5.30 in the same operational condition as (A).

curves of $1/I_p$ versus $1/[F]$ (Supplementary data Fig. S7A). The values were $2.78 \pm 0.06 \times 10^{-12}$ M and $8.27 \pm 0.65 \times 10^{-12}$ M, respectively. These values were close to those from graph-fitting by GraphPad Prism 8 software, which were $2.70 \pm 0.10 \times 10^{-12}$ M and $10.6 \pm 1.2 \times 10^{-12}$ M for MIP and NIP, respectively (Supplementary data Fig. S7B). For the MIP cryogel sensor, the coefficient of determination was 0.9910, indicating that the MIP cryogel sensor had a higher affinity for binding to insulin than the NIP cryogel sensor. The best known bioreceptors, such as the streptavidin-biotin pair, the barnase-barstar pair [57] and the antigen-antibody IgG complex [58] produce K_D values of 10^{-14} M, 10^{-14} M, and 10^{-8} – 10^{-10} M. Therefore, the proposed electrode exhibited a relatively high binding affinity to insulin, better than that of the antigen-antibody IgG complex.

3.4.3. Selectivity

To evaluate selectivity, the MIP sensor was used to determine typical interferences in human serum at normal levels. These included 6.0 mM glucose, 0.50 mM uric acid (UA), 80.0 μM creatinine, 0.50 μM dopamine (DA), 85.0 μM ascorbic acid (AA), 7.25 μM human serum albumin (HSA), 7.25 nM carcinoembryonic antigen (CEA) and 7.25 nM alpha-fetoprotein (AFP). The current response of all interferences was very much lower than that of 0.80 pM insulin (Fig. 5A). Moreover, the current responses of these interferences mixed with 0.80 pM of insulin were not

significantly different ($P > 0.05$ two-way ANOVA) from those of insulin alone. These results showed that the sensor is highly selective for insulin.

At much higher concentrations of AA, UA, and DA, current responses remained relatively small, similar to that of the LOD of insulin (33 fM) (Fig. 5B). As a result, their presence should not interfere with insulin measurement by the proposed sensor. The responses of binary mixtures at the higher concentrations were also not significantly different from those of the very low concentration (0.050 pM) of insulin alone. The high selectivity of the modified electrode is most likely due to the morphological complementarity of the imprinted cavities and insulin molecules, and the reversibility of the non-covalent binding between the functional monomers and insulin. The proposed flow system also plays a key role by removing matrix compounds present in the solution during the insulin rebinding step.

3.4.4. Reproducibility

The reproducibility of the electrode fabrication was evaluated by using six modified electrodes to determine insulin at 0.050, 0.10, 0.20, 0.30, and 0.40 pM. The relative standard deviations (RSDs) of the five concentrations were in the range of 2.90–7.83% while the sensitivities of the six electrodes were 195 ± 3 , 200 ± 5 , 190 ± 11 , 199 ± 5 , 198 ± 8 , 196 ± 4 nA pM^{-1} (Supplementary data Fig. S8A). The RSD values were very much better than the acceptable limit of 32–45% for 0.1–0.050 pM

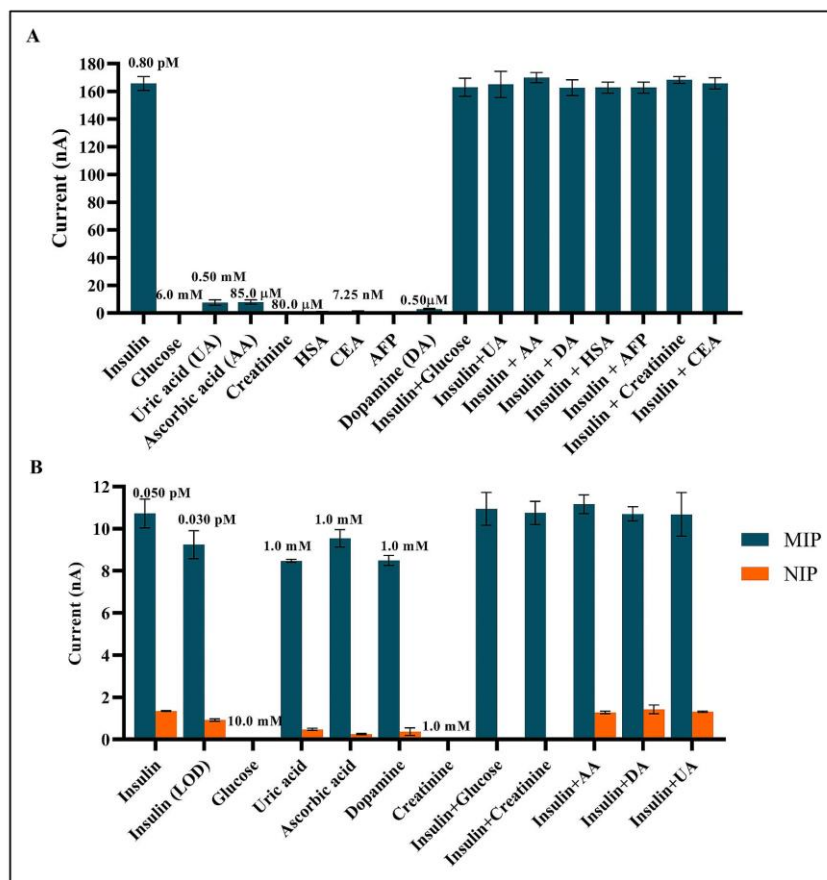


Fig. 5. (A) Shows the current responses of interferences at normal physiological levels and binary mixtures with 0.80 pM insulin in phosphate buffer solution at pH 5.30. (B) Shows the current responses of electro-active interferences (10.0 mM glucose, 1.0 mM uric acid (UA), 1.0 mM ascorbic acid (AA), 1.0 mM dopamine (DA), and 1.0 mM creatinine) and binary mixture with 0.050 pM insulin in 1.0 M phosphate buffer pH 5.30. The operating condition was a sample loop of 500 μ L and a flow rate of 100 μ L min^{-1} .

[50]. These findings demonstrated that the modified electrode preparation procedure was highly reproducible for insulin detection.

3.4.5. Stability of the MIP-modified electrode

The operational stability of the MIP cryogel sensor was investigated by continuously measuring the current response of 0.80 pM insulin in the optimal condition. The sensor was stable for up to 46 detections with a relative average response of $99.1 \pm 1.4\%$ (Supplementary data Fig. S8B), after which the response decreased to below 90%. This was most likely due to the loss of the MIP cryogel layer from the electrode surface, which was confirmed by the increase in redox peak height seen in the CV of the modified electrode evaluated after the operational stability test.

The stability of the modified electrodes was also tested after 0, 1, 3, 8, 9, 10, and 11 weeks of dry storage. The electrode retained more than 90% of its original sensitivity for 10 weeks (Supplementary data Fig. S8C). Furthermore, a single modified electrode exhibited long-term stability for 4 weeks of dry storage, retaining more than 90% of its original sensitivity after repeated weekly use (Supplementary data Fig. S8D). This result demonstrated the robustness of the modified

electrode. The stability of the electrode was most likely due to the f-MWCNTs platform which enabled an even distribution of MIP cryogel. Compared to antibody and aptamer receptors [12,59], the proposed electrode exhibited much greater stability and is easier to handle because it can be stored dry at room temperature.

3.4.6. Comparison to other sensors

The analytical performances of this sensor were compared with performances of other insulin sensors. The developed MIP sensor exhibited a lower limit of detection (33 fM) than most of the other sensors (Table 1), and although the linear range was not as wide, it was more than sufficient for the direct detection of insulin in human serum samples with as much as 250 times dilution (Section 3.5). This sensor offers a significant advantage in terms of stability because, unlike other sensors, special storage is not required. In dry storage at room temperature, this sensor can keep its stability for up to ten weeks. Furthermore, it is reusable for up to 46 cycles, making it useful in real-time sample analysis. Another advantage of the sensor is its high affinity for insulin binding, as demonstrated by the low K_D value.

Table 1
A comparison of the performances of sensors for insulin detection.

Sensor	Detection method	Linear range (pM)	LOD (fM)	K_D (mol L ⁻¹)	Selectivity	Stability	Ref.
EMMIPs	DPV (Fe (CN) ₆) ^{3-/4-}	10–1000	3000	NR	BSA, BHB, HRP, AA, DA, GSH, Na ⁺ , K ⁺ , Mg ²⁺ , Ca ²⁺ , Cl ⁻ , HCO ₃ ⁻	20 days* (stored at 4 °C)	[39]
Epitope imprinting	DPV (Fe (CN) ₆) ^{3-/4-}	0.010–0.50	7.24	NR	L-tryptophan, hlg, BSA, L-proline	2 weeks* (stored at 4 °C)	[40]
Insulin MIP QCM	QCM	1.38–1720	270	6.3×10^{-10}	NR	3 months (stored at 4 °C)	[60]
NanoMIP/SPPE	DPV (Ferrocene)	50–2000	81	0.9×10^{-9}	Hb, HSA, HPC	168 days (stored at 4 °C)	[61]
Immunosensor	DPV	1.72×10^{-2} –8608	0.043	NR	PSA, HBSAg, CEA, HSA	2 weeks* (stored at 4 °C)	[59]
Aptasensor	EIS	500–10000	106.8×10^3	NR	L-cysteine, AA, UA, BSA	1 week* (stored at 4 °C)	[12]
MIP cryogel/f-MWCNTs/AuE	SWV	0.050–1.40	33	2.6×10^{-12}	HSA, CEA, AFP, glucose, creatinine, UA, AA, DA	Operational stability for 46 times and 10 weeks (stored at room temperature)	This work

EMMIPs: electromagnetic molecularly imprinted polymers; QCM: quartz crystal microbalance; NanoMIP: molecularly imprinted polymer nanoparticles; SPPE: screen printed platinum electrode; DPV: differential pulse voltammetry; EIS: electrochemical impedance spectroscopy; SWV: square wave voltammetry; K_D : equilibrium dissociation constant; NR: not reported; *: no further experiment.

3.5. Analysis of blood serum samples

The developed sensing system was applied to detect insulin in human serum samples. Type 1 diabetes is caused by the auto-immune destruction of insulin-producing pancreatic β -cells, which leads to the loss of insulin production. Over time, insulin production may decrease by 76% from the normal level (12–150 pM) [30,62]. Since the linear range of this system is 0.050–1.40 pM, a sample dilution of 40 times should be applied to ensure that the lowest insulin level will fall within the linear range. In type 2 diabetes, insulin levels may appear normal or elevated because blood glucose levels cannot be normalized due to insulin resistance [2]. To test for type 2 diabetes and normal insulin levels, a 250-times dilution should be applied. Before analyzing real samples, the effect of the serum matrix was studied by comparing the calibration plots of insulin standards (0.050–0.40 pM) and spiked sample solutions. At 250 times dilution, no matrix effect was observed; a result confirmed by two-way ANOVA ($P > 0.05$). At 40 times dilution, the matrix effect was observed initially, but after a longer washing time of 10 min, rather than the normal 3 min, the spiked samples showed no significant difference to the standard insulin ($P > 0.05$ two-way ANOVA). The accuracy of the sensor was evaluated from recoveries of spiked insulin at 40- and 250-times dilutions. Recoveries were in the range of $90 \pm 10\%$ – $111 \pm 3\%$ (Supplementary data Table S2). Since the acceptable recommended recovery is 40–120% [50], the sensor could be considered accurate for real sample analysis.

Since there was no matrix effect after dilution, the insulin concentration could be calculated from the standard solution calibration equation and then multiplied by the appropriate dilution factor to obtain the concentration in a human serum sample. Samples were first tested with 250 times dilution. If the response was out of the range, a 40-times dilution was used. Fig. 6 shows the comparison between insulin concentrations obtained from the proposed sensor and the Elecsys insulin assay used in the hospital. The insulin concentrations from both methods were compared using the paired Student's t-test (two-tailed). The Student's t-test revealed that there is no statistically significant difference between the proposed sensor and the Elecsys insulin assay ($t = -0.872$, $p = 0.406$). The results indicated that seven samples showed levels likely to be found within the normal range while three samples were likely from type 2 diabetic patients based on typical insulin levels (>150 pM) [30,62].

4. Conclusions

An MIP cryogel/f-MWCNTs/AuE incorporated with a flow system for insulin detection was successfully developed. This sensor was able to

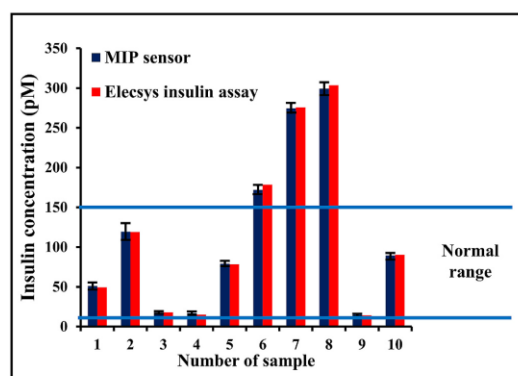


Fig. 6. Insulin was determined in human serum samples using the proposed sensor and the Elecsys insulin assay used by the hospital.

perform the direct detection of insulin with high selectivity over a wide range of interferences and provided high operational and storage stability. A low limit of detection and very good recoveries were achieved that showed the potential of the developed system for the quantification of insulin in human serum from type 1 and type 2 diabetic patients. This sensor has a very satisfactory reusability (46 times), which will lead to further research into the reusability of the sensor with real samples. Since the matrix of various real samples can diversely affect reusability, further flow system optimization may be required.

Credit author statement

Nur Indah Wardani: Conceptualization, Formal analysis, Writing – original draft. **Tawatchai Kangkamano:** Conceptualization, Validation, Formal analysis. **Rodtichoti Wannapob:** Conceptualization, Validation, Formal analysis. **Proespichaya Kanatharana:** Validation, Formal analysis. **Panote Thavarungkul:** Conceptualization, Writing – review & editing, Formal analysis, Supervision. **Warakorn Limbut:** Conceptualization, Writing – review & editing, Formal analysis, Supervision.

Declaration of competing interest

The authors declare that they have no known competing financial interests or personal relationships that could have appeared to influence

the work reported in this paper.

Data availability

Data will be made available on request.

Acknowledgements

This work was supported by a grant from The Thailand Research Fund (TRF: BRG6080009). We would like to thank the Center of Excellence for Trace Analysis and Biosensor at Prince of Songkla University. Financial support for Nur Indah Wardani, in the form of a scholarship from the Thailand's Education Hub for Southern Region of ASEAN Countries (TEH-AC 109/2016), is also gratefully acknowledged. The authors would like to thank Thomas Duncan Coyne, Faculty of Science, Prince of Songkla University, Hat Yai, Songkhla, for proof-reading the manuscript.

Appendix A. Supplementary data

Supplementary data to this article can be found online at <https://doi.org/10.1016/j.talanta.2022.124137>.

References

- M. Jim, T. Stewart, *Essentials of Human Nutrition*, fourth ed., Oxford University Press Inc., New York, United States, 2012. Fourth edition ed.
- A. Amer, Diabet, diagnosis and classification of diabetes mellitus, *Diabetes Care* 37 (2014) S81–S90.
- A. Amer, Diabet, classification and diagnosis of diabetes: standards of medical care in diabetes-2018, *Diabetes Care* 41 (2018) S13–S27.
- R. Soffe, V. Nock, J.G. Chase, Towards point-of-care insulin detection, *ACS Sens.* 4 (1) (2019) 3–19.
- F. Poulsen, K.B. Jensen, A luminescent oxygen channeling immunoassay for the determination of insulin in human plasma, *J. Biomol. Screen* 12 (2) (2007) 240–247.
- M. Mecklenburg, C. Lindbladh, H. Li, K. Mosbach, B. Danielsson, Enzymatic amplification of a flow-injected thermometric enzyme-linked immunoassay for human insulin, *Anal. Biochem.* 212 (2) (1993) 388–393.
- C. Lei, C. Xu, O. Noonan, A.K. Meka, L. Zhang, A. Nouwens, C. Yu, Mesoporous materials modified by aptamers and hydrophobic groups assist ultra-sensitive insulin detection in serum, *Chem. Commun.* 51 (71) (2015) 13642–13645.
- H. Henry, D. Lannoy, N. Simon, D. Seguy, M. D'Herbomez, C. Barthélémy, B. Décaudin, T. Dine, P. Odou, Immunoassay quantification of human insulin added to ternary parenteral nutrition containers: comparison of two methods, *Anal. Bioanal. Chem.* 409 (14) (2017) 3677–3684.
- Z.H. Chen, M.P. Caulfield, M.J. McPhaul, R.E. Reitz, S.W. Taylor, N.J. Clarke, Quantitative insulin analysis using liquid chromatography-tandem mass spectrometry in a high-throughput clinical laboratory, *Clin. Chem.* 59 (9) (2013) 1349–1356.
- A. Thomas, P.T. Brinkkotter, W. Schanzer, M. Thevis, Simultaneous determination of insulin, DesB30 insulin, proinsulin, and C-peptide in human plasma samples by liquid chromatography coupled to high resolution mass spectrometry, *Forensic Toxicol.* 35 (1) (2017) 106–113.
- S.Q. Dong, Y. Gu, G.L. Wei, D.Y. Si, C.X. Liu, Direct comparison of LC-MS/MS and RIA methods for the pharmacokinetics assessment of human insulin in preclinical development, *Biomed. Chromatogr.* 32 (11) (2018) 8.
- F. Abazar, A. Noorbakhsh, Chitosan-carbon quantum dots as a new platform for highly sensitive insulin impedimetric aptasensor, *Sens. Actuator B-Chem.* 304 (2020) 7.
- Y. Wu, B. Midinow, R.J. White, Electrochemical aptamer-based sensor for real-time monitoring of insulin, *ACS Sens.* 4 (2) (2019) 498–503.
- I. Sisolakova, J. Hovancova, R. Orinakova, A. Orinak, L. Trnkova, D.R. Garcia, J. Radonak, Influence of a polymer membrane on the electrochemical determination of insulin in nanomodified screen printed carbon electrodes, *Bioelectrochemistry* 130 (2019) 11.
- M. Taib, L.L. Tan, N.H. Abd Karim, G.C. Ta, L.Y. Heng, B. Khalid, Reflectance aptasensor based on metal salphen label for rapid and facile determination of insulin, *Talanta* 207 (2020) 9.
- S. Tan, R. Han, S.L. Wu, H. Liang, Y.T. Zhao, H. Zhao, C.P. Li, A novel fluorescent sensing platform for insulin detection based on competitive recognition of cationic pillar 6 arene, *Talanta* 197 (2019) 130–137.
- S.K. Arya, S.P. Singh, B.D. Malhotra, *Electrochemical Techniques in Biosensors, Handbook of Biosensors and Biochips* 2007.
- T.S.A.A.J.B. Marian, The electrochemistry of proteins and related substances: Part II. Insulin, *J. Electroanal. Chem. Interfacial Electrochem.* 85 (1) (1977) 173–183.
- J.J. Berzas Nevado, J. Rodriguez Flores, G. Castañeda Peñalvo, Adsorptive stripping square-wave voltammetric behavior of insulin, *Fresen. J. Anal. Chem.* 364 (8) (1999) 753–757.
- W. Zong, R. Liu, F. Sun, M. Wang, P. Zhang, Y. Liu, Y. Tian, Cyclic voltammetry: a new strategy for the evaluation of oxidative damage to bovine insulin, *Protein Sci.* 19 (2) (2010) 263–268.
- E. Habibi, E. Omidinia, H. Heidari, M. Fazli, Flow injection amperometric detection of insulin at cobalt hydroxide nanoparticles modified carbon ceramic electrode, *Anal. Biochem.* 495 (2016) 37–41.
- Y. Yu, M. Guo, M. Yuan, W. Liu, J. Hu, Nickel nanoparticle-modified electrode for ultra-sensitive electrochemical detection of insulin, *Biosens. Bioelectron.* 77 (2016) 215–219.
- H. Belkhalifa, F. Teodorescu, G. Queniat, Y. Coffinier, N. Dokhan, S. Sam, A. Abderrahmani, R. Boukherroub, S. Szunerits, Insulin impregnated reduced graphene oxide/Ni(OH)₂ thin films for electrochemical insulin release and glucose sensing, *Sens. Actuator B-Chem.* 237 (2016) 693–701.
- J. Wang, T. Tangkuaram, S. Loyprasert, T. Vazquez-Alvarez, W. Veerasai, P. Kanatharana, P. Thavarungkul, Electrochemical detection of insulin at RuO₂/carbon nanotube-modified carbon electrodes, *Anal. Chim. Acta* 581 (1) (2007) 1–6.
- M.G. Zhang, C. Mullens, W. Gorski, Insulin oxidation and determination at carbon electrodes, *Anal. Chem.* 77 (19) (2005) 6396–6401.
- J. Wang, M. Musameh, Electrochemical detection of trace insulin at carbon-nanotube-modified electrodes, *Anal. Chim. Acta* 511 (1) (2004) 33–36.
- I. Šišoláková, J. Hovancová, R. Orínková, A. Orínak, D. Rueda Garcia, O. Shylenko, J. Radonák, Comparison of insulin determination on NiNPs/chitosan-MWCNTs and NiONPs/chitosan-MWCNTs modified pencil graphite electrode, *Electroanalysis* 31 (1) (2019) 103–112.
- E. Martinez-Perinan, M. Revenga-Parra, M. Gennari, F. Pariente, R. Mas-Balleste, F. Zamora, E. Lorenzo, Insulin sensor based on nanoparticle-decorated multiwalled carbon nanotubes modified electrodes, *Sens. Actuator B-Chem.* 222 (2016) 331–338.
- B. Rafiee, A.R. Fakhari, Electrochemical oxidation and determination of insulin at nickel oxide nanoparticles-multiwalled carbon nanotube modified screen printed electrode, *Biosens. Bioelectron.* 46 (2013) 130–135.
- C.A. Burtis, E.R. Ashwood, D.E. Bruns, N.W. Tietz, *Tietz Textbook of Clinical Chemistry and Molecular Diagnostics*, Elsevier/Saunders 2012.
- H.Y. Zhang, C.J. Liu, L. Chen, B. Dai, Control of ice crystal growth and its effect on porous structure of chitosan cryogels, *Chem. Eng. Sci.* 201 (2019) 50–57.
- A. Fatoni, A. Numnuam, P. Kanatharana, W. Limbut, P. Thavarungkul, A novel molecularly imprinted chitosan-acrylamide, graphene, ferrocene composite cryogel biosensor used to detect microalbumin, *Analyst* 139 (23) (2014) 6160–6167.
- S. Aslyuce, L. Uzun, A. Yousefi Rad, S. Unal, R. Say, A. Denizli, Molecular imprinting based composite cryogel membranes for purification of anti-hepatitis B surface antibody by fast protein liquid chromatography, *J. Chromatogr. B* 889–890 (2012) 95–102.
- T. Kangkamoto, A. Numnuam, W. Limbut, P. Kanatharana, P. Thavarungkul, Chitosan cryogel with embedded gold nanoparticles decorated multiwalled carbon nanotubes modified electrode for highly sensitive flow based non-enzymatic glucose sensor, *Sens. Actuator. B Chem.* 246 (2017) 854–863.
- S. Aslyuce, B. Mattiasson, A. Denizli, Combined protein A imprinting and cryogelation for production of spherical affinity material, *Biomed. Chromatogr.* 33 (10) (2019), e4605.
- S. Ramanavicius, A. Ramanavicius, Development of molecularly imprinted polymer based phase boundaries for sensors design (review), *Adv. Colloid Interface Sci.* 305 (2022), 102693.
- V. Ratautaite, R. Boguzaitė, E. Brazys, A. Ramanaviciene, E. Ciplys, M. Juozapaitis, R. Slibinskas, M. Bechelany, A. Ramanavicius, Molecularly imprinted polypyrrole based sensor for the detection of SARS-CoV-2 spike glycoprotein, *Electrochim. Acta* 403 (2022), 139581.
- R. Gui, H. Jin, H. Guo, Z. Wang, Recent advances and future prospects in molecularly imprinted polymers-based electrochemical biosensors, *Biosens. Bioelectron.* 100 (2018) 56–70.
- W.Y. Zhu, L. Xu, C.H. Zhu, B.Z. Li, H. Xiao, H.J. Jiang, X.M. Zhou, Magnetically controlled electrochemical sensing membrane based on multifunctional molecularly imprinted polymers for detection of insulin, *Electrochim. Acta* 218 (2016) 91–100.
- C.J. Zhao, X.H. Ma, J.P. Li, An insulin molecularly imprinted electrochemical sensor based on epitope imprinting, *Chin. J. Anal. Chem.* 45 (9) (2017) 1360–1366.
- R. Dan, Y.Z. Wang, L. Du, S.H. Du, M.D. Huang, S. Yang, M. Zhang, The synthesis of molecular imprinted chitosan-gels copolymerized with multifunctional monomers at three different temperatures and the recognition for the template ovalbumin, *Analyst* 138 (12) (2013) 3433–3443.
- W.R. Zhao, T.F. Kang, L.P. Lu, F.X. Shen, S.Y. Cheng, A novel electrochemical sensor based on gold nanoparticles and molecularly imprinted polymer with binary functional monomers for sensitive detection of bisphenol A, *J. Electroanal. Chem.* 786 (2017) 102–111.
- C. Yang, Y. Zhang, W.Q. Cao, X.F. Ji, J. Wang, Y.N. Yan, T.L. Zhong, Y. Wang, Synthesis of molecularly imprinted cryogels to deplete abundant proteins from bovine serum, *Polymers* 10 (1) (2018) 11.
- A. Fatoni, A. Numnuam, P. Kanatharana, W. Limbut, P. Thavarungkul, A novel molecularly imprinted chitosan-acrylamide, graphene, ferrocene composite cryogel biosensor used to detect microalbumin, *Analyst* 139 (23) (2014) 6160–6167.

- [45] K. Toth, K. Stulik, W. Kutner, Z. Feher, E. Lindner, Electrochemical detection in liquid flow analytical techniques: characterization and classification - (IUPAC Technical Report), *Pure Appl. Chem.* 76 (6) (2004) 1119–1138.
- [46] A.C.B. Dias, E.C. Figueiredo, V. Grassi, E.A.G. Zagatto, M.A.Z. Arruda, Molecularly imprinted polymer as a solid phase extractor in flow analysis, *Talanta* 76 (5) (2008) 988–996.
- [47] J. Erdőssy, V. Horváth, A. Yarman, F.W. Scheller, R.E. Gyurcsányi, Electro-synthesized molecularly imprinted polymers for protein recognition, *TrAC, Trends Anal. Chem.* 79 (2016) 179–190.
- [48] D.R. Thevenot, K. Toth, R.A. Durst, G.S. Wilson, Electrochemical biosensors: recommended definitions and classification, *Biosens. Bioelectron.* 16 (1–2) (2001) 121–131.
- [49] J.S. Daniels, N. Pourmand, Label-free impedance biosensors: opportunities and challenges, *Electroanalysis* 19 (12) (2007) 1239–1257.
- [50] I. Taverniers, M. De Loose, E. Van Bockstaele, Trends in quality in the analytical laboratory. II. Analytical method validation and quality assurance, *TrAC, Trends Anal. Chem.* 23 (8) (2004) 535–552.
- [51] D.M. Hawkins, D. Stevenson, S.M. Reddy, Investigation of protein imprinting in hydrogel-based molecularly imprinted polymers (HydroMIPs), *Anal. Chim. Acta* 542 (1) (2005) 61–65.
- [52] Z. Jie, H. Xiwen, Study of the nature of recognition in molecularly imprinted polymer selective for 2-aminopyridine, *Anal. Chim. Acta* 381 (1) (1999) 85–91.
- [53] J. Gao, M. Mrksich, F.A. Gomez, G.M. Whitesides, Using capillary electrophoresis to follow the acetylation of the amino groups of insulin and to estimate their basicities, *Anal. Chem.* 67 (18) (1995) 3093–3100.
- [54] K. Promsuwan, P. Thayarungkul, P. Kanatharana, W. Limbut, Flow injection amperometric nitrite sensor based on silver microcubics-poly (acrylic acid)/poly (vinyl alcohol) modified screen printed carbon electrode, *Electrochim. Acta* 232 (2017) 357–369.
- [55] A. Shrivastava, V.B. Gupta, Methods for the determination of limit of detection and limit of quantitation of the analytical methods, *Chronicles Young Sci.* 2 (2011) 21–25.
- [56] R.J. Ansell, Characterization of the binding properties of molecularly imprinted polymers, in: B. Mattiasson, L. Ye (Eds.), *Molecularly Imprinted Polymers in Biotechnology*, Springer Int Publishing Ag, Cham, 2015, pp. 51–93.
- [57] T. Wang, S. Tomic, R.R. Gabdouliline, R.C. Wade, How optimal are the binding energetics of barnase and barstar? *Biophys. J.* 87 (3) (2004) 1618–1630.
- [58] H.F. El-Sharif, D.M. Hawkins, D. Stevenson, S.M. Reddy, Determination of protein binding affinities within hydrogel-based molecularly imprinted polymers (HydroMIPs), *Phys. Chem. Chem. Phys.* 16 (29) (2014) 15483–15489.
- [59] Y.Y. Li, L.H. Tian, L. Liu, M.S. Khan, G.H. Zhao, D.W. Fan, W. Cao, Q. Wei, Dual-responsive electrochemical immunosensor for detection of insulin based on dual-functional zinc silicate spheres-palladium nanoparticles, *Talanta* 179 (2018) 420–425.
- [60] F. Kartal, D. Cimen, N. Bereli, A. Denizli, Molecularly imprinted polymer based quartz crystal microbalance sensor for the clinical detection of insulin, *Mater. Sci. Eng. C-Mater. Biol. Appl.* 97 (2019) 730–737.
- [61] A.G. Cruz, I. Haq, T. Cowen, S. Di Masi, S. Trivedi, K. Alanazi, E. Piletska, A. Mujahid, S.A. Piletsky, Design and fabrication of a smart sensor using in silico epitope mapping and electro-responsive imprinted polymer nanoparticles for determination of insulin levels in human plasma, *Biosens. Bioelectron.* 169 (2020) 7.
- [62] C. Steele, W.A. Hagopian, S. Gitelman, U. Masharani, M. Cavaghan, K.I. Rother, D. Donaldson, D.M. Harlan, J. Bluestone, K.C. Herold, Insulin secretion in type 1 diabetes, *Diabetes* 53 (2) (2004) 426–433.

Supplementary Data

Electrochemical Sensor Based on Molecularly Imprinted Polymer Cryogel and Multiwalled Carbon Nanotubes for Direct Insulin Detection

Nur Indah Wardani^{a,b,c}, Tawatchai Kangkamano^{a,b,c,d}, Rodtichoti Wannapob^{a,b,c}, Proespichaya Kanatharana^{a,b,c}, Panote Thavarungkul^{a,b,c}, and Warakorn Limbut^{a,b,e,*}

^a*Center of Excellence for Trace Analysis and Biosensor, Prince of Songkla University, Hat Yai, Songkhla, 90110, Thailand*

^b*Center of Excellence for Innovation in Chemistry, Faculty of Science, Prince of Songkla University, Hat Yai, Songkhla 90110, Thailand*

^c*Division of Physical Science, Faculty of Science, Prince of Songkla University, Hat Yai, Songkhla 90110, Thailand*

^d*Department of Chemistry, Faculty of Science, Thaksin University (Phatthalung Campus), Papayom, Phatthalung, 93110, Thailand*

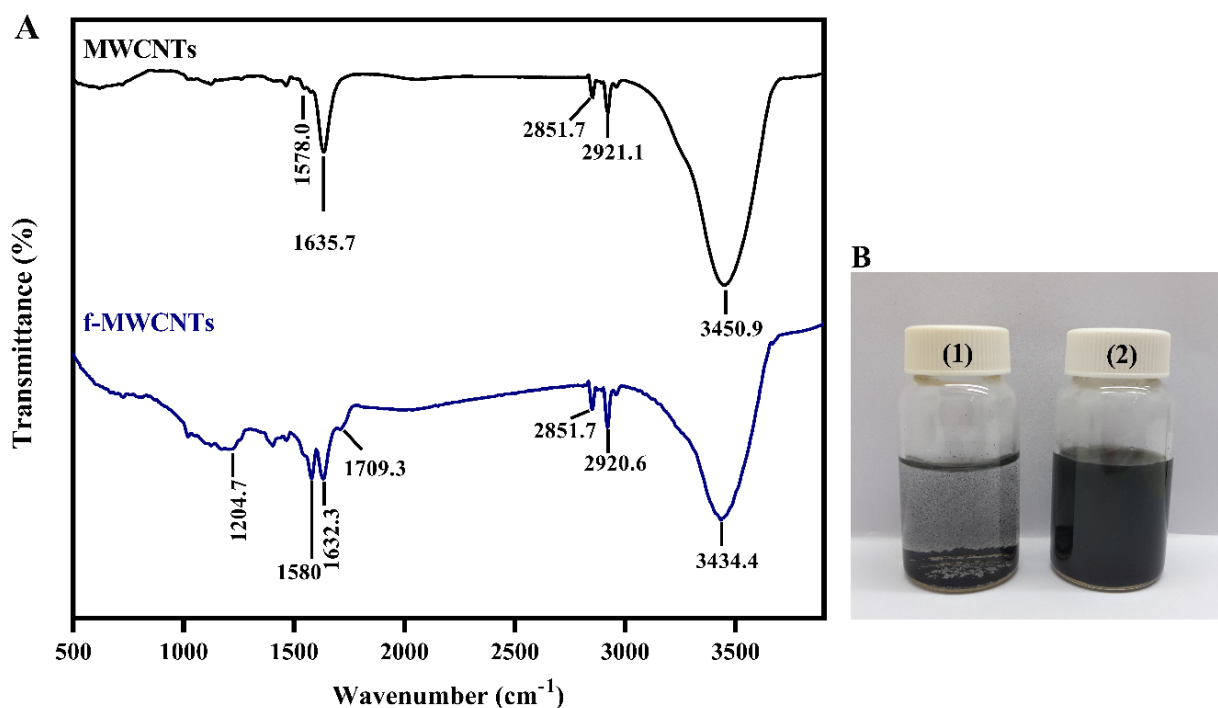
^e*Division of Health and Applied Sciences, Faculty of Science, Prince of Songkla University, Hat Yai, Songkhla, 90110, Thailand*

* *Corresponding author at: Division of Health and Applied Sciences, Faculty of Science, Prince of Songkla University, Hat Yai, Songkhla 90110, Thailand.*

E-mail address: warakorn.l@psu.ac.th (W. Limbut).

S1. Fourier transform infrared (FT-IR) spectroscopy of carboxylated MWCNTs (f-MWCNTs)

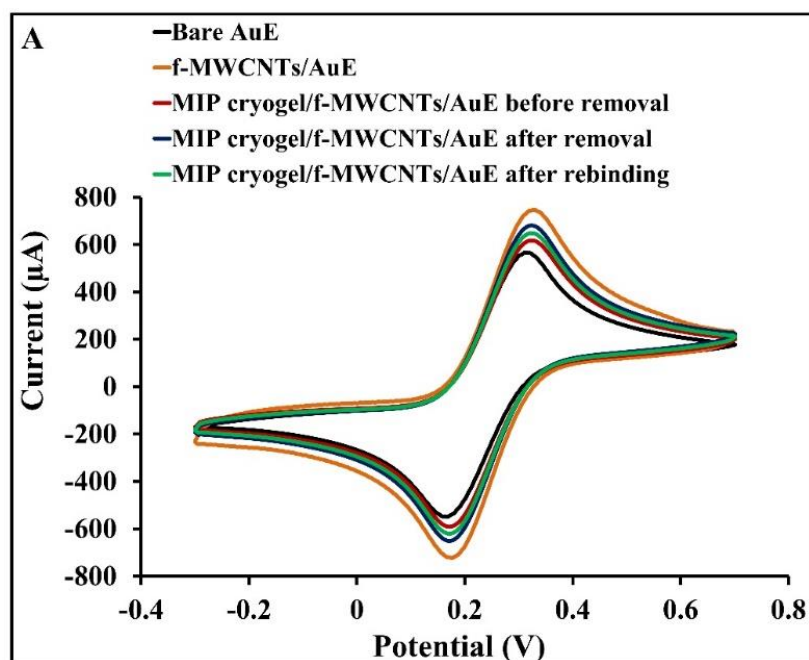
Fig. S1(A) shows the FT-IR spectra of MWCNTs and f-MWCNTs. The MWCNTs spectrum displayed O-H stretching band at 3450.9 cm^{-1} and CH_2 stretching vibration at 2921.1 and 2851.7 cm^{-1} . The bands at 1638.16 cm^{-1} and 1636.22 cm^{-1} were assigned to C=C stretching vibrations of the aromatic rings. After functionalization of the MWCNTs, bands corresponding to C=O and C-O in the carboxylic group were observed at 1709.3 cm^{-1} and 1204.7 cm^{-1} , respectively (Entezari et al., 2014; Shao et al., 2022). This confirmed the presence of carboxylic groups on the surface of f-MWCNTs. Furthermore, the f-MWCNTs dispersed more completely (**Fig. S1B**), which is advantageous for further modification by improving drop-casting uniformity and stability on the gold electrode (AuE) surface.

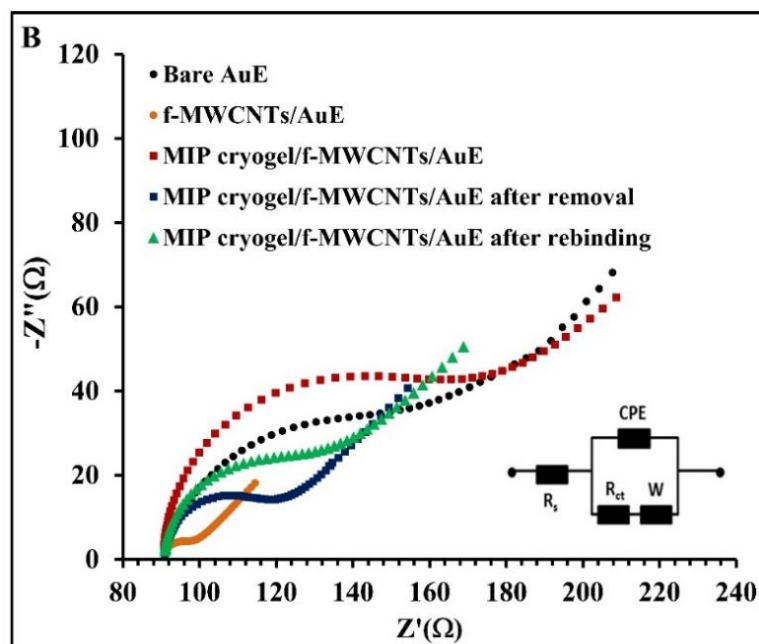


Supplementary data Fig. S1 (A) FT-IR spectra and (B) photo images of (1) MWCNTs and (2) f-MWCNTs in DI water.

S2. Electrochemical characterization of modified electrode

The bare AuE, f-MWCNTs/AuE, MIP cryogel/f-MWCNTs/AuE before template removal, MIP cryogel/f-MWCNTs/AuE after template removal and MIP cryogel/f-MWCNTs/AuE after rebinding were characterized electrochemically by cyclic voltammetry and electrochemical impedance spectroscopy using a redox probe of 5.0 mM $[\text{Fe}(\text{CN})_6]^{4-/3-}$. The effect of each step of modification can be seen in the change of redox peaks in **Fig. S2A**. EIS produced similar results (**Fig. S2B**), Changes in charge transfer resistance (R_{ct}) after each step of modification were displayed in Nyquist plots.

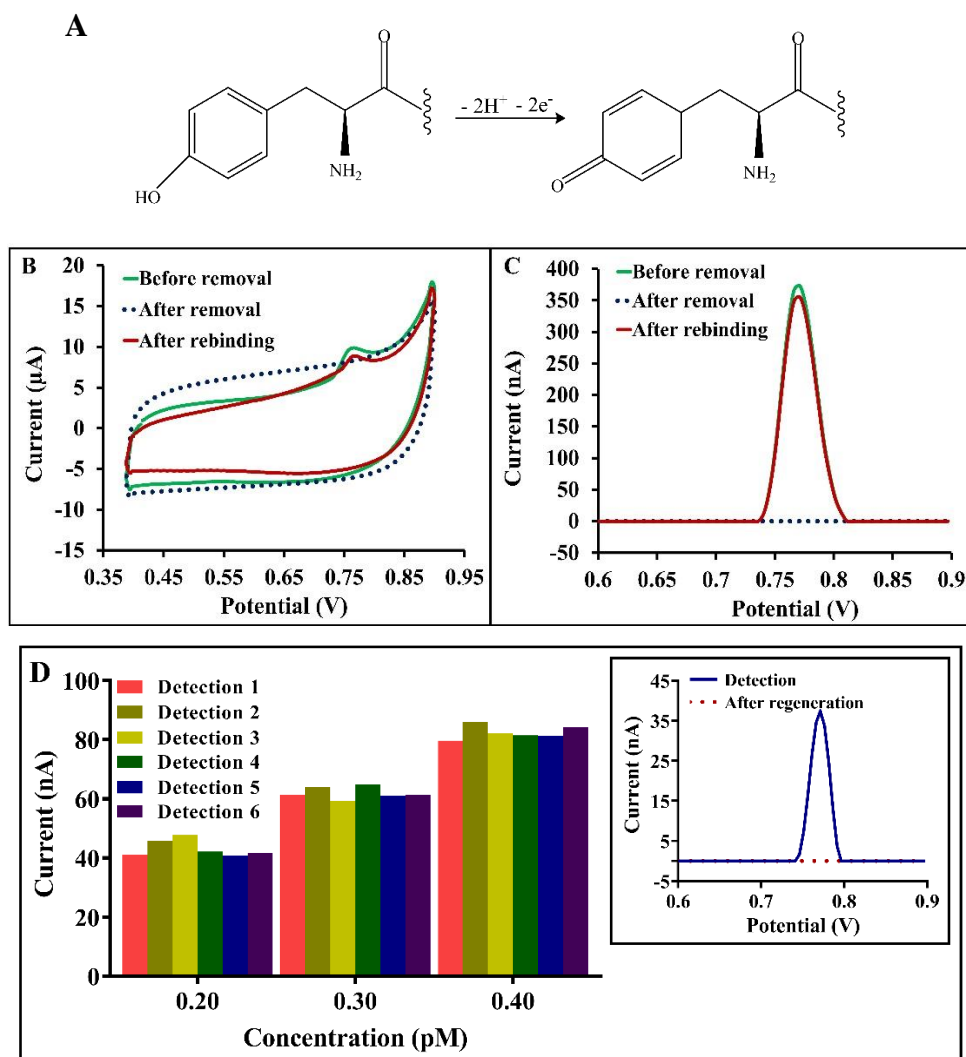




Supplementary data Fig. S2 Electrochemical characterization of the modified electrode: (A) Cyclic voltammograms and (B) Nyquist plots of electrochemical impedance responses in 5.0 mM $[\text{Fe}(\text{CN})_6]^{4-/3-}$. Inset: Randles equivalent circuit composed of the solution resistance (R_s), charge transfer resistance (R_{ct}), constant phase element (CPE) and the Warburg impedance (W). Rebinding condition: 1.0 μM insulin in phosphate buffer at pH 5.30.

S3. Insulin oxidation

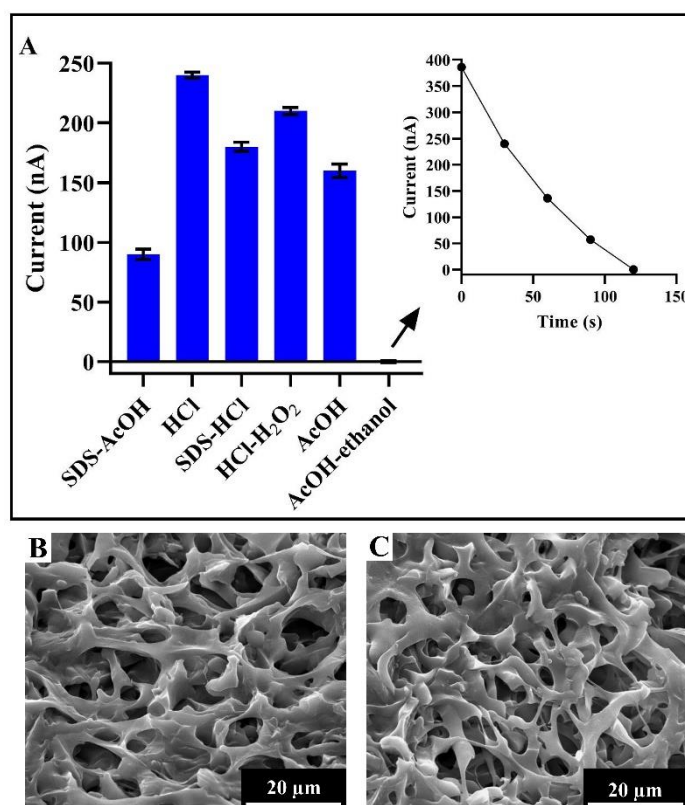
The oxidation of tyrosine involves its hydroxyl group and results in the release of a proton, as shown in **Fig. S3A**. **Fig. S3** shows the CV (**B**) and SWV (**C**) of insulin oxidation at the MIP cryogel/f-MWCNTs/AuE. The oxidation peak was observed at 0.76 V, and was produced by the oxidation of tyrosine residues in the insulin molecule (Sisolakova et al., 2019; Zhang et al., 2005). The reversibility of insulin binding to the MIP cryogel/f-MWCNTs/AuE was investigated by performing a series of binding-regeneration cycles. In **Fig. S3D**, the stable oxidation current of insulin after binding and regeneration cycles shows the good reversibility of insulin binding to the electrode.



Supplementary data Fig. S3 (A) The oxidation of tyrosine (Sisolakova et al., 2019), (B) CV and (C) SWV of the MIP cryogel/f-MWCNTs/AuE before template removal, after template removal, and after rebinding of 1.0 μM insulin in phosphate buffer at pH 5.30, using a flow rate of 100 $\mu\text{L min}^{-1}$. (D) Insulin was detected at concentrations of 0.20 pM, 0.30 pM, and 0.40 pM in phosphate buffer solution at pH 5.30 in a flow rate of 100 $\mu\text{L min}^{-1}$. After each detection, the electrode was regenerated and insulin was detected again. The chart shows the current responses of insulin. Inset: A typical SWV curve of current response during insulin detection and after regeneration.

S4. Optimization of template removal

Fig. S4 The template was removed from the MIP cryogel/f-MWCNTs/AuE using different solvents for 4 h. During template removal, the oxidation current of insulin was measured by SWV (A) and the structure of MIP cryogel was observed by SEM before and after template removal.



Supplementary data Fig. S4 (A) The chart shows oxidation currents of insulin in 1.0 mM phosphate buffer solution at pH 5.30, at a flow rate of 100 $\mu\text{L min}^{-1}$, after 4-hour template removal. The inset shows the oxidation current of insulin after template removal for 2 h using a mixture of acetic acid and ethanol (9:1 (v/v)). SEM images show the MIP cryogel/f-MWCNTs/AuE (B) before template removal and (C) after template removal.

S5. Optimization of amount of f-MWCNTs

The effects of f-MWCNTs loading were seen in the CVs of insulin oxidation (**Fig. S5A**) and redox current of $\text{Fe}(\text{CN})_6^{3-/4-}$ probe (**B**). The amount of f-MWCNTs increased the effective surface area (**Table S1**) for deposition of MIP cryogel, which was calculated by using the Randles-Sevcik equation (Eq.1) (Bard & Faulkner, 2000) with data from **Fig. S5B**.

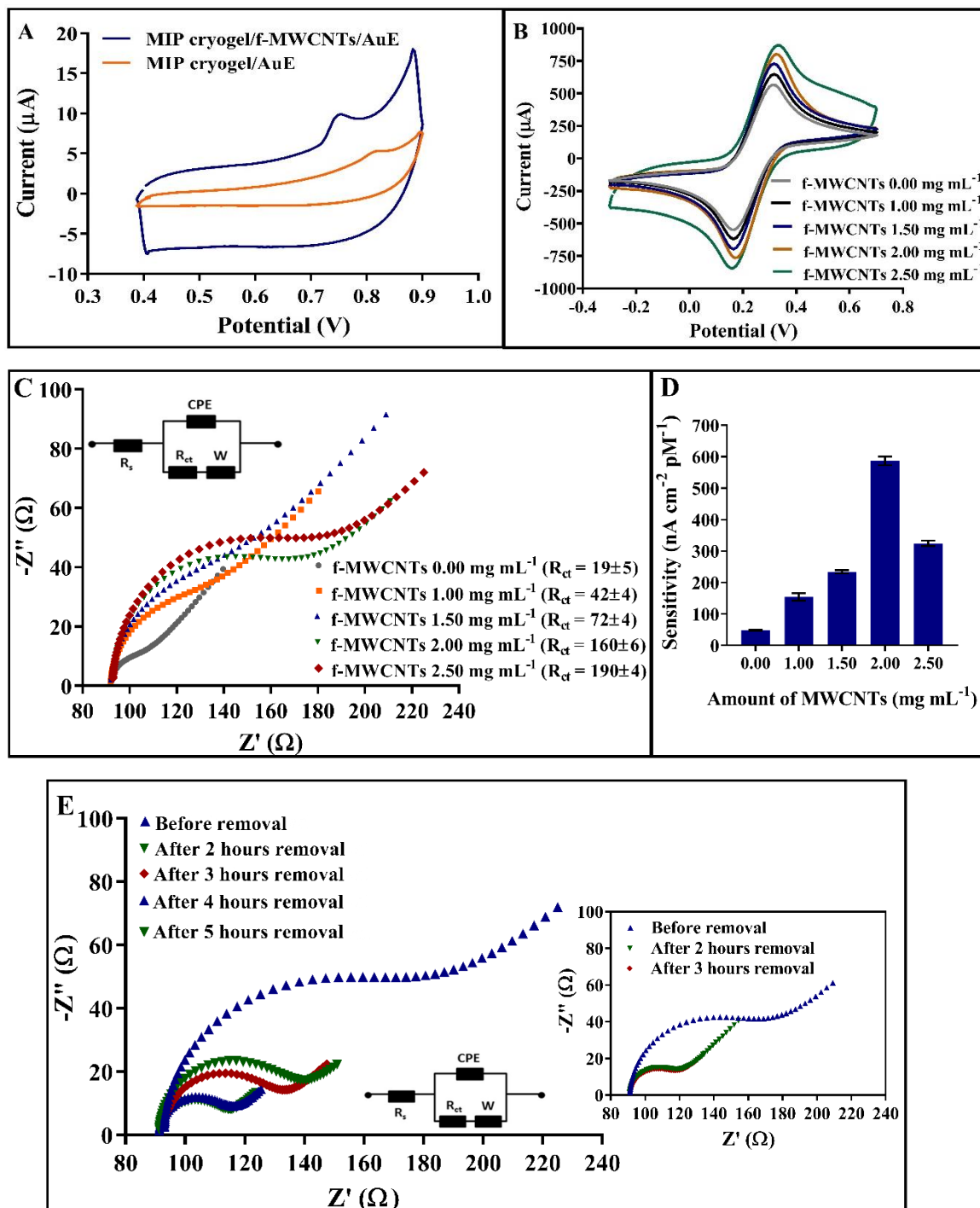
$$I_{p,a} = (2.687 \times 10^5) n^{3/2} A \cdot C (D \cdot \nu)^{1/2} \quad (1)$$

where $I_{p,a}$ is the peak current (μA), n is the number of electrons transferred, A is the area (cm^2), C is the concentration of $\text{Fe}(\text{CN})_6^{3-/4-}$ solution (mol cm^{-3}), D is the diffusion coefficient ($7.6 \times 10^{-6} \text{ cm}^2 \text{ s}^{-1}$) (Krejci et al., 2014) and ν is the scan rate (V s^{-1})

Increasing the platform surface area enabled more MIP cryogel to be deposited (**Fig. S5C**), which increased sensitivity (**Fig. S5D**) toward insulin. Too long a time was needed to remove template completely at 2.50 mg mL^{-1} f-MWCNTs (**Fig. S5E**). Hence, a loading of 2.00 mg mL^{-1} was considered optimal.

Table S1. The effective surface area of the electrode with different amounts of f-MWCNTs

Amount of f-MWCNTs	A (cm^2)
0.00 mg mL^{-1}	0.242
1.00 mg mL^{-1}	0.282
1.50 mg mL^{-1}	0.298
2.00 mg mL^{-1}	0.315
2.50 mg mL^{-1}	0.327

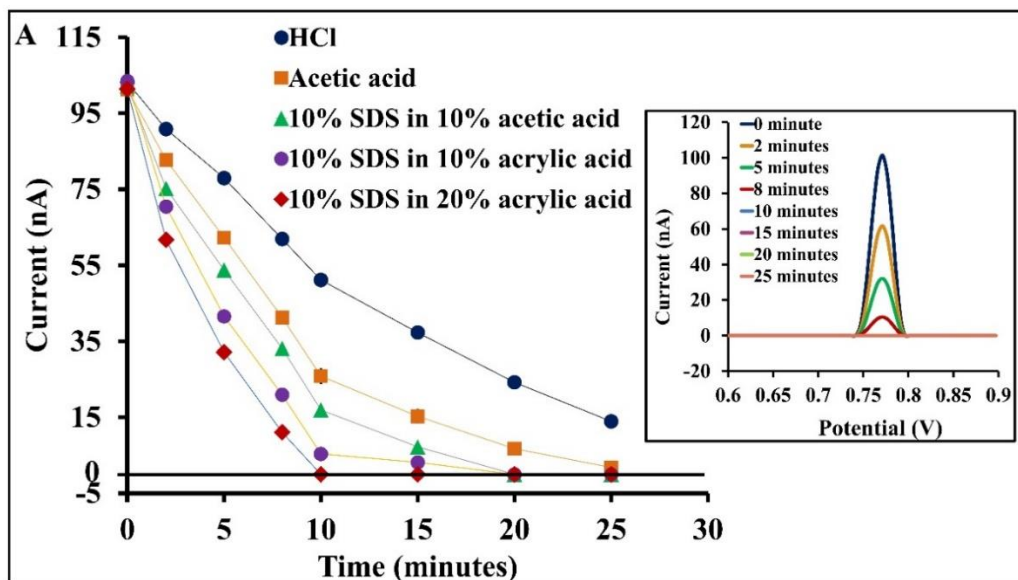


Supplementary data Fig. S5 (A) CVs of 1.0 μM insulin were produced using the MIP cryogel/f-MWCNTs/AuE and MIP cryogel/AuE in 1.0 mM phosphate buffer at pH 5.30 at a flow rate of 100 $\mu\text{L min}^{-1}$. (B) CVs of 10 mM $\text{Fe}(\text{CN})_6^{3-/4-}$ were produced at a scan rate 0.10 V s^{-1} on the f-MWCNTs/AuE with different amounts of f-MWCNTs. (C) EIS responses in 5.0 mM $[\text{Fe}(\text{CN})_6]^{4-/3-}$ were produced at the MIP cryogel/f-

MWCNTs/AuE with different f-MWCNTs loadings before insulin template removal. Inset: Randles equivalent circuit composed of the solution resistance (R_s), charge transfer resistance (R_{ct}), constant phase element (CPE) and the Warburg impedance (W). (D) The effect of different loadings of f-MWCNTs on the sensitivity of insulin detection (0.050-0.40 pM) in 1.0 phosphate buffer at pH 5.30 and a flow rate of 100 $\mu\text{L min}^{-1}$. (E) EIS responses were produced at the MIP cryogel/f-MWCNTs/AuE loaded with 2.50 mg mL^{-1} f-MWCNTs in 5.0 mM $[\text{Fe}(\text{CN})_6]^{4-/3-}$ solution after insulin template removal. The inset shows the EIS response of 2.00 mg mL^{-1} f-MWCNTs after template removal.

S6. Optimization of type of regeneration solution, pH, and flow rate

Oxidation current of insulin after regeneration using different solutions was shown in **Fig. S6A**. Also, the highest sensitivity can be obtained with optimum pH (**Fig. S6B**) and flow rate (**Fig. S6C**).



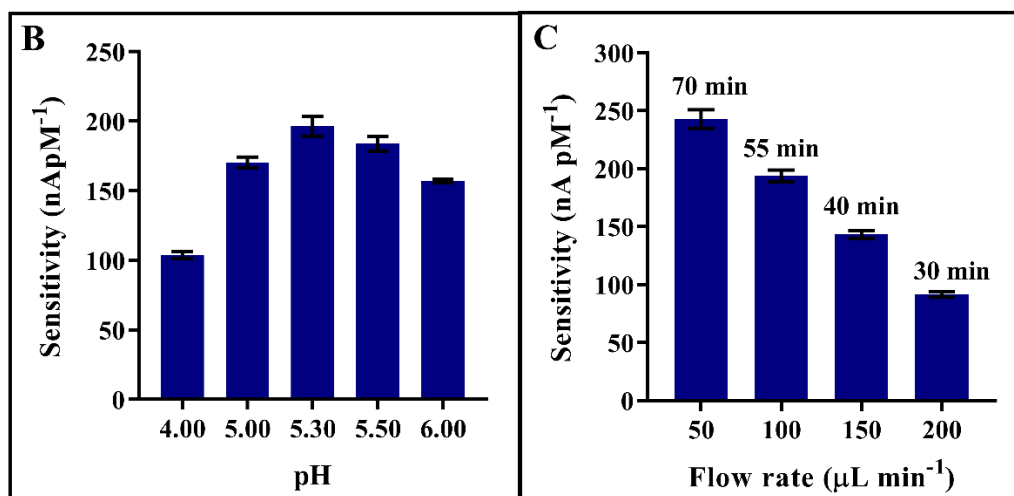


Fig. S6 (A) The chart shows the effects of different regeneration solutions on the removal of 0.50 pM insulin from the recognition sites of the molecularly imprinted polymer (inset: SWV of insulin after regeneration with 10% SDS in 20% acrylic acid). Chart (B) shows the effect of buffer pH on electrode sensitivity toward insulin (0.050-0.40 pM) and chart (C) shows the effect on sensitivity of flow rate with analysis time in 1.0 mM phosphate buffer.

S7. Binding Isotherm

The dissociation constant (K_D) of insulin binding to the modified electrode was obtained by plotting the current response (I_F) and concentration of insulin $[F]$ (Fig. S7A) and fitting with the Langmuir isotherm using GraphPad Prism 8 (Fig. S7B).

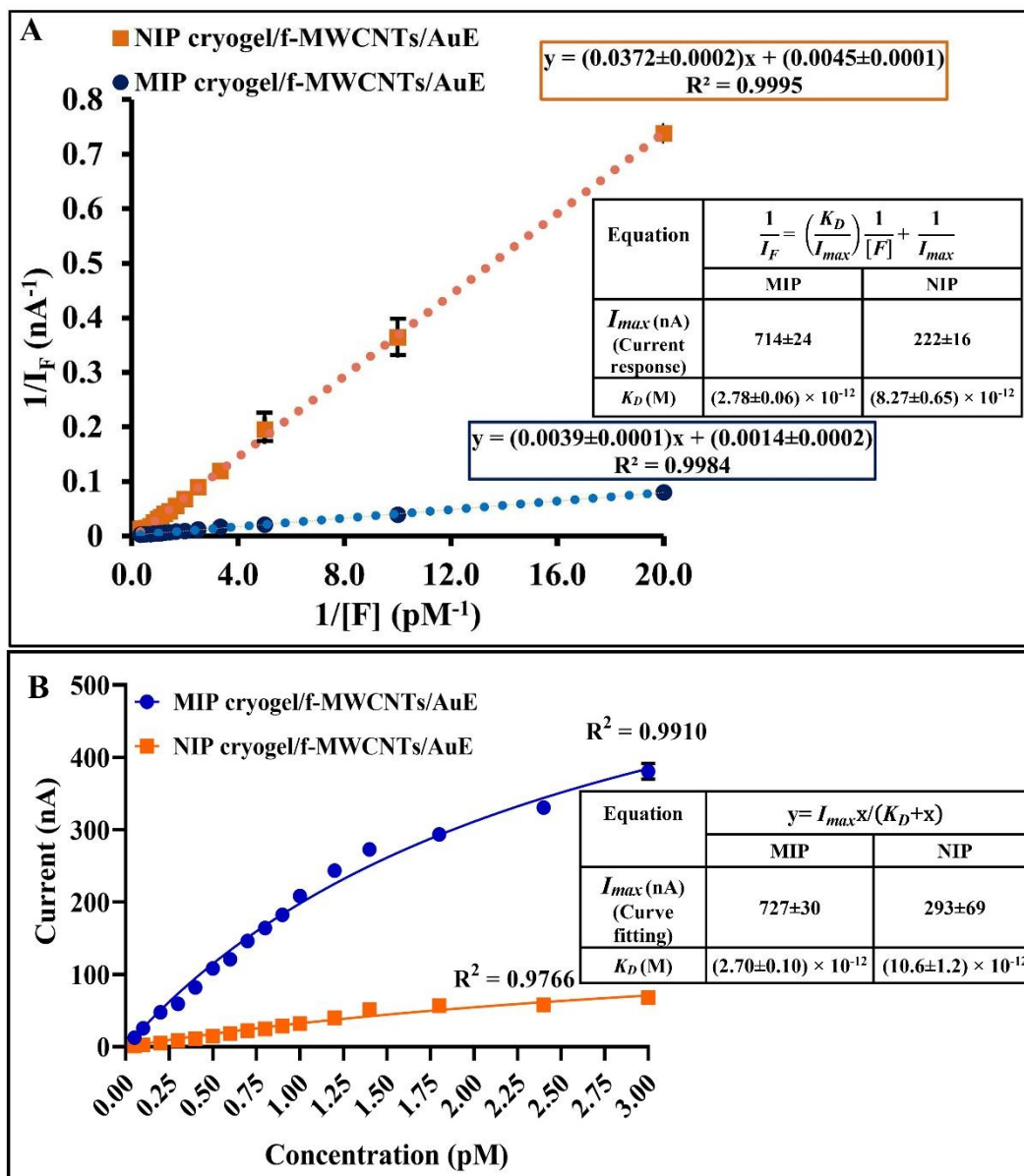
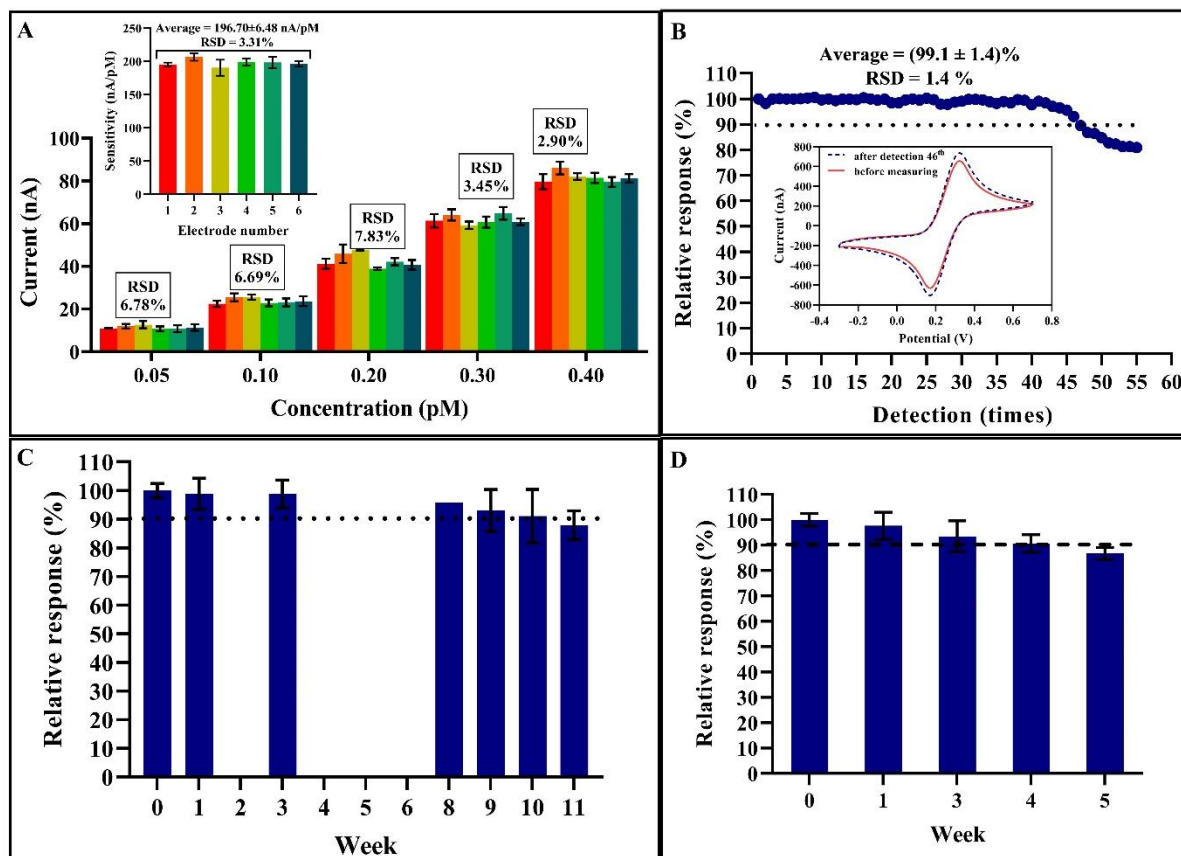


Fig. S7 (A) The linearized Langmuir plotting between $1/I_F$ and $1/[F]$ of insulin on the NIP cryogel/f-MWCNTs/AuE and MIP cryogel/f-MWCNTs/AuE. (B) Plots of current response change versus concentration of insulin at the MIP and NIP sensors were fitted with the Langmuir isotherm using GraphPad Prism 8.

S8. Reproducibility and stability of the MIP modified electrode

The reproducibility and stability of the modified electrode were evaluated using the oxidation current and sensitivity of insulin detection.



Supplementary data Fig. S8 The chart (A) shows current responses obtained from six modified electrodes (inset: sensitivity of the modified electrode for insulin detection (0.050-0.40 pM)). Chart (B) shows the operational stability of the MIP cryogel/f-MWCNTs/AuE toward repeated detection of 0.80 pM insulin. Chart (C) shows the relative sensitivity of different electrodes after various storage times. Chart (D) shows the long-term stability of the proposed electrode after repeated weekly use for four weeks. Between measurements, the electrode was stored in dry conditions at room temperature.

S9. Real samples

Table. S2 The results of a spike and recovery test using human blood serum samples

40-times dilution factor				
Spiked concentration (pM)	Sample 1		Sample 2	
	Measured concentration (pM)	%recovery	Measured concentration (pM)	%recovery
0.0	17±2	-	14.2±0.3	-
2.0	18.8±0.2	90±10	16.1±0.2	95±11
4.0	20.9±0.1	98±3	17.8±0.3	90±8
8.0	25.6±0.4	108±5	21.4±0.5	90±6
12.0	29.5±0.7	104±6	27.48±0.01	111±3
16.0	33.9±0.4	106±2	29.99 ±0.02	99±5
250-times dilution factor				
Spiked concentration (pM)	Sample 3		Sample 4	
	Measured concentration (pM)	%recovery	Measured concentration (pM)	%recovery
0.0	51±4	-	120 ±10	-
12.5	63±1	96±10	132 ±1	96±4
25.0	77±3	104±3	143 ±2	92±8
50.0	100±2	98±3	169 ±3	98±5
75.0	127±1	101±2	194 ±5	99±7
100.0	153±1	102±1	219 ±4	99±4

References

- [1] W. Shao, J. Mai, Z. Wei, Nonenzymatic Lactic Acid Detection Using Cobalt Polyphthalocyanine/Carboxylated Multiwalled Carbon Nanotube Nanocomposites Modified Sensor, Chemosensors 10(2) (2022).

- [2] M. Entezari, M. Safari, M. Hekmati, S. Hekmat, A. Azin, Modification of carboxylated multiwall nanotubes with benzotriazole derivatives and study of their anticancer activities, *Medicinal Chemistry Research* 23(1) (2014) 487-495.
- [3] M.G. Zhang, C. Mullens, W. Gorski, Insulin oxidation and determination at carbon electrodes, *Anal. Chem.* 77(19) (2005) 6396-6401.
- [4] I. Sisolakova, J. Hovancova, R. Orinakova, A. Orinak, L. Trnkova, D.R. Garcia, J. Radonak, Influence of a polymer membrane on the electrochemical determination of insulin in nanomodified screen printed carbon electrodes, *Bioelectrochemistry* 130 (2019) 11.
- [5] A.J. Bard, L.R. Faulkner, *Electrochemical Methods: Fundamentals and Applications*, 2nd Edition, John Wiley & Sons, Incorporated 2000.
- [6] J. Krejci, Z. Sajdlova, V. Nedela, E. Flodrova, R. Sejnohova, H. Vranova, R. Plicka, Effective Surface Area of Electrochemical Sensors, *Journal of The Electrochemical Society* 161(6) (2014) B147.

PAPER II**Molecularly imprinted dual electrochemical sensor for the one-step
determination of albuminuria to creatinine ratio (ACR)****Wardani, N. I., Kanatharana, P., Thavarungkul, P., Limbut, W***Reprinted from Talanta (2023) 265, 124769**with permission of Elsevier*



Contents lists available at ScienceDirect

Talanta

journal homepage: www.elsevier.com/locate/talanta

Molecularly imprinted polymer dual electrochemical sensor for the one-step determination of albuminuria to creatinine ratio (ACR)

Nur Indah Wardani^{a,b,c}, Proespichaya Kanatharana^{a,b,c}, Panote Thavarungkul^{a,b,c}, Warakorn Limbut^{a,c,d,*}

^a Center of Excellence for Trace Analysis and Biosensor, Prince of Songkla University, Hat Yai, Songkhla, 90110, Thailand

^b Division of Physical Science, Faculty of Science, Prince of Songkla University, Hat Yai, Songkhla, 90110, Thailand

^c Center of Excellence for Innovation in Chemistry, Faculty of Science, Prince of Songkla University, Hat Yai, Songkhla, 90110, Thailand

^d Division of Health and Applied Sciences, Faculty of Science, Prince of Songkla University, Hat Yai, Songkhla, 90110, Thailand

ARTICLE INFO

Keywords:

Simultaneous determination
Electrochemical sensor
Dual MIP
Urinary ACR

ABSTRACT

The urinary albumin to creatinine ratio (ACR) is a convenient and accurate biomarker of chronic kidney disease (CKD). An electrochemical sensor for the quantification of ACR was developed based on a dual screen-printed carbon electrode (SPdCE). The SPdCE was modified with carboxylated multiwalled carbon nanotubes (f-MWCNTs) and redox probes of polymethylene blue (PMB) for creatinine and ferrocene (Fc) for albumin. The modified working electrodes were then molecularly imprinted with coated with polymerized poly-o-phenylenediamine (PoPD) to form surfaces that could be separately imprinted with creatinine and albumin template molecules. The seeded polymer layers were polymerized with a second coating of PoPD and the templates were removed to form two different molecularly imprinted polymer (MIP) layers. The dual sensor presented recognition sites for creatinine and albumin on different working electrodes, enabling the measurement of each analyte in one potential scan of square wave voltammetry (SWV). The proposed sensor produced linear ranges of 5.0–100 ng mL⁻¹ and 100–2500 ng mL⁻¹ for creatinine, and 5.0–100 ng mL⁻¹ for albumin. LODs were 1.5 ± 0.2 ng mL⁻¹ and 1.5 ± 0.3 ng mL⁻¹, respectively. The dual MIP sensor was highly selective and stable for seven weeks at room temperature. The ACRs obtained using the proposed sensor compared well ($P > 0.05$) with the results from immunoturbidimetric and enzymatic methods.

Credit author statement

Nur Indah Wardani: Conceptualization, Formal analysis, Validation, Writing – original draft; Proespichaya Kanatharana: Conceptualization, Formal analysis, Validation; Panote Thavarungkul: Conceptualization, Formal analysis, Validation, Supervision, Writing – review & editing; Warakorn Limbut: Conceptualization, Formal analysis, Validation, Supervision, Writing – review & editing.

1. Introduction

Chronic kidney disease (CKD) is a progressive condition that involves reduced kidney function and structural damage. Global morbidity and mortality are high but treatment outcomes and cost-effectiveness could be improved by early diagnosis and staging [1]. In clinical assessments, the criteria for CKD are decreasing glomerular filtration rate (GFR) and

albuminuria. The albuminuria, or urine albumin, to creatinine ratio (ACR) is the preferred indicator in initial screening for CKD due to the convenience of determining ACR in random urine sampling. The test is easy and can avoid the potential errors of random sampling [2,3].

The determination of urine albumin and creatinine commonly relies on methods such as immunoturbidimetry, fluoro-immunoassays, and enzymatic assays, which are all relatively time consuming, expensive and call for professional expertise. Less expensive colorimetric methods that do not require professional expertise can also be used, but have relatively low sensitivity [4,5]. Recent developments of optical and electrochemical sensors have focused on the dual detection of albumin and creatinine to determine the ACR. Simple assay platforms have been developed from paper-based analytical devices (PADs) that used dye-binding for albumin determination and colorimetry for creatinine determination, but this approach was prone to reading errors and individual interpretation [6–8]. A more sensitive optical sensor used

* Corresponding author. Division of Health and Applied Sciences, Faculty of Science, Prince of Songkla University, Hat Yai, Songkhla, 90110, Thailand.
E-mail address: warakorn.l@psu.ac.th (W. Limbut).

<https://doi.org/10.1016/j.talanta.2023.124769>

Received 13 March 2023; Received in revised form 2 June 2023; Accepted 4 June 2023

Available online 7 June 2023

0039-9140/© 2023 Elsevier B.V. All rights reserved.

copper nanoclusters as a fluorescent probe, but albumin and creatinine had to be detected separately under different conditions [9]. A recently developed dual electrochemical sensor integrated with a circuit board enabled the successive monitoring of albumin or creatinine levels by two different electrochemical methods, using a dual working electrode i.e., chronoamperometry (CA) and cyclic voltammetry (CV) [10] or chronoamperometry (CA) and differential pulse voltammetry (DPV) [11]. While these sensors can determine the ACR, they need a complicated circuit board and suffer from poor selectivity for creatinine. Thus, a simpler single detection protocol that can selectively detect the two analytes at the same time would be beneficial. For the selective simultaneous determination of albumin and creatinine, an electrochemical sensor based on a molecularly imprinted polymer (MIP) could have great potential.

MIP presents specific recognition sites to the target analyte. It is a biomimetic receptor with more stability and less expense than natural receptors [12]. A number of selective and sensitive MIP sensors have been reported for urine albumin [13,14] and creatinine [15,16]. The simultaneous detection of more than one analyte has been achieved by using different templates in one MIP [17–19], and by synthesizing an array of MIPs with different templates [20,21]. The dual template MIP is easier to fabricate but the uneven distribution of binding sites and disturbance during rebinding could affect the performance. The size difference between albumin (66.7 kDa) and creatinine (113.1 Da), the non-electroactive property of albumin and the high oxidation potential of creatinine might also hinder electrochemical detection. Thus, for the simultaneous determination of albumin and creatinine, an array of MIPs with different recognition sites is the preferable approach.

Surface imprinting has emerged as an efficient method of molecular imprinting because it produces binding sites at or near the MIP surface for easier removal and rebinding of the analyte. Moreover, the preliminary anchoring of the analyte to the electrode surface generates uniformly distributed binding sites [22,23]. The integration of the MIP layer with the electrode surface has mostly been performed using electropolymerization, whether imprinting small or large template molecules. Electropolymerization enables the thickness of the MIP layer to be controlled [24] and the surface thickness can be better controlled if an electroactive functional monomer is electropolymerized. The imprinting of binding sites is improved, the binding and removal of analytes to and from the imprinted sites is facilitated, and quantification becomes more reliable [25]. *Ortho*-phenylenediamine (*o*-PD) is a monomer that can easily be electropolymerized on various materials and forms film with good chemical and mechanical stability. The presence of abundant amine groups ($-NH_2$) may help to bind the support layer to the platform and the template molecule to the support layer [26].

The performance of the proposed MIP sensor could be improved by integrating multiwalled carbon nanotubes (MWCNTs). Their large surface area and high conductivity could increase the number of imprinted cavities and the conductivity of the MIP [27]. Functionalizing the MWCNTs using carboxylic acid could help raise their dispersibility [28, 29]. Therefore, carboxylated MWCNTs (f-MWCNTs) were used in this work to obtain an evenly distributed layer of f-MWCNTs on the electrode surface and enhance the conductivity of the modified electrode. For the detection of the analyte binding to the MIP, square wave voltammetry (SWV) was employed. SWV is highly sensitive and enables scanning in the potential range required to detect the compounds of interest [30]. By coupling redox probes such as polymethylene blue (oxidation potential at -0.37 V) and ferrocene (oxidation potential at 0.13 V) with the MIPs, their distinct oxidation potentials could improve the separation of creatinine and albumin binding. The two analytes could then be better monitored simultaneously in one potential scan.

Herein, we report the determination of ACR, obtained through the simultaneous determination of urine albumin and creatinine, using a dual MIP sensor. This sensor was prepared on the surface of a dual screen-printed carbon electrode (SPdCE), that comprised one working electrode for creatinine with polymethylene blue (PMB) as the detecting

element and another for albumin using ferrocene (Fc) as the detecting element. The f-MWCNTs coated on the SPdCE were employed to increase the surface area of the MIP layer, thus, allowing a large number of recognition sites to be imprinted. The surface imprinting was carried out by first anchoring the analytes on an electropolymerized layer followed by the electropolymerization of *ortho*-phenylenediamine (*o*-PD) at a suitable thickness to optimize the selectivity of the MIP sensor. The PMB and Fc oxidation currents were monitored in a single potential scan. The current responses corresponded to the amount of creatinine and albumin bound to the sensor. The sensor was characterized and optimized for the determination of creatinine and albumin. The developed MIP dual electrochemical sensor was then applied to detect creatinine and albumin in urine samples to obtain the ACR.

2. Experimental

2.1. Reagents and materials

Human serum albumin (HSA, $\geq 96\%$) and creatinine (anhydrous, 98%) were from Sigma-Aldrich (Steinheim, Germany). *Ortho*-phenylenediamine monomer (*o*-PD) was from BDH Laboratory Supplies (Poole, England). Ferrocene (F408– 98%), poly (3,4-ethylenedioxythiophene): poly (styrenesulfonate) (PEDOT:PSS), glutaraldehyde (25% in H_2O), oxalic acid (98%) were from Sigma-Aldrich (Steinheim, Germany). Methylene blue (MB) was from Gurr Certistain, England. Glucose anhydrous was from Fluka (Buchs, Switzerland). L-ascorbic acid, dopamine hydrochloride, and cysteine were from Sigma-Aldrich (Darmstadt, Germany). Sodium chloride (NaCl) was from Merck (Copenhagen, Denmark). Uric acid was from Sigma-Aldrich (Budapest, Hungary) and urea was from Riedel-de Haën (Bucharest, Romania). The supporting electrolyte, phosphate buffered saline (PBS) pH 7.40, consisted of sodium dihydrogen o-phosphate and disodium hydrogen o-phosphate (Ajax Finechem, Sydney, Australia) with potassium chloride (Merck, Germany). All aqueous solutions were prepared using water purified with a Mili-Q purification system (resistivity ≥ 18 M Ω cm). MWCNTs (purity $\geq 95\%$, average diameter 60–100 nm, length 2–5 μm) (Shenzhen Nano-Techbnologies Port Co., Ltd., Shenzhen, China) were functionalized to form carboxylated MWCNTs with a 3:1 (v/v) concentrated H_2SO_4 and HNO_3 mixture, filtered and left in a vacuum desiccator before use. All other chemicals used were of analytical grade. Dual screen-printed carbon electrodes (SPdCEs, DRP-X1110) were supplied by Metrohm-DropSens (Asturias, Spain).

2.2. Apparatus

The electrode modification steps were evaluated with electrochemical impedance spectroscopy (EIS) and cyclic voltammetry (CV) performed on the μ Autolab Type III potentiostat-galvanostat controlled by NOVA 2.1 software (Metrohm Autolab B.V., The Netherlands). The impedance spectra were fitted to a Randle's equivalent circuit by FRA software to obtain the charge transfer resistance (R_{ct}). Electrode surface morphology was observed by scanning electron microscopy (SEM) (Quanta 400, FEI, USA). Fourier-transform infrared spectroscopy (FT-IR) (VERTEX 70, Bruker, Germany) was used to characterize the MIP and NIP (see Section 3.1). The electrochemical determination of creatinine and albumin was performed in a batch system by SWV using the μ Autolab Type III.

2.3. Electrode modification

Surface organic substances were removed from the bare SPdCE by applying a constant 1.20 V potential for 5 min in saturated Na_2CO_3 [31]. The SPdCE was then rinsed with de-ionized water, and dried with nitrogen gas. The steps of electrode modification are illustrated in Fig. 1. The two working electrodes were modified with 15.0 μg of f-MWCNTs (in dimethylformide, DMF see 3.3.1), and then allowed to dry. To

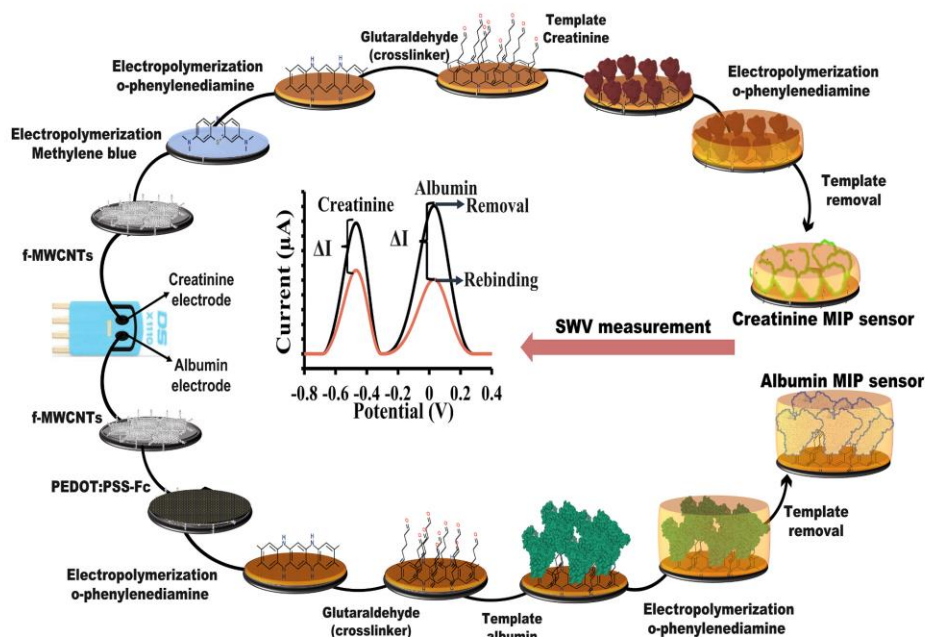


Fig. 1. The preparation of creatinine MIP sensor and albumin MIP sensor.

fabricate the creatinine electrode (WE1), a PMB redox probe layer was electropolymerized onto the f-MWCNTs in 0.25 mmol L^{-1} MB in 50 mmol L^{-1} PBS, pH 7.40, by applying a fixed potential of 1.50 V for 900 s [32]. This was followed by applying a range of potentials from -0.70 to 0.40 V at a scan rate of 100 mV s^{-1} . Preliminary testing with 20, 30, 35, and 40 cycles demonstrated that the strongest signal was produced by a redox probe polymerized with 30 cycles, and this condition was applied in the fabrication process. After this step, the PMB/f-MWCNTs electrode was washed with PBS solution. To fabricate the albumin electrode (WE2), PEDOT:PSS and DMF were mixed at a ratio of 1:1 and 5.0 mg of Fc were added to $50.0 \mu\text{L}$ of the solution [33]. Preliminary testing with 1.5, 2.0, and $2.5 \mu\text{L}$ of the mixture demonstrated that the strongest signal was obtained from an electrode modified with $2.0 \mu\text{L}$, and this amount was drop-casted onto the f-MWCNTs/albumin electrode and dried at room temperature.

The MIPs of the two electrodes were prepared separately, each with two layers of PoPD. The first layer, used as a platform for amine groups, was produced with three scans of CV from 0.00 to $+0.80 \text{ V}$ at 50 mV s^{-1} in 5.0 mmol L^{-1} o-PD in 0.20 mol L^{-1} acetate buffer at pH 5.20 [34]. The dual electrode was then immersed in 2.0% (v/v) glutaraldehyde (GA) for 30 min , to activate the amine ($-\text{NH}_2$) groups of PoPD and as a linker to bind with the template molecule [35]. After washing, $2.0 \mu\text{L}$ each of 1.0 mg mL^{-1} creatinine and albumin templates were drop-casted on the respective working electrodes and left for 24 h at 4°C . After rinsing with de-ionized water, the second layer of PoPD was electropolymerized on the working electrodes to form an MIP layer of optimal thickness (see section 3.3.2). The dual creatinine and albumin MIP sensor was obtained after removing the templates in 0.10 mol L^{-1} oxalic acid [33] for the appropriate time (see section 3.3.3), followed by washing in PBS with stirring. For comparison, a non-imprinted polymer (NIP) sensor was prepared using the same steps, but without the creatinine and albumin templates.

2.4. Characterizations of the modified electrode and electrochemical measurements

The surface morphology of the modified electrodes was observed by scanning electron microscopy (SEM) (Quanta 400, FEI, USA). Electrochemical measurements were taken using the SPdCE, which comprised WE1 for creatinine detection, WE2 for albumin detection, a silver pseudo-reference electrode (RE), and an auxiliary electrode (AE) (Fig. 1 and Fig. 4A). The determination of creatinine or albumin singly was performed by connecting only WE1 or WE2 to the potentiostat. To simultaneously determine both analytes, WE1 and WE2 were connected to the same potentiostat port. Electrochemical characterization and determination were performed in a batch system in 8.0 mL 0.050 mol L^{-1} PBS (pH 7.40) at room temperature using the $\mu\text{Autolab Type III}$. The use of pH 7.40, the highest physiological pH [36], was based on the preliminary study that provided the PMB with a more negative oxidation potential at higher pH [37] that led to two well separated peak potentials between PMB and ferrocene. Electrode modification steps were characterized by CV and EIS. For this study, CV was performed from -0.70 V to 0.60 V at a scan rate of 50 mV s^{-1} in 0.050 mol L^{-1} PBS (pH 7.40) at room temperature. EIS was performed in a frequency range of $10,000\text{--}0.01 \text{ Hz}$ using an amplitude of 5.0 mV at 0.00 V in $5.0 \text{ mM Fe}(\text{CN})_6^{3-/4-}$ solution.

To study analyte rebinding, the dual MIP sensor was immersed in 5.0 mL of 0.050 mol L^{-1} PBS containing creatinine and albumin. The rebinding time was preliminary tested at 10, 15, 20, 25, and 30 min . However, when the time was less than 30 min , the responses did not correlate with the change in concentration, probably due to the insufficient rebinding contact time. The shortest time that provides linear correlation between rebinding response and concentration was 30 min . Therefore 30 min was used in this study. After rebinding the sensor was rinsed in PBS with stirring for 15 min to remove matrix compounds that may have bound non-specifically. The dual sensor was then immersed in

0.050 mol L⁻¹ PBS without stirring before determining creatinine and albumin bound to the WE1 and WE2. The analytes were determined by SWV, applying a potential range from -0.80 V to +0.40 V with a modulation amplitude of 0.10 V, which produced well separated oxidation peaks of PMB and Fc. The binding of creatinine and albumin to the imprinted cavities hindered the electron transfer of PMB and Fc to the electrode surface, reducing the oxidation current (Fig. 1). The current change (ΔI) was taken in proportion to the concentration of creatinine and albumin. The simultaneous electrochemical measurement of the dual MIP sensor was monitored by connecting both working electrodes via the same port. The ACR was calculated as follows:

$$\text{ACR (mg g}^{-1}\text{)} = \frac{\text{albumin (mg mL}^{-1}\text{)}}{\text{creatinine (g mL}^{-1}\text{)}}$$

2.5. Electrode modification optimization

The amount of f-MWCNTs used to modify the working electrodes, the thickness of the MIP layer, and the template removal time were investigated. A series of standard solutions (mixtures of creatinine and albumin, $n = 3$) was tested in 0.050 mol L⁻¹ PBS (pH 7.40) with a 30 min incubation time. The optimal was the one with the highest sensitivity (slope of the calibration plot).

2.6. Reproducibility, reusability, and long-term stability

Reproducibility was examined by comparing the standard deviation and sensitivity of six different modified electrodes. Reusability was examined by repeatedly measuring a series of creatinine and albumin mixtures ($n = 3$). The long-term stability was evaluated with the modified electrodes that were prepared at the same time in which the responses of each modified electrode were tested after different span of storage time and compared to those of the freshly prepared.

2.7. Selectivity

The effects of possible interfering species present in urine were tested with glucose, uric acid (UA), urea, ascorbic acid (AA), dopamine (DA), cysteine (Cys), Cl⁻, Na⁺, and K⁺. They were examined individually and mixed with creatinine and albumin. The interfering species were detected at slightly higher concentrations than those seen in typical urine samples of CKD patients [38–40]. The current responses were compared to those of creatinine and albumin. All measurements were carried out in triplicate.

2.8. Real sample analysis

Human urine samples were obtained from Songklanagarind Hospital, Hat Yai, Songkhla, Thailand. The sample collection and handling protocol were approved by the Human Research Ethics Committee of the Faculty of Medicine, Prince of Songkla University. The matrix effect was first evaluated to obtain an appropriate dilution factor. Slopes from standard insulin solutions and spiked samples were compared by two-way ANOVA at the 95% confidence level ($P > 0.05$). Real samples were diluted with an appropriate dilution factor, using 0.050 mol L⁻¹ PBS. Urine creatinine concentration was determined using the proposed sensor and the enzymatic standard method. The results of creatinine measurement showed normally distributed data; the paired Student's *t*-test (two-tailed) was used to compare results from the proposed sensor and the enzymatic method used by the hospital at a significance level of 0.05. Urine albumin concentration was determined using the proposed sensor and an immunoturbidimetric method. The obtained albumin concentrations showed non-normally distributed data, and thus the Wilcoxon signed-rank test was used to compare the two sets of results at a significance level of 0.05.

3. Results and discussion

3.1. Characterization of the MIP sensors

Observed by SEM, the f-MWCNTs/SPdCE showed a filamentous surface structure (Fig. S1A and I), made thicker by the polymerized PMB (Fig. S1B), and rougher by the deposition of Fc (Fig. S1J). Before the template removal, small beads were observed on the MIP/PMB/f-MWCNTs/SPdCE (Fig. S1C), and a significantly rough surface on the MIP/Fc/f-MWCNTs/SPdCE (Fig. S1K). The presence of templates were also confirmed by the FT-IR spectra (Figs. S2A–B). Following the template removal (Fig. S1D), the small beads were no longer visible on the MIP/PMB/f-MWCNTs/SPdCE. After the rebinding of creatinine, the beads reappeared (Fig. S1G) and were similar to those observed before the template was removed. The surface of the MIP/Fc/f-MWCNTs/SPdCE was smoother after the albumin template was removed (Fig. S1L). After analyte rebinding (Fig. S1O), due to the reoccupation of the cavities by albumin, the surface of the electrode resembled the surface of the electrode before the albumin template was removed (Fig. S1K). The NIP electrodes exhibited the same surface features both before and after template removal and rebinding of both creatinine (Figs. S1E, F, H) and albumin (Figs. S1M, N, P). The FT-IR characteristic peaks also substantiated the before and after template removal, as well as the rebinding steps (Fig. S2). These results confirmed the formation of MIPs for the determination of creatinine and albumin.

The electrode modification was also examined stepwise by CV and EIS. No redox peaks were present in the voltammograms of the bare SPdCE (Figs. S3A and B curve (a)) and the f-MWCNTs/SPdCE, that produced larger background currents (Figs. S3A and B curve (b)) due to the increased surface area and conductivity. Redox peaks were produced at the PMB/f-MWCNTs/SPdCE (Fig. 3A curve (c)) and f-MWCNTs/SPdCE (Fig. 3B curve (c)). The voltammograms of the PoPD/PMB/f-MWCNTs/SPdCE (Fig. S3A curve (d,e)) and the PoPD/Fc/f-MWCNTs/SPdCE (Fig. S3B curve (d,e)) presented reduced redox peaks. Following template removal, the redox peaks of the MIP/PoPD/PMB/f-MWCNTs/SPdCE and MIP/PoPD/Fc/f-MWCNTs/SPdCE were significantly increased (Figs. S3A and B curve (f)), before decreasing after analyte rebinding (Figs. S3A and B curve (g)). The reduction in the redox peaks indicated the occupation of the imprinted cavities on the respective working electrodes by creatinine and albumin, which blocked electron transfer.

EIS revealed similar behaviors. Smaller R_{ct} s, were observed at the f-MWCNTs/SPdCE (Figs. S4A and B curve (b)) compared to the bare SPdCEs (Figs. S4A and B curve (a)). The larger R_{ct} s of the PMB/f-MWCNTs/SPdCE (Fig. S4A curve (c)) and Fc/f-MWCNTs/SPdCE circuits (Fig. S4B curve (c)) indicated that the redox probes were bound to the electrode.

The R_{ct} of both circuits increased after the first layer of PoPD (Figs. S4A and B curve (d)) was electropolymerized because the polymer layer hindered electron transfer. The R_{ct} of both circuits increased again after the electropolymerization of the second PoPD layer (Figs. S4A and B curve (e)). After the imprinted cavities were exposed by template removal, R_{ct} s decreased (Figs. S4A and B curve (f)), and then increased after the rebinding of creatinine and albumin (Fig. S4 curve (g)).

3.2. Electrochemical response of dual MIP sensor

Fig. 2A shows the PMB and Fc responses during a single sweep of SWV in PBS (pH 7.40) solution, prior to the rebinding when only the creatinine MIP (WE1) or albumin MIP (WE2) electrodes was connected, as well as the simultaneous SWV of the dual MIP sensor, when WE1 and WE2 were connected to the same potentiostat port. When the electrodes were scanned singly by SWV in 0.050 mol L⁻¹ PBS pH 7.40, the oxidation peak of PMB at the WE1 was observed at -0.37 V. The oxidation peak of Fc at the WE2 occurred at +0.13 V (Fig. 2A). When electrodes were scanned together, two well-separated oxidation peaks with lower

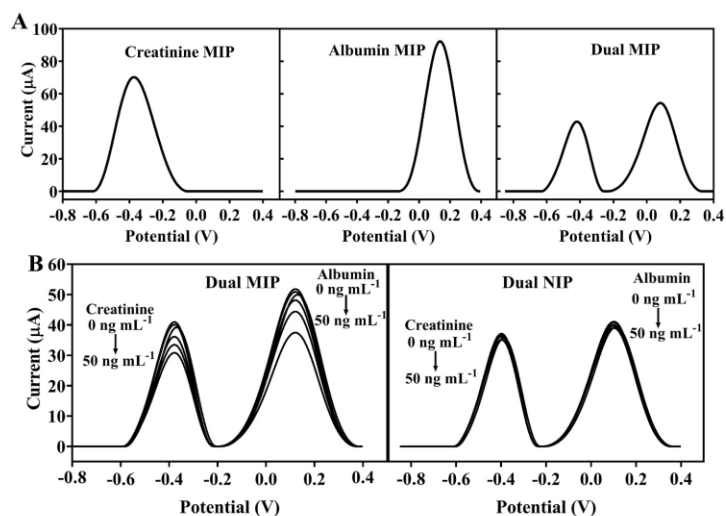


Fig. 2. SWV waveforms were obtained from (A) the creatinine MIP, albumin MIP, and dual MIP sensor before analyte rebinding in 0.050 mol L⁻¹ PBS pH 7.40. (B) The waveforms of the dual MIP and the dual NIP sensors were obtained in 0.050 mol L⁻¹ PBS pH 7.40 with the addition of various creatinine and albumin mixtures.

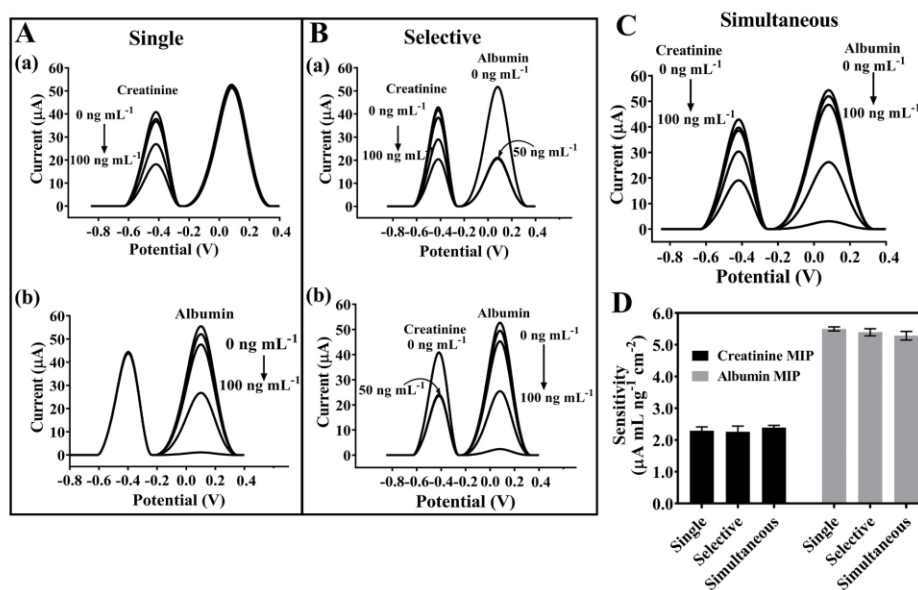


Fig. 3. SWV waveforms were produced by the dual MIP in the presence of creatinine and/or albumin in 0.050 mol L⁻¹ PBS (pH 7.40). (A) Shows the responses to single determinations of creatinine and albumin. (B) Shows the results of selective determination of varying concentrations of one analyte and a stable concentration of the other. (C) Shows the results of simultaneous determination of creatinine and albumin. (D) Sensitivities of creatinine and albumin determination.

amplitudes were observed at -0.41 V for PMB and $+0.08$ V for Fc. The slight shifts in peak potential were probably due to the shared auxiliary (AE) and reference (RE) electrodes of the two WEs, since all other connections of the electrodes were the same [41] (Fig. S5A). Also, when the WE1 and 2 were connected together, the background current was larger than when they were connected singly, thus, contributing to the

lower response (Fig. S5B).

To confirm the imprinting effect and rebinding ability, SWV was applied to determine a series of creatinine and albumin mixtures (0–50 ng mL⁻¹) at the dual MIP and NIP sensors. The rebinding of creatinine and albumin reduced the oxidation peaks of PMB and Fc (Fig. 2B). The very small decrease in current at the dual NIP sensor was due to the

absence of imprinted cavities for creatinine and albumin. The much higher decrease in the currents at the dual MIP sensor was due to the imprinted cavities on the MIP layer, and indicated their specificity towards creatinine and albumin.

3.3. Optimization of electrode preparation

3.3.1. Amount of f-MWCNTs

The amount of f-MWCNTs used to fabricate WE1 and 2 (0.0 μg , 5.0 μg , 10.0 μg , 15.0 μg , and 20.0 μg) was optimized to obtain a larger surface area, and thus more binding sites. Larger amounts of f-MWCNTs increased conductivity and effective surface area up to 15.0 μg (Figs. S6A–B). The sensitivity of creatinine and albumin rebinding (Fig. S6C) also increased with greater loadings of f-MWCNTs from 0.0 to 15.0 μg and became stable at 20.0 μg , in agreement with the surface area data (Fig. S6B). Hence, 15.0 μg of MWCNTs were used to fabricate WE1 and 2.

3.3.2. MIP layer thickness

The thickness of the MIP has an influence on creatinine and albumin rebinding. The MIP layer should be thick enough to allow the formation of molecular cavities. The thickness of the layer is determined by the number of cycles of electropolymerization used and can be estimated from the total charge used during electropolymerization. The total charge used here was estimated using the equation below [42,43]:

$$d = \frac{QM}{nFA\rho}$$

where Q is the total charge used during electropolymerization (obtained by integration of the oxidation peaks, Fig. S7A), M is the molecular weight of *o*-PD (108.1 g mol^{-1}), n is the number of electrons (2), F is Faraday's constant (96,485 C mol^{-1}), A is the electrode surface area and ρ is the density of *o*-PD (1.03 g cm^{-3}).

The dimensions of the creatinine molecule are about 0.39 nm \times 0.53 nm \times 0.38 nm [44]. The MIP layer thicknesses produced by 1, 3, 5, and 7 scanning cycles were calculated to be 1.4, 4.1, 6.8, and 9.6 nm, respectively. The sensitivity of the creatinine MIP sensor was highest at the electrode produced with three cycles of electropolymerization (Fig. S7B). This layer (4.1 nm) was thicker than the creatinine molecule. The dimensions of the albumin molecule are about 13.6 nm \times 2.7 nm \times 2.7 nm [45]. The MIP layer thicknesses produced by 5, 7, 10, and 15 scanning cycles were calculated to be 7.4, 10.3, 14.8, and 22.2 nm, respectively. The sensitivity of the albumin MIP sensor was highest at the electrode produced with 10 scan cycles (Fig. S7B), which provided the most suitable thickness (14.8 nm) for the binding of albumin with the imprinted cavities. Hence, three scans and ten scans were used, respectively, for the preparation of the dual creatinine-albumin MIP sensor.

3.3.3. Template removal time

Oxalic acid (0.10 mol L^{-1}) was employed to remove both templates due to its ability to break the interaction in the MIP polymer such as the imine bond (C=N) formed between the template and *o*-PD [46,47]. Removal times of 15, 30, 60, 90, and 120 min were tested, and monitored by observing the increase in the SWV response of PMB and Fc, which indicated the removal of creatinine and albumin template from the polymer (Fig. S7C). The current responses increased with removal time up to 60 min and then became relatively stable, most likely due to the complete removal of template. Therefore 60 min was chosen as the optimal removal time for both templates.

3.4. Simultaneous determination of creatinine and albumin

The reliability of this dual MIP sensor for simultaneous determination of creatinine and albumin was investigated by comparing the

sensitivity of single analyte determination, selective determination, and simultaneous determination. The determination of creatinine and albumin singly was monitored via the SWV response of the dual MIP sensor to different concentrations of creatinine or albumin. When only creatinine (5.0–100 ng mL^{-1}) was present, rebinding on the creatinine sensor was indicated by the decrease in PMB current, while the Fc current response at the albumin sensor was relatively stable (Fig. 3A(a)). Similarly, for the determination of albumin singly (5.0–100 ng mL^{-1}), rebinding was only indicated at the albumin sensor, as shown by the decrease in Fc current and relatively stable PMB current (Fig. 3A(b)).

In the selective determination test, the concentration of one analyte was varied while the concentration of the other analyte was unchanged. The SWV responses of the dual MIP to mixtures of 50 ng mL^{-1} albumin and 5.0–100 ng mL^{-1} creatinine were observed. The PMB current decreased in proportion to the increases in creatinine concentration, while the response to 50 ng mL^{-1} albumin was almost unchanged (Fig. 3B(a)). This result showed that the presence of albumin will likely not interfere with creatinine determination. A similar behavior was shown by the SWV response to mixtures of 50 ng mL^{-1} creatinine and 5.0–100 ng mL^{-1} albumin (Fig. 3B(b)).

In the simultaneous determination study, the concentration of both targets was increased from 5.0 to 100 ng mL^{-1} . Both the PMB and Fc currents decreased gradually, and did not interfere with each other (Fig. 3C). There was no significant difference ($P > 0.05$) in the sensitivity of the three methods (Fig. 3D), which indicated that the selectivity of the dual MIP sensor was good and could allow for the simultaneous determination of creatinine and albumin since each sensor only responded to the intended target analyte.

3.5. Analytical performances

3.5.1. Linear range, limit of detection (LOD) and limit of quantification (LOQ)

The simultaneous determination of the two analytes was investigated between 5.0 and 2500 ng mL^{-1} (Fig. 4A). There were two linear ranges for creatinine, 5.0–100 ng mL^{-1} and 100–2500 ng mL^{-1} , and one for albumin, 5.0–100 ng mL^{-1} (Fig. 4B and C). For creatinine, the LOD was $1.5 \pm 0.2 \text{ ng mL}^{-1}$ ($3S_a/b$, where S_a is the standard deviation of the intercept, and b is the slope of the calibration curve [48]) and the LOQ was $5.1 \pm 0.7 \text{ ng mL}^{-1}$ ($10S_a/b$). For albumin, the LOD was $1.5 \pm 0.3 \text{ ng mL}^{-1}$ and the LOQ $5.2 \pm 0.3 \text{ ng mL}^{-1}$. The linear ranges and LOQs are acceptable for the determination of the ACR (creatinine = 0.30–3.00 mg mL^{-1} [49] and albumin $>0.3 \text{ mg mL}^{-1}$ [50]), because they allow dilution by up to 3000 times prior to analysis, which would reduce sample matrix effects.

3.5.2. Binding isotherm

The binding affinity of the dual MIP sensor toward creatinine and albumin was evaluated from the SWV responses of creatinine-albumin mixtures at concentrations of 5.0–4000 ng mL^{-1} . The obtained data were fitted to the Langmuir adsorption isotherm model [51] based on the following equation:

$$I_F = \frac{I_{\max}[F]}{K_D + [F]}$$

where I_F is the current response due to binding, $[F]$ is the concentration of creatinine or albumin (ng mL^{-1}), I_{\max} is the maximum current response at saturated binding, and K_D is the dissociation constant (ng mL^{-1}). The K_D values of the MIP and NIP sensors were determined based on the slope of the linear region of the curves of $1/I_F$ against $1/[F]$ (Figs. S8A and B). For creatinine, the K_D values for the MIP and NIP sensors were $43.7 \pm 7.9 \text{ ng mL}^{-1}$ and $91 \pm 11 \text{ ng mL}^{-1}$, respectively (Fig. S8A). These K_D values were close to those obtained from graph-fitting with GraphPad Prism 8 software, which were $39.8 \pm 2.5 \text{ ng mL}^{-1}$ and $96 \pm 12 \text{ ng mL}^{-1}$, respectively (Fig. S8C). For albumin, the K_D values for

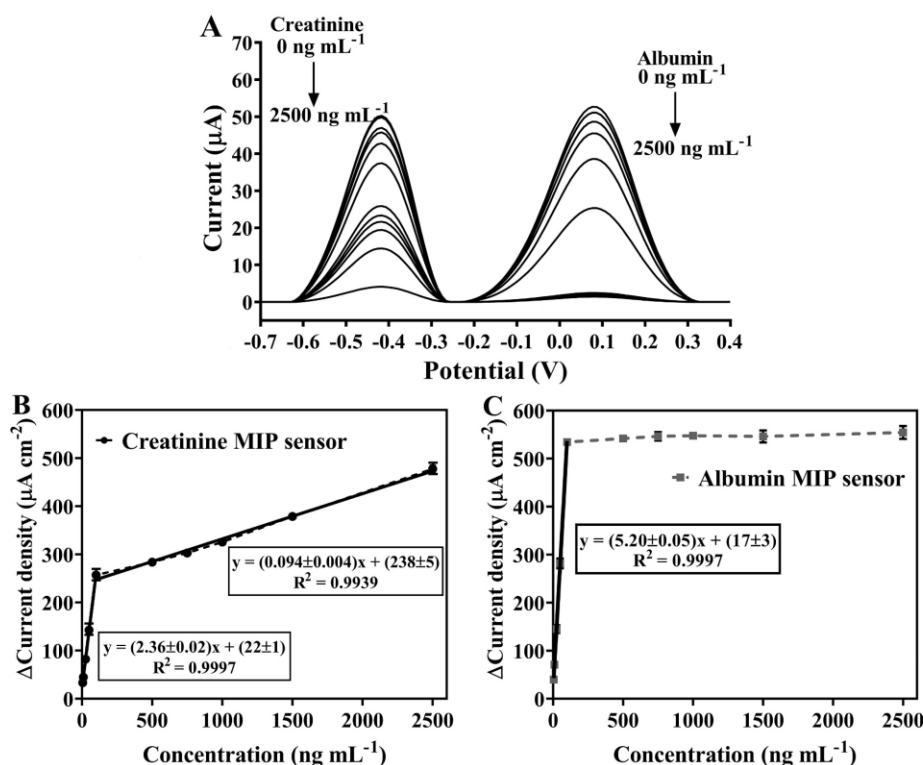


Fig. 4. (A) The SWV waveforms were obtained at the dual MIP sensor after the rebinding of creatinine and albumin mixtures in the range of 0–2500 ng mL⁻¹ in 0.050 mol L⁻¹ PBS (pH 7.40). Calibration plots were constructed for simultaneous determination at different concentrations of (B) creatinine and (C) albumin under optimal conditions.

the MIP and NIP sensors were 49.5 ± 2.3 ng mL⁻¹ and 90 ± 4 ng mL⁻¹, respectively (Fig. S8B). These values were also close to those from the graph-fitting, which were 44.6 ± 4.2 ng mL⁻¹ and 100 ± 11 ng mL⁻¹, respectively (Fig. S8D). The K_D s of the dual MIP sensor were more than two-fold lower than those of the dual NIP sensor, indicating that the dual MIP sensor had a much higher binding affinity for creatinine and albumin. Moreover, the K_D values of the proposed dual MIP sensor were much lower than those of other reported sensors, including a creatinine-MAA MIP K_D 8.3×10^3 ng mL⁻¹ [52], a creatinine-Al³⁺ MIP K_D 29.2×10^3 ng mL⁻¹ [53], a multi stimuli responsive (MSR) albumin-MIP K_D 166.7 ng mL⁻¹ [54] and a polyscopoletin-based albumin-MIP K_D 186.2×10^3 ng mL⁻¹ [55], indicated exceptional binding affinity.

3.5.3. Reproducibility

The reproducibility of the electrode fabrication was evaluated using six modified electrodes to determine mixtures of 5.0, 10, 25, 50 and 100 ng mL⁻¹ of creatinine and albumin. The relative standard deviations (RSDs) of the five concentrations were in the range of 1.2–4.5% for creatinine and 0.4–7.2% for albumin (Fig. S9). The RSDs were much better than the acceptable range of 32–45% for ng mL⁻¹ [56], indicating the excellent reliability of the modification process of the electrode.

3.5.4. Reusability and long-term stability

The reusability of the dual MIP sensor was investigated by repeatedly measuring mixtures of 500, 750, 1000, and 1500 ng mL⁻¹ of creatinine and 5.0, 10, 25, and 50 ng mL⁻¹ of albumin. After each cycle of

measurement, the dual MIP sensor was immersed for 30 min in 0.10 mol L⁻¹ oxalic acid with stirring to remove bound creatinine and albumin. After washing the sensor with 0.050 mol L⁻¹ PBS solution, the regenerated sensor was used for the next cycle of measurement. The relative sensitivities were stable up to seven cycles (a total of 84 measurements), with average sensitivities of $96 \pm 4\%$ (RSD of 4.5%) for creatinine and $98 \pm 2\%$ (RSD of 2.1%) for albumin (Fig. S10A). After seven cycles, sensitivity decreased to below 90%; most likely due to the loss of some of the modified layer, indicated by the reduced redox peaks of PMB and Fc after eight cycles (Figs. S10B and C).

The long-term stability of the modified electrodes was tested over nine weeks. The electrodes were stored in 0.050 mol L⁻¹ PBS pH 7.40 at room temperature, and one electrode was tested every week. The electrodes retained more than 90% of their sensitivity for seven weeks (Fig. S11A). The stability of the electrode was most likely due to the highly stable f-MWCNTs platform and the MIP layer. The reduced responses were most likely due to the loss of some of the redox probe activity. At 8 and 9 weeks, the observed decreases in the redox peak currents of PMB and Fc (Figs. S11B and C) were probably due to the hydrophilicity of PMB [57,58] which led to the swelling and disintegration of PEDOT:PSS during storage [59]. These results showed that the dual MIP sensor could be reused for several cycles of analyte binding and removal and had good storage stability.

3.5.5. Selectivity

The selectivity of the dual sensor was tested by comparing the change

in current density response to mixtures of 500 ng mL⁻¹ of creatinine and 50 ng mL⁻¹ of albumin (the middle of the linear range [60]) in the absence and presence of interferences typically found in the urine of CKD patients (Fig. 5). The response of the dual MIP sensor was much higher toward creatinine and albumin than toward the interferences. Moreover, the responses toward mixtures of the interferences and creatinine and albumin were not significantly different ($P > 0.05$ two-way ANOVA) to the responses toward creatinine and albumin alone. For comparison, the dual NIP sensor was tested and showed very low responses (Fig. S12) similar to the very low interference responses on the dual MIP sensor. These results showed that the sensor was highly selective toward creatinine and albumin.

3.5.6. Comparison with other sensors

The analytical performances of the dual MIP sensor were compared with those of other analytical methods and MIP electrochemical sensors for the determination of creatinine and albumin. Among the different methods that can analyze both analytes (Table 1(1–7)), the present sensor exhibits the lowest LOD, and only the present sensor enables the simultaneous determination of creatinine and albumin. LOQs and stability are good compared with other methods. Among the electrochemical sensors, the present sensor is the only one that can simultaneously measure creatinine and albumin in one scan with low LODs and LOQs (Table 1(6–18)). Although, the linear ranges of the proposed sensor are not wide, they are more than sufficient for the determination of creatinine and albumin in human urine samples with 3000x dilutions. This sensor also exhibits satisfactory storage stability at room temperature. Another advantage of the proposed sensor is the high binding affinity of the respective MIPs for creatinine and albumin. Compared to the only other work that reported the K_D of albumin MIP (Table 1(16)) [55], the proposed sensor demonstrated a very much lower K_D value: 49.5 ± 2.3 ng mL⁻¹ versus 186×10^3 ng mL⁻¹.

3.6. Analysis of real samples

The developed dual MIP sensor was applied to determine creatinine and albumin in human urine samples. The effect of the urine matrix was studied by comparing the calibration plots of both target analytes in standard solution and spiked sample solution. At 3000x dilutions, the matrix effect was not observed, as confirmed by two-way ANOVA ($P > 0.05$). The selectivity of the sensors together with their very low LODs, allowing thousands folds of dilution, helped to minimize the interfering effect of the matrix. Average recoveries were in the range of 93 ± 2 – $102 \pm 3\%$ for creatinine and 96 ± 4 – $105 \pm 2\%$ for albumin (Table S1). These

ranges are within the acceptable limits for analytical analysis in the mg mL⁻¹ concentration range, which are 80 and 110% [56]. Therefore, the determination of creatinine and albumin in human urine samples could be calculated from the calibration equation of the standard solution (Table 2). The creatinine concentrations determined by the proposed sensor were compared with the results obtained from the enzymatic method used by the hospital. No statistically significant difference was observed (the Student's t-test, $t = 1.432$, $p = 0.180$). Similarly, for albumin, there was no statistically significant difference between the results obtained from the proposed sensor and the immunoturbidimetric method used by the hospital (the Wilcoxon signed-rank test, $p = 0.469$).

Moreover, the ACR values obtained from the proposed sensor showed no statistically significant difference to those from the hospital method (Table 2) (the Student's t-test, $t = 0.321$, $p = 0.754$). The ACR is a measure of albuminuria in random urine samples, which is recommended by the global nonprofit organization Kidney Disease: Improving Global Outcomes (KDIGO) for monitoring the risk of CKD. Urine ACR categories <10–29, 30–300, and > 300 mg g⁻¹ are high normal, high, and very high, respectively [3,68]. The results indicated that the levels of albuminuria in five of the tested samples were likely to be normal, those of three were high, and the others very high.

4. Conclusions

An MIP dual electrochemical sensor was developed from a dual screen-printed carbon electrode with carboxylated multiwalled carbon nanotubes as a platform and *o*-phenylenediamine as a functional monomer. The simultaneous determination of creatinine and albumin in human urine was successfully performed without interferences between the two analytes. This sensor was able to perform the highly sensitive and selective simultaneous measurement of creatinine and albumin within the same square wave voltammetry scan with high reproducibility and good long-term stability. This dual MIP sensor was successfully applied for the measurement of urinary creatinine and albumin in the same sample to establish the albumin to creatinine ratio. The proposed sensor showed good reusability for a total of 84 measurements over seven cycles. The reusability of the sensor could be improved by increasing the stability of the redox probes. The developed dual MIP sensor would be potentially useful for the monitoring of CKD patients.

Declaration of competing interest

The authors declare that they have no known competing financial interests or personal relationships that could have appeared to influence

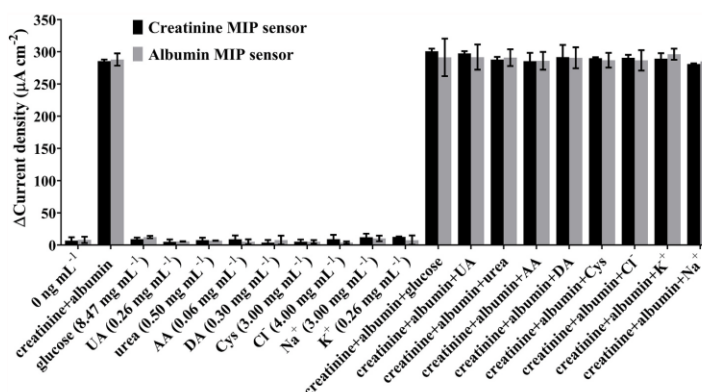


Fig. 5. Responses of the dual MIP sensor were produced in the presence of creatinine, albumin and various possible interferences. The relative current responses of analytes and mixtures with possible interferences were compared.

Table 1
A comparison of the performances of analytical methods for the determination of urine creatinine and albumin.

	Detection system	Method	Linear range (ng mL ⁻¹)		LOD (ng mL ⁻¹)		Detection	Incubation time	Stability	Ref.
			Albumin	Creatinine	Albumin	Creatinine				
1	SIA system	Spectrophotometry	0–2 × 10 ⁴	0–1 × 10 ⁵	600	3500	Non-simultaneous	–	–	[61]
2	Bromocresol green/Jaffé reaction PADS	Colorimetry	1 × 10 ⁵ –3.5 × 10 ⁶	1 × 10 ⁵ –3.5 × 10 ⁶	7100	5400	Non-simultaneous	30 s	–	[6]
3	Microfluidic sliding paper-based	Colorimetry	7500–1 × 10 ⁵	1 × 10 ⁵ –3 × 10 ⁶	5000	50000	Non-simultaneous	3 min	–	[8]
4	Drawing-PADS	Colorimetry	0–1 × 10 ⁶	0–3 × 10 ⁶	–	–	Non-simultaneous	15 min	2 months (room temperature)	[7]
5	GSH-CuNCs fluorescent probe	Fluorescence	300–10000	3390–113000	100	1469	Non-simultaneous	15 min	14 weeks (stored at 4 °C)	[9]
6	SPCE ABTS-CNT Nafion	CV	1000–1 × 10 ⁵	9.4 × 10 ⁴ –2.5 × 10 ⁶	–	–	Non-simultaneous	30 min	–	[10]
7	Creatinine sensor-albumin sensor	DPV	1 × 10 ⁴ –3 × 10 ⁵	1 × 10 ⁵ –2 × 10 ⁶	63000	93000	Non-simultaneous	3 min	50 days (creatinine sensor)	[11]
8	TMSPMA-GO-co-HEMA/MMA sensor	DPV	–	5000–30000	–	1878	–	2 min	–	[15]
9	CuO@MIP/CPE	Amperometry	–	56.5–22600	–	9.4	–	2 min	2 weeks (stored at 4 °C)	[62]
10	MIP/Au-SPE	DPV	–	0.1–1000	–	0.081	–	30 min	–	[63]
11	MIES/Fe ₃ O ₄ @PANI NPs	DPV	–	2.3–113	–	0.04	–	20 min	30 days (stored at 4 °C)	[64]
12	Ni@PANI/MGCEs	DPV	–	0.45–11.3 11.3–90.4	–	0.02	–	30 min	4 weeks	[16]
13	CoTe-GCE	CV	13–100	–	6	–	–	–	–	[13]
14	CNT/ABTS _(CV)	CV	1 × 10 ⁴ –1 × 10 ⁵	–	4000	–	–	–	>28 days, Reusability >5cycles	[14]
15	GE/AuNPs/PTH-MB/MIP	DPV	1.0 × 10 ⁻⁴ –100	–	3.0 × 10 ⁻⁵	–	–	20 min	25 days (stored at 4 °C)	[65]
16	HSA MIP film	CV	2 × 10 ⁴ –1 × 10 ⁵	–	3700	–	–	10 min	–	[55]
17	MIP-HSA chemosensor	DPV	800–2000	–	16.6	–	–	60 min	–	[66]
18	CS-AM-Grp-Fc-HSA MIP	DPV	0.1–1000	–	0.05	–	–	10 min	5 weeks (stored at room temperature)	[67]
19	Dual-MIP sensor	SWV	5.0–100	5.0–100 100–2500	1.5 ± 0.3	1.5 ± 0.2	Simultaneous	30 min	7 weeks (stored at room temperature)	This work

CV: cyclic voltammetry; CA: chronoamperometry; DPV: differential pulse voltammetry; SWV: square wave voltammetry.

Table 2
Results obtained with the dual MIP sensor (n = 3) and hospital method for determination of urinary creatinine and albumin. ACR values were also calculated and compared.

Sample	Creatinine		Albumin		ACR (mg g ⁻¹)	
	Found(mg mL ⁻¹)	Enzymatic method	Found(mg mL ⁻¹)	Immuno-turbidimetric	MIP sensor	Immuno-turbidimetric +Enzymatic method
1	0.138 ± 0.007	0.14	0.078 ± 0.008	0.078	568 ± 17	557
2	2.41 ± 0.06	2.44	0.054 ± 0.005	0.049	22.3 ± 2.5	20.1
3	1.84 ± 0.03	5.25	0.049 ± 0.002	0.048	27.1 ± 1.2	26.1
4	0.102 ± 0.004	0.10	0.049 ± 0.002	0.050	484 ± 20	485
5	0.79 ± 0.08	0.78	0.433 ± 0.009	0.434	552 ± 17	556
6	0.58 ± 0.03	0.61	0.132 ± 0.005	0.134	228 ± 8	220
7	1.35 ± 0.11	1.35	0.061 ± 0.003	0.063	45.6 ± 3.2	46.7
8	1.23 ± 0.13	1.21	0.210 ± 0.005	0.211	171 ± 15	175
9	1.22 ± 0.04	1.23	0.157 ± 0.005	0.157	129 ± 6	128
10	1.47 ± 0.25	1.52	0.992 ± 0.019	1.008	672.5 ± 47.6	663.2
11	1.92 ± 0.16	2.06	0.040 ± 0.004	0.042	20.8 ± 3.3	20.2
12	1.56 ± 0.13	1.55	0.011 ± 0.001	0.011	7.31 ± 1.2	7.1

the work reported in this paper.

Acknowledgements

This work was supported by an International Research Network grant (IRN62W0002) from Thailand Science Research and Innovation (TSRI). We would like to thank the Center of Excellence for Trace

Data availability

Data will be made available on request.

Analysis and Biosensor (TAB-CoE) and the Talent Management Project, Faculty of Science, Prince of Songkla University and the Center of Excellence for Innovation in Chemistry (PERCH-CIC). Financial support for Nur Indah Wardani, in the form of a scholarship from the Thailand's Education Hub for Southern Region of ASEAN Countries (TEH-AC 109/2016), is gratefully acknowledged. The authors would like to thank Thomas Duncan Coyne, Faculty of Science, Prince of Songkla University, Hat Yai, Songkhla, for proofreading the manuscript.

Appendix A. Supplementary data

Supplementary data to this article can be found online at <https://doi.org/10.1016/j.talanta.2023.124769>.

References

- [1] A.C. Webster, E.V. Nagler, R.L. Morton, P. Masson, Chronic kidney disease, *Lancet* 389 (10075) (2017) 1238–1252.
- [2] W.F. Keane, G. Eknoyan, Proteinuria, albuminuria, risk, assessment, detection, elimination (PARADE): a position paper of the National Kidney Foundation, *Am. J. Kidney Dis.* 33 (5) (1999) 1004–1010.
- [3] N.K. Foundation, K/DOQI clinical practice guidelines for chronic kidney disease: evaluation, classification, and stratification, *Am. J. Kidney Dis.* 39 (2 Suppl 1) (2002) S1–S266.
- [4] K. Inoue, E. Streja, T. Tsujimoto, H. Kobayashi, Urinary albumin-to-creatinine ratio within normal range and all-cause or cardiovascular mortality among U.S. adults enrolled in the NHANES during 1999–2015, *Ann. Epidemiol.* 55 (2021) 15–23.
- [5] M.B. Jensen, I. Viken, F. Høgh, K.K. Jacobsen, Quantification of urinary albumin and -creatinine: a comparison study of two analytical methods and their impact on albumin to creatinine ratio, *Clin. Biochem.* (2022).
- [6] S. Chaiyo, K. Kalcher, A. Apllux, O. Chailapakul, W. Siangproh, A novel paper-based colorimetry device for the determination of the albumin to creatinine ratio, *Analyst* 143 (22) (2018) 5453–5460.
- [7] R. Hiraoka, K. Kuwahara, Y.-C. Wen, T.-H. Yen, Y. Hiruta, C.-M. Cheng, D. Citterio, Paper-based device for naked eye urinary albumin/creatinine ratio evaluation, *ACS Sens.* 5 (4) (2020) 1110–1118.
- [8] S.-J. Chen, C.-C. Tseng, K.-H. Huang, Y.-C. Chang, L.-M. Fu, Microfluidic sliding paper-based device for point-of-care determination of albumin-to-creatinine ratio in human urine, *Biosensors* 12 (7) (2022).
- [9] S. Thammajinn, C. Buranachai, P. Kanatharana, P. Thavarungkul, C. Thammakhet-Buranachai, A copper nanoclusters probe for dual detection of microalbumin and creatinine, *Spectrochim. Acta Mol. Biomol. Spectrosc.* 270 (2021), 120816.
- [10] S.Y. Lee, H.Y. Lee, D.S. Ciou, Z.X. Liao, P.W. Huang, Y.T. Hsieh, Y.C. Wei, C.Y. Lin, M.D. Shieh, J.Y. Chen, A portable wireless urine detection system with power-efficient electrochemical readout ASIC and ABTS-CNT biosensor for UACR detection, *IEEE Transact. Biomed. Circuits Syst.* 15 (3) (2021) 537–548.
- [11] Y. Jia, G. Liu, G. Xu, X. Li, Z. Shi, C. Cheng, D. Xu, Y. Lu, Q. Liu, Battery-free and wireless tag for in situ sensing of urinary albumin/creatinine ratio (ACR) for the assessment of albuminuria, *Sensor. Actuator. B Chem.* 367 (2022), 132050.
- [12] J.J. BelBruno, Molecularly imprinted polymers, *Chem. Rev.* 119 (1) (2019) 94–119.
- [13] U. Saeed, B. Fatima, D. Hussain, R. Ashiq, M. Naeem Ashiq, M. Najam-ul-Haq, CoTe nanorods based electrochemical sensor for quantitative detection of albumin from chronic kidney disease patients, *J. Electroanal. Chem.* 906 (2022).
- [14] S.-Y. Lin, C.-Y. Lin, Electrochemically-functionalized CNT/ABTS nanozyme enabling sensitive and selective voltammetric detection of microalbuminuria, *Anal. Chim. Acta* 1197 (2022), 339517.
- [15] T.S. Anirudhan, J.R. Deepa, N. Stanly, Fabrication of a molecularly imprinted silylated graphene oxide polymer for sensing and quantification of creatinine in blood and urine samples, *Appl. Surf. Sci.* 466 (2019) 28–39.
- [16] H. Rao, Z. Lu, H. Ge, X. Liu, B. Chen, P. Zou, X. Wang, H. He, X. Zeng, Y. Wang, Electrochemical creatinine sensor based on a glassy carbon electrode modified with a molecularly imprinted polymer and a Ni@polyaniline nanocomposite, *Microchim. Acta* 184 (1) (2017) 261–269.
- [17] W. Zheng, M. Zhao, W. Liu, S. Yu, L. Niu, G. Li, H. Li, W. Liu, Electrochemical sensor based on molecularly imprinted polymer/reduced graphene oxide composite for simultaneous determination of uric acid and tyrosine, *J. Electroanal. Chem.* 813 (2018) 75–82.
- [18] T. Zhang, X. Xuan, M. Li, C. Li, P. Li, H. Li, Molecularly imprinted Ni-polyacrylamide-based electrochemical sensor for the simultaneous detection of dopamine and adenine, *Anal. Chim. Acta* 1202 (2022), 339689.
- [19] M. Johari-Ahmar, P. Karami, M. Ghanei, A. Afkhami, H. Bagheri, Development of a molecularly imprinted polymer tailored on disposable screen-printed electrodes for dual detection of EGFR and VEGF using nano-liposomal amplification strategy, *Biosens. Bioelectron.* 107 (2018) 26–33.
- [20] J. Liu, Y. Wang, X. Liu, Q. Yuan, Y. Zhang, Y. Li, Novel molecularly imprinted polymer (MIP) multiple sensors for endogenous redox couples determination and their applications in lung cancer diagnosis, *Talanta* 199 (2019) 573–580.
- [21] M. Wang, X. Cetó, M. del Valle, A novel electronic tongue using electropolymerized molecularly imprinted polymers for the simultaneous determination of active pharmaceutical ingredients, *Biosens. Bioelectron.* 198 (2022), 113807.
- [22] Y. Liu, G. Dykstra, Recent progress on electrochemical (bio)sensors based on aptamer-molecularly imprinted polymer dual recognition, *Sensor. Actuat. Rep.* 4 (2022), 100112.
- [23] E. Mazzotta, T. Di Giulio, C. Maltesta, Electrochemical sensing of macromolecules based on molecularly imprinted polymers: challenges, successful strategies, and opportunities, *Anal. Bioanal. Chem.* 414 (18) (2022) 5165–5200.
- [24] R.D. Crapnell, A. Hudson, C.W. Foster, K. Eersels, B.V. Grinsven, T.J. Cleij, C. E. Banks, M. Peeters, Recent advances in electrosynthesized molecularly imprinted polymer sensing platforms for bioanalyte detection, *Sensors* 19 (5) (2019).
- [25] T. Di Giulio, E. Mazzotta, C. Maltesta, Molecularly imprinted polycapotein for the electrochemical detection of the chronic disease marker lysozyme, *Biosensors* 11 (1) (2021).
- [26] C. Maltesta, E. Mazzotta, R.A. Picca, A. Poma, I. Chianella, S.A. Piletsky, MIP sensors – the electrochemical approach, *Anal. Bioanal. Chem.* 402 (5) (2012) 1827–1846.
- [27] M.A. Beluomini, J.L. da Silva, A.C. de Sá, E. Buffon, T.C. Pereira, N.R. Stradiotto, Electrochemical sensors based on molecularly imprinted polymer on nanostructured carbon materials: a review, *J. Electroanal. Chem.* 840 (2019) 343–366.
- [28] F. Huang, B. Zhu, H. Zhang, Y. Gao, C. Ding, H. Tan, J. Li, A glassy carbon electrode modified with molecularly imprinted poly(aniline boronic acid) coated onto carbon nanotubes for potentiometric sensing of sialic acid, *Microchim. Acta* 186 (5) (2019) 270.
- [29] M. Ni, Y. Xu, C. Wang, P. Zhao, P. Yang, C. Chen, K. Zheng, H. Wang, X. Sun, C. Li, Y. Xie, J. Fei, A novel thermo-controlled acetaminophen electrochemical sensor based on carboxylated multi-walled carbon nanotubes and thermosensitive polymer, *Diam. Relat. Mater.* 107 (2020), 107877.
- [30] M. Lovrić, Square-wave voltammetry, in: F. Scholz, A.M. Bond, R.G. Compton, D. A. Fiedler, G. Inzelt, H. Kahlert, S. Komorsky-Lovrić, H. Löhse, M. Lovrić, F. Marken, A. Neudeck, U. Retter, F. Scholz, Z. Stojek (Eds.), *Electroanalytical Methods: Guide to Experiments and Applications*, Springer Berlin Heidelberg, Berlin, Heidelberg, 2010, pp. 121–145.
- [31] G. Cui, J.H. Yoo, J.S. Lee, J. Yoo, J.H. Uhm, G.S. Cha, H. Nam, Effect of pre-treatment on the surface and electrochemical properties of screen-printed carbon paste electrodes, *Analyst* 126 (8) (2001) 1399–1403.
- [32] X. Xiao, B. Zhou, L. Tan, H. Tang, Y. Zhang, Q. Xie, S. Yao, Poly(methylene blue) doped silica nanocomposites with crosslinked cage structure: electropolymerization, characterization and catalytic activity for reduction of dissolved oxygen, *Electrochim. Acta* 56 (27) (2011) 10055–10063.
- [33] S. Khumgern, P. Thavarungkul, P. Kanatharana, A. Numnuam, Molecularly imprinted electrochemical sensor based on poly(o-phenylenediamine-co-o-aminophenol) incorporated with poly(styrenesulfonate) doped poly(3,4-ethylenedioxythiophene) ferrocene composite modified screen-printed carbon electrode for highly sensitive and selective detection of prostate cancer biomarker, *Microchem. J.* 177 (2022), 107311.
- [34] R.A.S. Couto, S.S. Costa, B. Mounsef, J.G. Pacheco, E. Fernandes, F. Carvalho, C.M. P. Rodrigues, C. Delerue-Matos, A.A.C. Braga, L. Moreira Gonçalves, M.B. Quinaz, Electrochemical sensing of ecstasy with electropolymerized molecularly imprinted poly(o-phenylenediamine) polymer on the surface of disposable screen-printed carbon electrodes, *Sensor. Actuator. B Chem.* 290 (2019) 378–386.
- [35] K. Phonklam, R. Wannapob, W. Sriwimol, P. Thavarungkul, T. Phairatana, A novel molecularly imprinted polymer PMB/MWNTs sensor for highly-sensitive cardiac troponin T detection, *Sensor. Actuator. B Chem.* 308 (2020), 127630.
- [36] J. Sittiwong, F. Unob, Detection of urinary creatinine using gold nanoparticles after solid phase extraction, *Spectrochim. Acta Mol. Biomol. Spectrosc.* 138 (2015) 381–386.
- [37] A. Esokkiya, S. Sudalaimani, K. Sanjeev Kumar, P. Sampathkumar, C. Suresh, K. Giribabu, Poly(methylene blue)-based electrochemical platform for label-free sensing of acrylamide, *ACS Omega* 6 (14) (2021) 9528–9536.
- [38] Y. Itano, H. Sobajima, N. Ohashi, T. Shibata, A. Fujiya, T. Nagata, M. Ando, T. Imaizumi, Y. Kubo, T. Ozeki, T. Katsuno, S. Kato, Y. Yasuda, S. Maruyama, High urinary glucose is associated with improved renal prognosis in patients with diabetes mellitus, *J. Diabetes Investig.* 12 (6) (2021) 998–1006.
- [39] H. Kanno, E. Kanda, A. Sato, K. Sakamoto, Y. Kanno, Estimation of daily protein intake based on spot urine urea nitrogen concentration in chronic kidney disease patients, *Clin. Exp. Nephrol.* 20 (2) (2016) 258–264.
- [40] F. Li, H. Guo, J. Zou, C. Fu, S. Liu, J. Xiao, Z. Ye, Clinical classification of hyperuricemia in patients with chronic kidney disease, *Int. Urol. Nephrol.* 53 (8) (2021) 1665–1674.
- [41] R. García-González, A. Costa-García, M.T. Fernández-Abedul, Dual screen-printed electrodes with elliptic working electrodes arranged in parallel or perpendicular to the strip, *Sensor. Actuator. B Chem.* 198 (2014) 302–308.
- [42] T.L. Panasyuk, V.M. Mirsky, S.A. Piletsky, O.S. Wolfbeis, Electropolymerized molecularly imprinted polymers as receptor layers in capacitive chemical sensors, *Anal. Chem.* 71 (20) (1999) 4609–4613.
- [43] D. Du, S. Chen, J. Cai, Y. Tao, H. Tu, A. Zhang, Recognition of dimethoate carried by bi-layer electrodeposition of silver nanoparticles and imprinted poly(o-phenylenediamine), *Electrochim. Acta* 53 (22) (2008) 6589–6595.
- [44] M.G. Cho, S. Hyeon, K.K. Park, S.H. Chough, Characterization of hydrogel type molecularly imprinted polymer for creatinine prepared by precipitation polymerization, *Polymer* 237 (2021), 124348.
- [45] M.A. Kiselev, I. Gryzunov, G.E. Dobretsov, M.N. Komarova, [Size of a human serum albumin molecule in solution], *Biofizika* 46 (3) (2001) 423–427.

- [46] T. Zhang, W. Zhang, L. Liu, Y. Chen, Simultaneous detection of site-specific histone methylations and acetylation assisted by single template oriented molecularly imprinted polymers, *Analyst* 145 (4) (2020) 1376–1383.
- [47] Y. Hao, R. Gao, D. Liu, B. Zhang, Y. Tang, Z. Guo, Preparation of biocompatible molecularly imprinted shell on superparamagnetic iron oxide nanoparticles for selective depletion of bovine hemoglobin in biological sample, *J. Colloid Interface Sci.* 470 (2016) 100–107.
- [48] B.M.a.U. Ö (Ed.), *Eurachem Guide: the Fitness for Purpose of Analytical Methods – A Laboratory Guide to Method Validation and Related Topics*, second ed. 2014, 2014.
- [49] D.B. Barr, L.C. Wilder, S.P. Caudill, A.J. Gonzalez, L.L. Needham, J.L. Pirkle, Urinary creatinine concentrations in the U.S. population: implications for urinary biologic monitoring measurements, *Environ. Health Perspect.* 113 (2) (2005) 192–200.
- [50] P.E. de Jong, R.T. Gansevoort, S.J. Bakker, Macroalbuminuria and microalbuminuria: do both predict renal and cardiovascular events with similar strength? *J. Nephrol.* 20 (4) (2007) 375–380.
- [51] R.J. Ansell, Characterization of the binding properties of molecularly imprinted polymers, in: B. Mattiasson, L. Ye (Eds.), *Molecularly Imprinted Polymers in Biotechnology*, Springer Int Publishing Ag, Cham, 2015, pp. 51–93.
- [52] C. Miura, N. Funaya, H. Matsunaga, J. Haginaka, Monodisperse, molecularly imprinted polymers for creatinine by modified precipitation polymerization and their applications to creatinine assays for human serum and urine, *J. Pharmaceut. Biomed. Anal.* 85 (2013) 288–294.
- [53] Q.Y. Ang, M.H. Zolkeflay, S.C. Low, Configuration control on the shape memory stiffness of molecularly imprinted polymer for specific uptake of creatinine, *Appl. Surf. Sci.* 369 (2016) 326–333.
- [54] J. Zhang, Y. Hao, X. Tian, Y. Liang, X. He, R. Gao, L. Chen, Y. Zhang, Multi-stimuli responsive molecularly imprinted nanoparticles with tailorable affinity for modulated specific recognition of human serum albumin, *J. Mater. Chem. B* (2022).
- [55] Z. Stojanovic, J. Erdőssy, K. Keltai, F.W. Scheller, R.E. Gyurcsányi, Electrosynthesized molecularly imprinted polyscopoletin nanofilms for human serum albumin detection, *Anal. Chim. Acta* 977 (2017) 1–9.
- [56] I. Taverniers, M. De Loose, E. Van Bockstaele, Trends in quality in the analytical laboratory. II. Analytical method validation and quality assurance, *TrAC, Trends Anal. Chem.* 23 (8) (2004) 535–552.
- [57] S. Kakhki, M.M. Barsan, E. Shams, C.M.A. Brett, Development and characterization of poly(3,4-ethylenedioxythiophene)-coated poly(methylene blue)-modified carbon electrodes, *Synth. Met.* 161 (23) (2012) 2718–2726.
- [58] L. Abad-Gil, C.M.A. Brett, Poly(methylene blue)-ternary deep eutectic solvent/Au nanoparticle modified electrodes as novel electrochemical sensors: optimization, characterization and application, *Electrochim. Acta* 434 (2022), 141295.
- [59] Z. Wang, J. Xu, Y. Yao, L. Zhang, Y. Wen, H. Song, D. Zhu, Facile preparation of highly water-stable and flexible PEDOT:PSS organic/inorganic composite materials and their application in electrochemical sensors, *Sensor. Actuator. B Chem.* 196 (2014) 357–369.
- [60] D.R. Thévenot, K. Toth, R.A. Durst, G.S. Wilson, Electrochemical biosensors: recommended definitions and classification, International union of pure and applied Chemistry: physical Chemistry division, commission I.7 (biophysical Chemistry); analytical Chemistry division, commission V.5 (electroanalytical Chemistry), *Biosens. Bioelectron.* 16 (1) (2001) 121–131.
- [61] W. Siangproh, N. Teshima, T. Sakai, S. Katoh, O. Chailapakul, Alternative method for measurement of albumin/creatinine ratio using spectrophotometric sequential injection analysis, *Talanta* 79 (4) (2009) 1111–1117.
- [62] N. Nontawong, M. Amatatongchai, S. Thimoonnee, S. Laosing, P. Jarujamrus, C. Karuwan, S. Chairam, Novel amperometric flow-injection analysis of creatinine using a molecularly-imprinted polymer coated copper oxide nanoparticle-modified carbon-paste-electrode, *J. Pharmaceut. Biomed. Anal.* 175 (2019), 112770.
- [63] A. Diouf, S. Motia, N. El Alami El Hassani, N. El Bari, B. Bouchikhi, Development and characterization of an electrochemical biosensor for creatinine detection in human urine based on functional molecularly imprinted polymer, *J. Electroanal. Chem.* 788 (2017) 44.
- [64] T. Wen, W. Zhu, C. Xue, J. Wu, Q. Han, X. Wang, X. Zhou, H. Jiang, Novel electrochemical sensing platform based on magnetic field-induced self-assembly of Fe₃O₄@Polyaniline nanoparticles for clinical detection of creatinine, *Biosens. Bioelectron.* 56 (2014) 180–185.
- [65] G. Zhang, Y. Yu, M. Guo, B. Lin, L. Zhang, A sensitive determination of albumin in urine by molecularly imprinted electrochemical biosensor based on dual-signal strategy, *Sensor. Actuator. B Chem.* 288 (2019) 564–570.
- [66] M. Cieplak, K. Szwabinska, M. Sosnowska, B.K.C. Chandra, P. Borowicz, K. Noworyta, F. D'Souza, W. Kutner, Selective electrochemical sensing of human serum albumin by semi-covalent molecular imprinting, *Biosens. Bioelectron.* 74 (2015) 960–966.
- [67] A. Fatoni, A. Numnuam, P. Kanatharana, W. Limbut, P. Thavarungkul, A novel molecularly imprinted chitosan-acrylamide, graphene, ferrocene composite cryogel biosensor used to detect microalbumin, *Analyst* 139 (23) (2014) 6160–6167.
- [68] A.S. Levey, J. Coresh, Chronic kidney disease, *Lancet* 379 (9811) (2012) 165–180.

Supplementary data

Molecularly imprinted polymer dual electrochemical sensor for the one-step determination of albuminuria to creatinine ratio (ACR)

Nur Indah Wardani^{a, b, c}, Proespichaya Kanatharana^{a, b, c}, Panote Thavarungkul^{a, b, c}, and Warakorn Limbut^{a, c, d *}

^a Center of Excellence for Trace Analysis and Biosensor, Prince of Songkla University, Hat Yai, Songkhla, 90110, Thailand

^b Division of Physical Science, Faculty of Science, Prince of Songkla University, Hat Yai, Songkhla 90110, Thailand

^c Center of Excellence for Innovation in Chemistry, Faculty of Science, Prince of Songkla University, Hat Yai, Songkhla 90110, Thailand

^d Division of Health and Applied Sciences, Faculty of Science, Prince of Songkla University, Hat Yai, Songkhla, 90110, Thailand

** Corresponding author at: Division of Health and Applied Sciences, Faculty of Science, Prince of Songkla University, Hat Yai, Songkhla 90110, Thailand*

Tel.: +66 74 288563; fax: +66 74 4481

E-mail address: warakorn.l@psu.ac.th (W. Limbut).

S1. Surface morphology characterization

The surface morphologies of the modified electrode were observed by scanning electron microscopy.

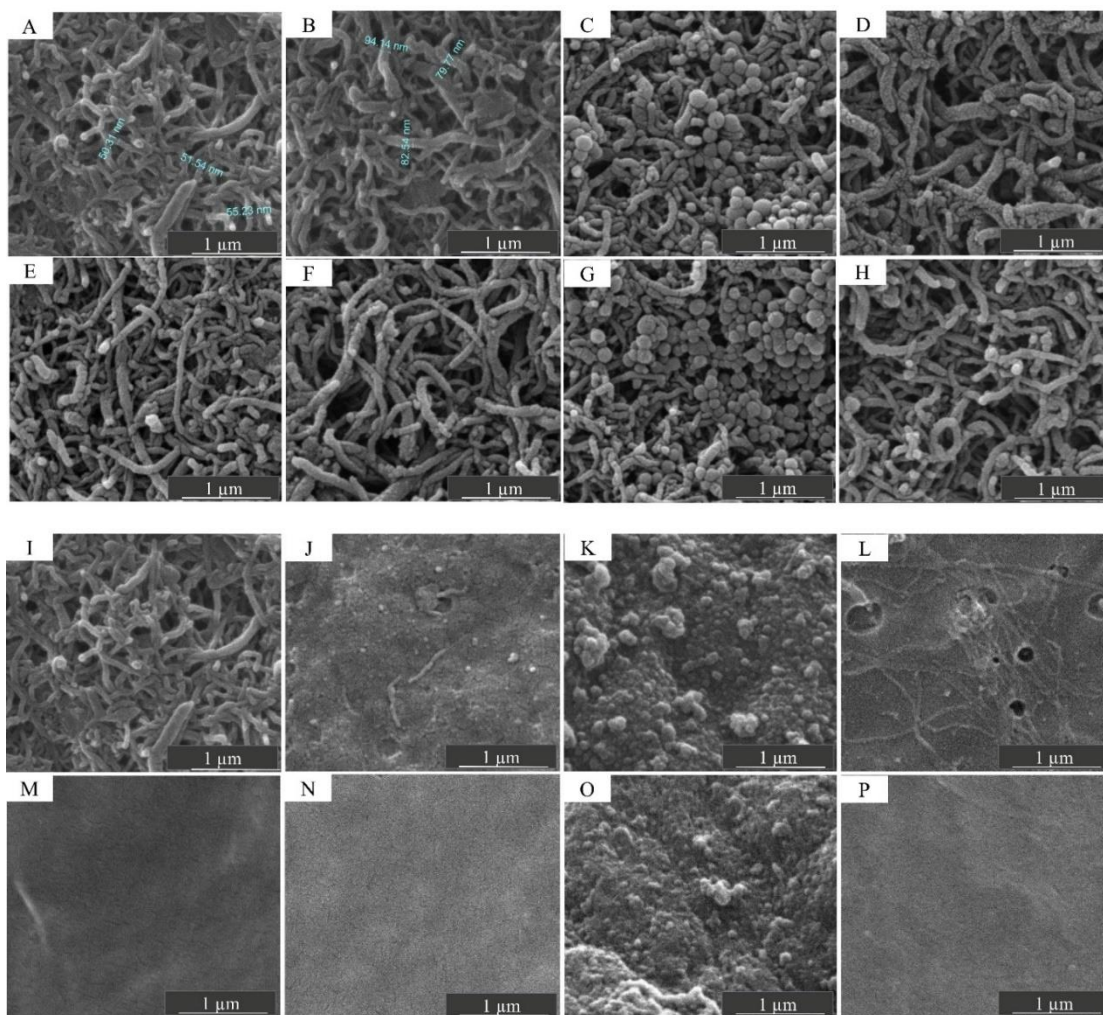
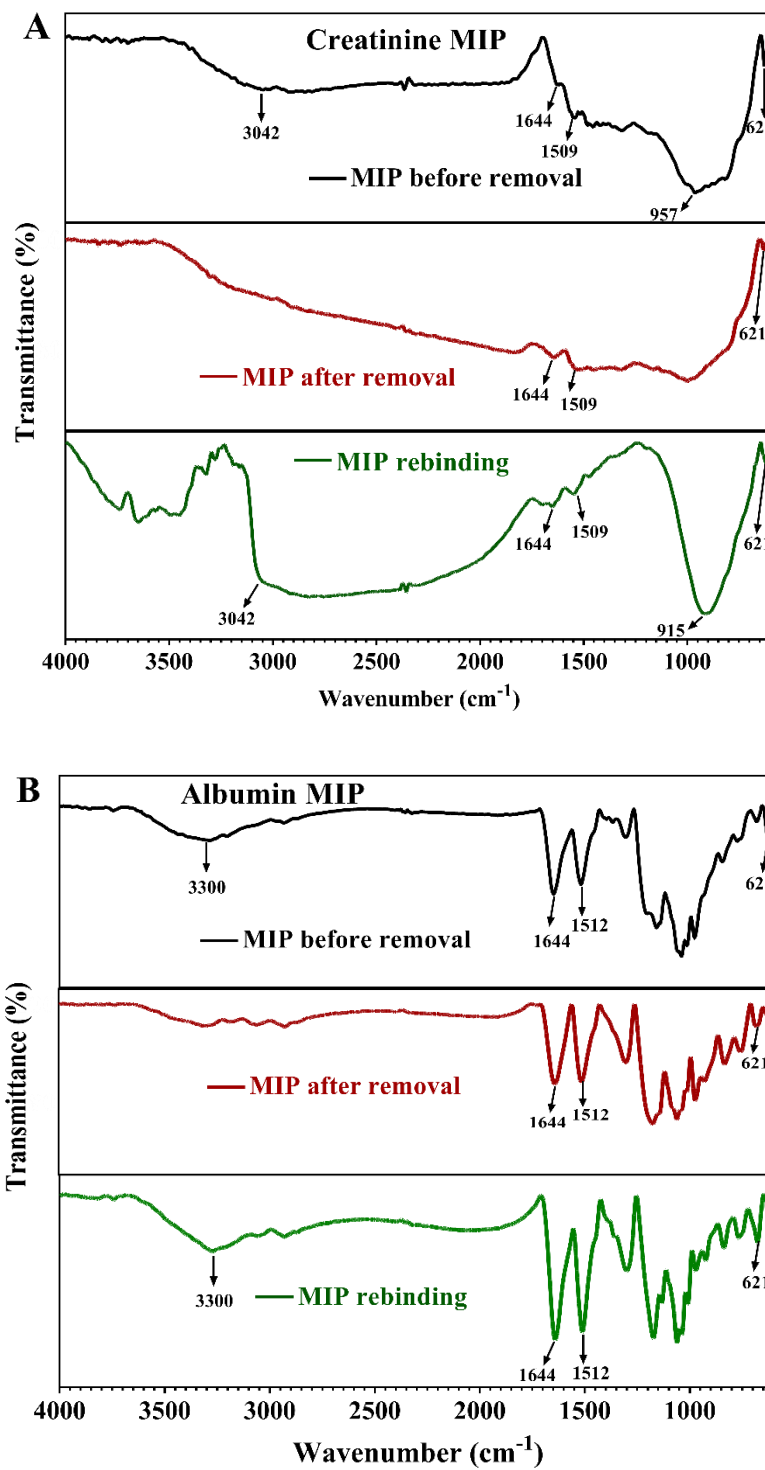


Fig. S1. SEM images A to D show the stepwise modification of an MIP/PMB/f-MWCNTs/SPCE for sensing creatinine: (A) f-MWCNTs/SPCE, (B) PMB/f-MWCNTs/SPCE, (C) MIP/PMB/f-MWCNTs/SPCE before template removal, and (D) after template removal; (E) NIP/PMB/f-MWCNTs/SPCE before removal and (F) after removal; (G) MIP/PMB/f-MWCNTs/SPCE after rebinding of 0.1 mg mL^{-1} creatinine and (H) NIP/PMB/f-MWCNTs/SPCE after rebinding of 0.1 mg mL^{-1} creatinine. SEM images I to L show the stepwise modification of an MIP/Fc/f-MWCNTs/SPCE for sensing albumin: (I) f-MWCNTs/SPCE, (J) Fc/f-MWCNTs/SPCE, (K) MIP/Fc/f-MWCNTs/SPCE before template removal and (L) after template removal; (M) NIP/Fc/f-MWCNTs/SPCE before template removal, and (N) after template removal; (O) MIP/Fc/f-MWCNTs/SPCE after rebinding of 0.1 mg mL^{-1} albumin and (P) NIP/Fc/f-MWCNTs/SPCE after rebinding of 0.1 mg mL^{-1} albumin.

S2. Fourier transform infrared (FT-IR) spectroscopy of MIP and NIP modified electrodes



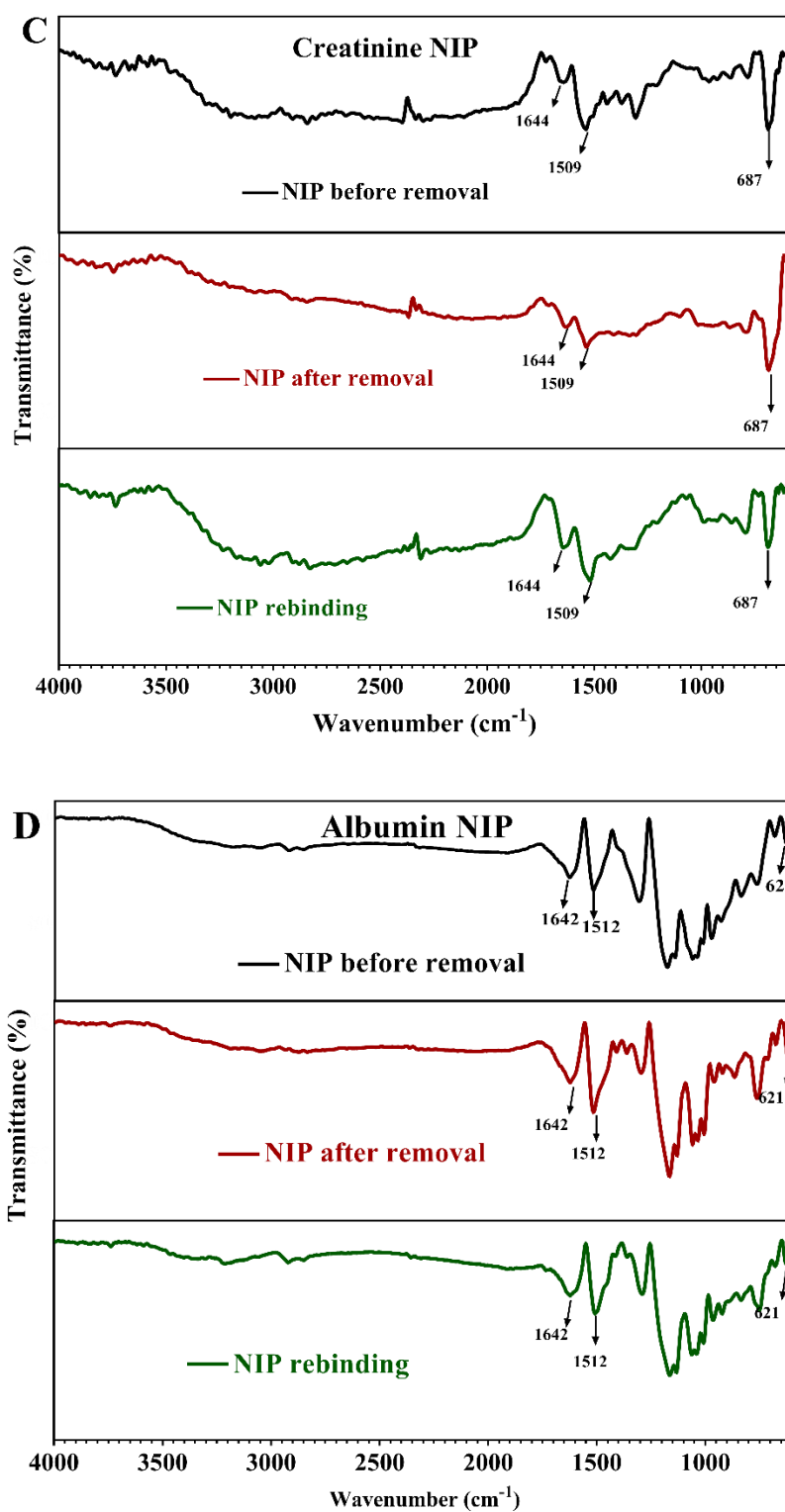


Fig.S2. The FT-IR characterization of MIP and NIP before removal, after removal, and rebinding. FT-IR spectra (A) creatinine MIP, (B) albumin MIP, (C) creatinine, and (D) albumin NIP.

The characteristic peaks of o-PD were displayed by the stretching vibration of C=C at 1509-1512 cm^{-1} , C=N at $\sim 1642\text{-}1644$ cm^{-1} , at $\sim 621\text{-}687$ cm^{-1} for the C-H bending vibration on the benzene ring [1, 2]. Before template removal, the stretching vibration at $\sim 915\text{-}957$ cm^{-1} of N-H, a broad absorption at 3042 cm^{-1} representing O-H bands corresponding to the creatinine template [3, 4] (**Fig. S2A**) and the vibration bands of albumin template at 3300 cm^{-1} related to protein amide band [5, 6] (**Fig. S2B**) were observed. Following the template removal, the characteristic peak of creatinine and albumin disappeared, demonstrating that the templates were removed. After the rebinding, the vibration bands of creatinine and albumin reappeared, due to the reoccupation of the cavities by both analytes. The creatinine (**Fig. S2C**) and albumin NIPs (**Fig. S2D**) exhibited only the same vibration bands corresponding to the functional monomer on every steps. These results confirm the formation of imprinted sites in the creatinine MIP and albumin MIP.

S3. Cyclic voltammetric responses of the modified electrodes

The preparation steps of the creatinine and albumin MIP sensors were monitored by observing the electrochemical behavior of PMB and Fc on the creatinine and albumin electrodes, respectively. They were studied separately in 0.050 mol L⁻¹ PBS (pH 7.40). The f-MWCNTs/SPCE provided a larger background current because f-MWCNTs enlarged the surface area and increased the conductivity of the electrode surface. The polymerization of the non-conductive PoPD on the electrodes reduced the redox peaks of PMB and Fc by blocking electron transfer. Template removal exposed the recognition cavities, increasing the current response, which decreased after the rebinding of the target analytes.

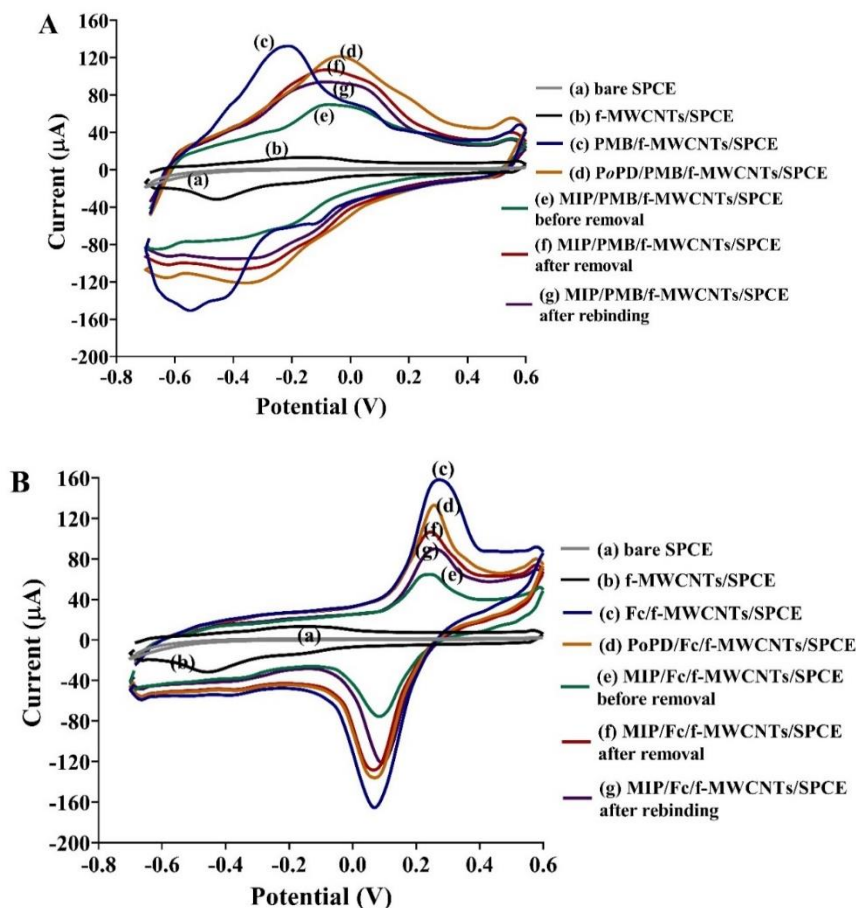


Fig. S3. CVs were produced in 0.050 mol L⁻¹ PBS (pH 7.40) at various electrodes tested during modification. (A) shows CVs of electrodes modified to detect creatinine and (B) shows CVs of electrodes modified to detect albumin. Rebinding condition: 500 ng mL⁻¹ creatinine and 50 ng mL⁻¹ albumin in PBS (pH 7.40).

S4. EIS response of the modified electrode

Each modification step of the creatinine and albumin electrodes was monitored by fitting the data to a Randles equivalent circuit. The semicircles in the Nyquist plots were used to calculate the electron transfer resistance (R_{ct}) of the electrode at each step of modification. The impedance of the circuit indicates the resistance of the electrode surface against electron transfer to and from the redox probe [1].

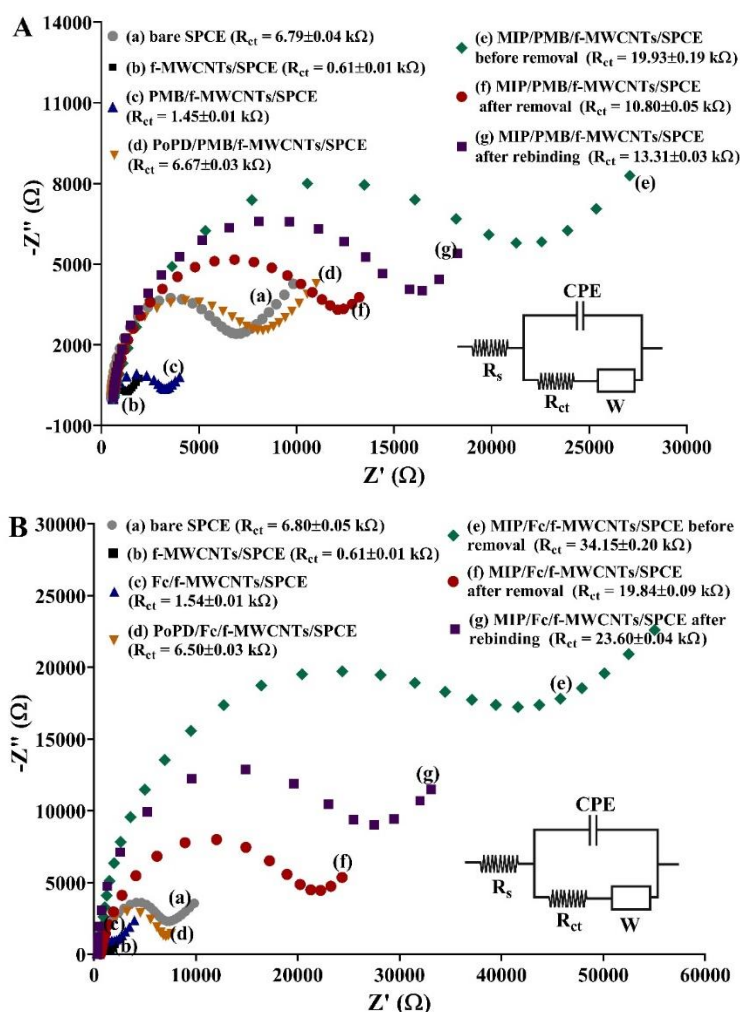


Fig. S3. EIS spectra were produced in $5.0 \text{ mM Fe(CN)}_6^{3-/4-}$ solution. The spectra show the resistance of various electrodes during modification. (A) shows EIS spectra of electrodes modified to detect creatinine, and (B) shows EIS spectra of electrodes modified to detect albumin. Inset: Randles equivalent circuit composed of the solution resistance (R_s), charge transfer resistance (R_{ct}), constant phase element (CPE) and the Warburg impedance (Z_w). Rebinding condition: 500 ng mL^{-1} creatinine and 50 ng mL^{-1} albumin in PBS (pH7.40).

S5. Electrode configuration

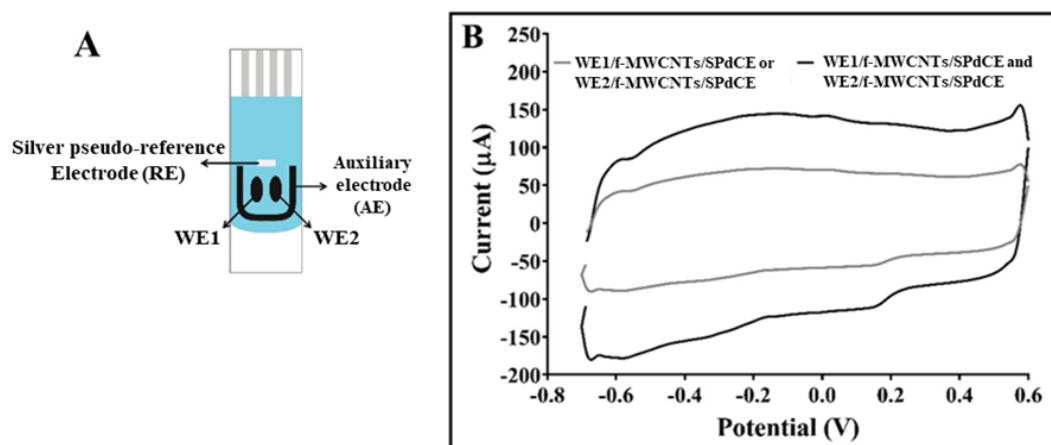


Fig. S5. (A) Schematic of the screen-printed carbon electrode (SPCE), showing the dual working electrodes (WE1 and WE2). (B) CVs were produced in 0.050 mol L^{-1} PBS (pH 7.40) at the f-MWCNTs/SPdCE when only WE1 or WE2 was connected, and when WE1 and WE2 were connected together.

S6. Optimization of the amount of f-MWCNTs

Larger loadings of f-MWCNTs increased the effective surface area (**Fig. S6B**) for the deposition of redox probes (Fc and PMB) and the MIP layer. The area was calculated using the Randle-Sevcik equation (Eq.1) [2] from the data of **Fig. S6A**.

$$I_{p,a} = (2.69 \times 10^5) n^{3/2} A C D^{1/2} v^{1/2} \quad (1)$$

where $I_{p,a}$ is the peak current (A), n is the number of electrons transferred (1), A is the electrode area (cm^2), C is the concentration of $\text{Fe}(\text{CN})_6^{3-/4-}$ solution (0.10 mol cm^{-3}), D is the diffusion coefficient ($7.6 \times 10^{-6} \text{ cm}^2 \text{ s}^{-1}$) [3] and v is the scan rate (0.050 V s^{-1}).

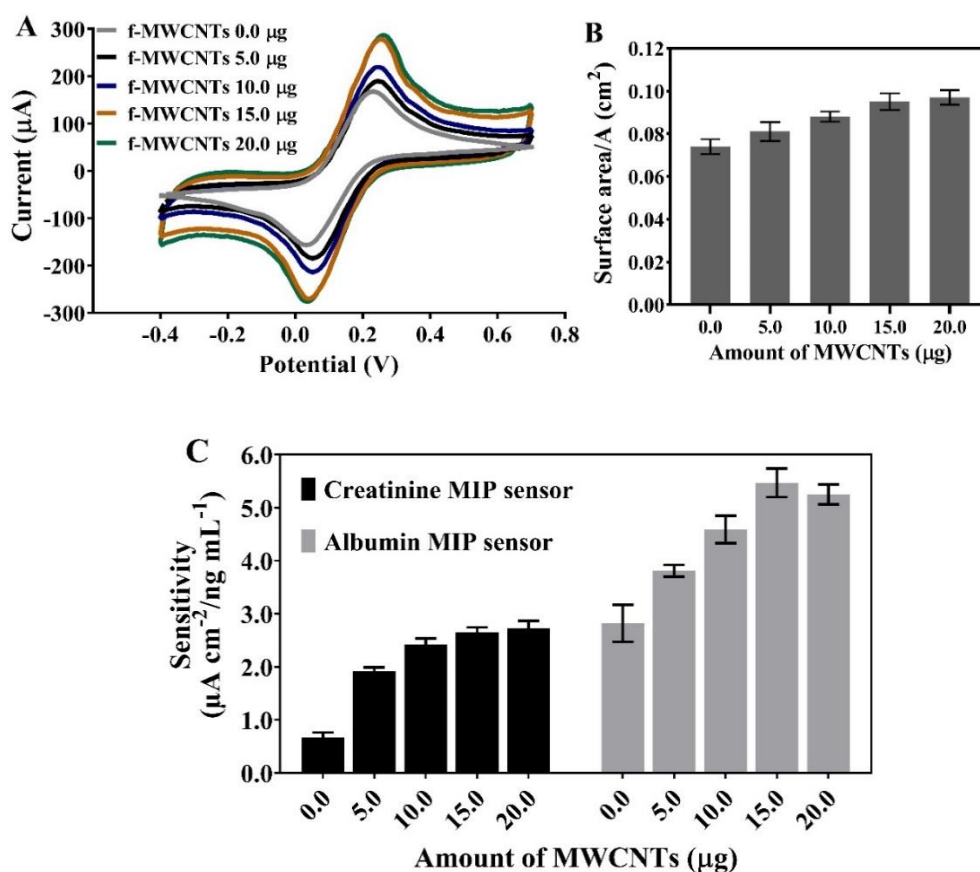


Fig. S6. (A) The CVs were produced by 10 mM $\text{Fe}(\text{CN})_6^{3-/4-}$ at the f-MWCNTs/SPCE at a scan rate of 0.050 V s^{-1} . (B) The effective surface area was calculated for electrodes fabricated with different amounts of f-MWCNTs. (C) sensitivity of electrodes fabricated with different amounts of f-MWCNTs was calculated toward mixtures of 5.0–100 ng mL^{-1} creatinine and albumin in 0.050 mol L^{-1} PBS (pH 7.40).

S7. Optimization of MIP layer thickness and template removal time

The cyclic voltammetric response observed during five scans of electropolymerization is shown in **Fig. S7A**. The charges used in each scan were added to estimate the MIP layer thickness. The number of electropolymerization scans that produced the optimal MIP layer thickness was determined based on the obtained sensitivity (**Fig. S7B**). To optimize template removal time, the dual MIP sensor was immersed in 0.10 mol L⁻¹ oxalic acid for 15, 30, 60, 90, and 120 min. A stable current response indicated the removal of the template. The current responses increased with time and were stable from 60 min on (**Fig. S7C**).

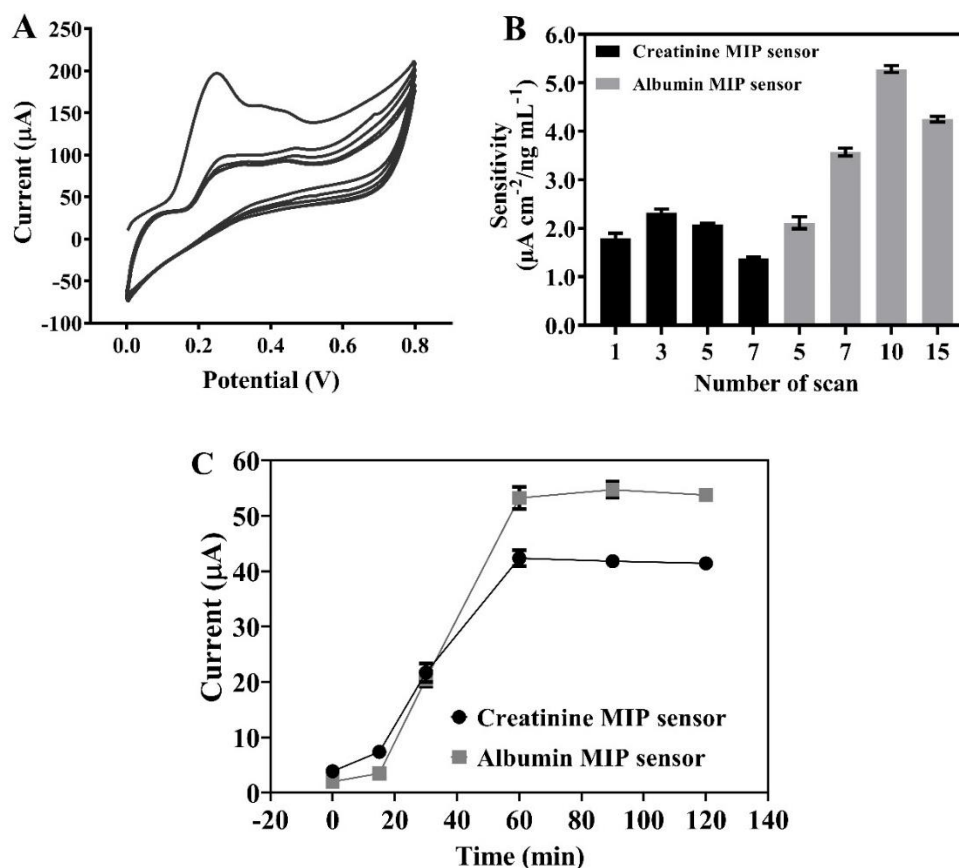


Fig. S7. (A) The CVs were produced by five scans of electropolymerization of 5.0 mmol L⁻¹ *o*-PD in 0.20 mol L⁻¹ acetate buffer at pH 5.20 at a scan rate of 50 mV s⁻¹. (B) The chart shows the effect of the number of electropolymerization scans on the sensitivity of creatinine and albumin (mixture 5.0-100 ng mL⁻¹) determination in 0.050 mol L⁻¹ PBS (pH 7.40). (C) The chart shows the current response of the dual MIP sensor at different template removal times.

S8. Binding Isotherm

The dissociation constant (K_D) of creatinine and albumin binding to each modified electrode was obtained by plotting the current response and concentration of both analytes and fitting the data with the Langmuir isotherm using GraphPad Prism 8.

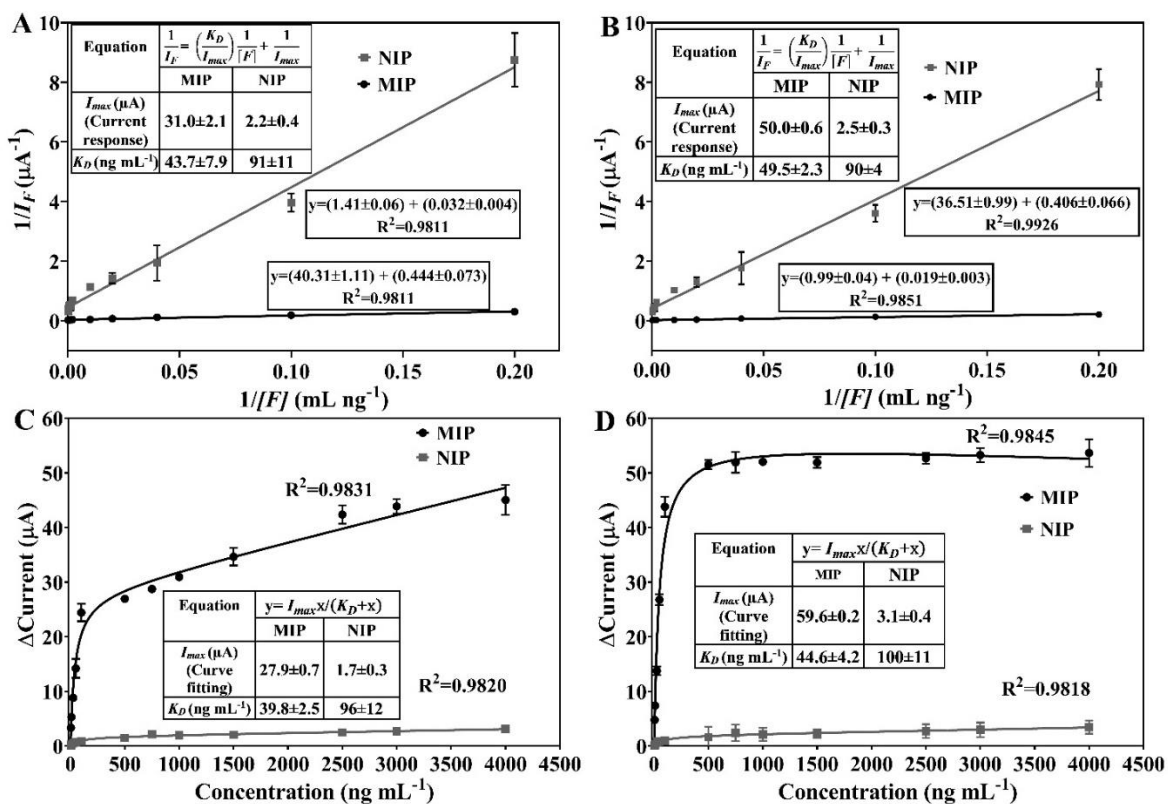


Fig. S8. The linearized Langmuir plots of $1/I_F$ vs. $1/[F]$ show of (A) creatinine and (B) albumin at the MIP and NIP sensors. Plots of the change in current response vs. concentration of (C) creatinine and (D) albumin at the MIP and NIP sensors were fitted with the Langmuir isotherm using GraphPad Prism 8.

S9. Reproducibility

The reproducibility of the preparation of the dual MIP sensor was observed from the current response of six electrodes.

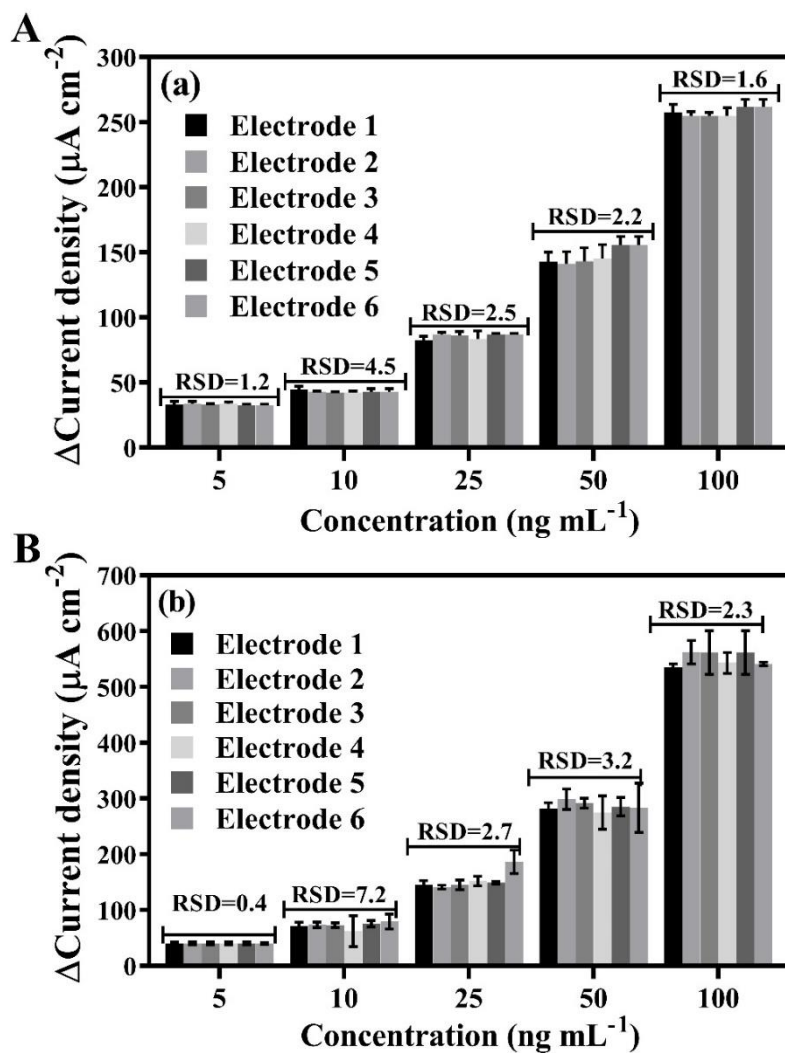


Fig. S9. The charts show the reproducibility of different electrode preparations of (A) the creatinine MIP sensor and (B) the albumin MIP sensor at different mixture concentrations of creatinine and albumin (5.0–100 ng mL⁻¹) in 0.050 mol L⁻¹ PBS at pH 7.40.

S10. Reusability

The reusability (**Fig. S10**) of the dual sensor was evaluated by comparing the sensitivity obtained from each cycle to the sensitivity obtained during the first cycle.

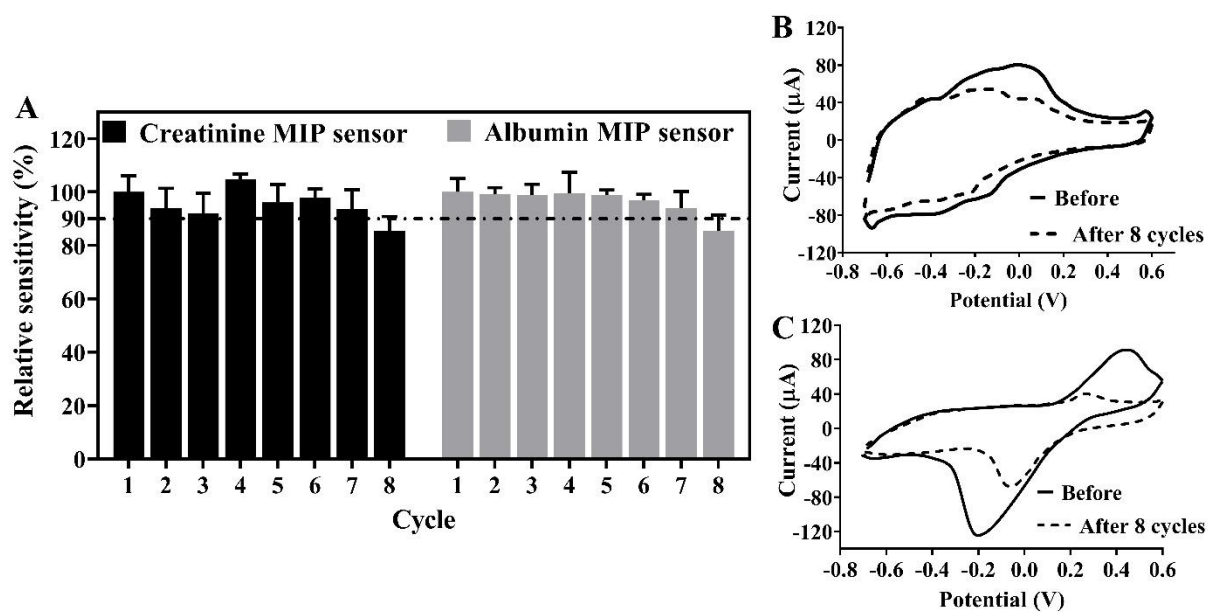


Fig. S10. (A) The sensitivities were obtained from repeatedly measuring mixtures of creatinine ($500, 750, 1000,$ and 1500 ng mL^{-1}) and albumin ($5.0, 10, 25,$ and 50 ng mL^{-1}) in 0.050 mol L^{-1} PBS at pH 7.40. The CVs are of (B) PMB and (C) Fc after eight cycle of creatinine and albumin measurement in 0.050 mol L^{-1} PBS pH 7.40

S11. Long-term stability

The long-term stability of the proposed sensor was evaluated by comparing sensitivity obtained from successive cycles of measurement and regeneration to the sensitivity obtained from the first cycle.

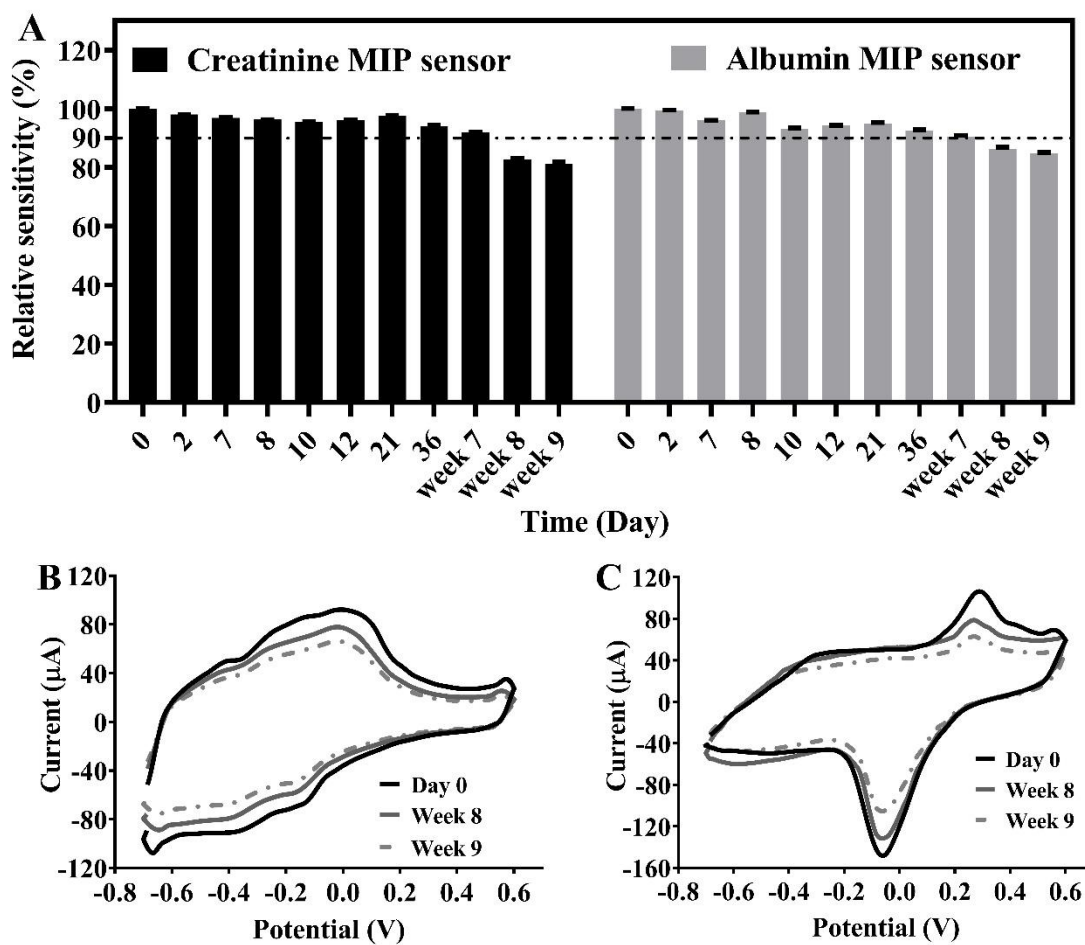


Fig. S11. (A) The chart shows the stability of the dual MIP sensor over 63 days. CVs show the reduced response with time of (B) PMB and (C) Fc of the dual MIP sensor in 0.050 mol L^{-1} PBS pH 7.40.

S12. Selectivity

Responses of the dual NIP sensor toward creatinine, albumin, and various possible interferences are shown in **Fig.S12**.

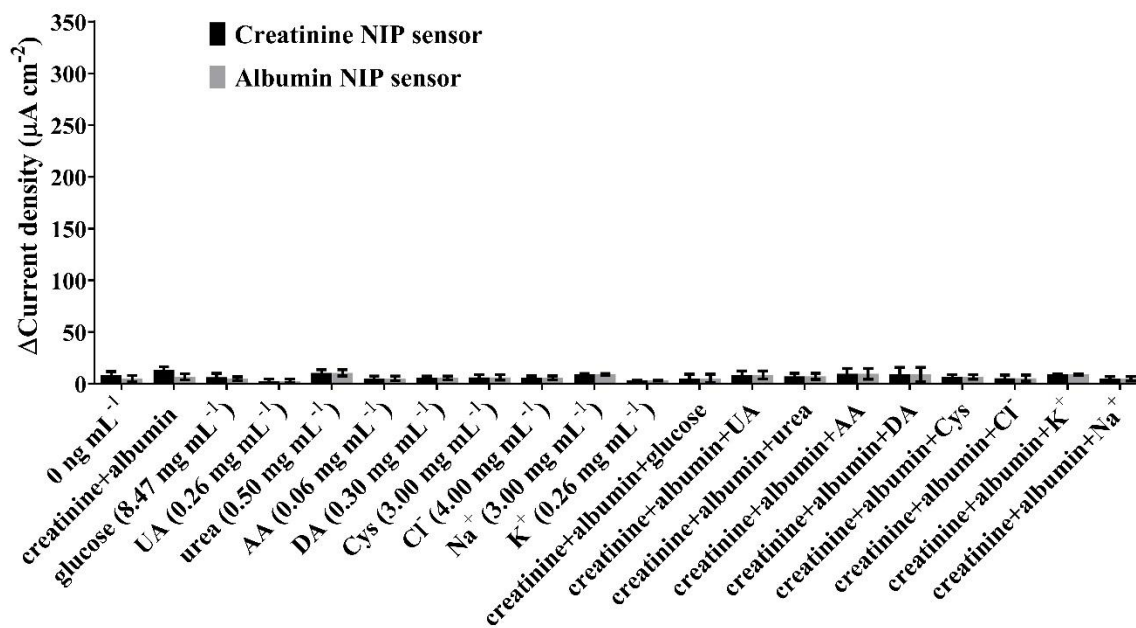


Fig.S12. Responses of the dual NIP sensor in the presence of creatinine, albumin, and various possible interferences.

S13. Recovery study

The recoveries of creatinine and albumin in **Table S1** were obtained from spiked samples obtained from Songklanagarind Hospital, Hat Yai, Thailand.

Table S1. Average recoveries and the relative standard deviations of urinary creatinine and albumin in hospital urine samples (n = 3).

Creatinine			HSA		
Spike concentration (mg mL ⁻¹)	Measured concentration (mg mL ⁻¹)	Recovery (%)	Spike concentration (mg mL ⁻¹)	Measured concentration (mg mL ⁻¹)	Recovery (%)
Sample 1					
0.0	0.305±0.015	-	0.0	0.078±0.001	-
0.015	0.320±0.001	98±4	0.015	0.109±0.001	101±7
0.030	0.335±0.001	99±4	0.030	0.109±0.001	103±4
0.075	0.380±0.003	100±4	0.075	0.151±0.003	97±4
0.150	0.458±0.005	101±4	0.150	0.229±0.003	100±3
Sample 2					
0.0	0.102±0.004	-	0.0	0.049±0.002	-
0.015	0.117±0.001	102±3	0.015	0.064±0.001	98±6
0.030	0.131±0.002	96±7	0.030	0.080±0.003	99±6
0.075	0.178±0.003	101±4	0.075	0.128±0.003	105±2
0.150	0.254±0.003	101±2	0.150	0.198±0.008	99±6
Sample 3					
0.0	1.917±0.158	-	0.0	0.040±0.004	-
1.50	3.353±0.143	95±10	0.015	0.056±0.001	99±4
2.25	4.051±0.090	95±4	0.030	0.071±0.001	102±3
3.00	4.939±0.090	101±3	0.075	0.116±0.006	101±7
4.50	6.498±0.112	102±3	0.150	0.185±0.007	97±5
Sample 4					
0.0	1.560±0.134	-	0.0	0.011±0.001	-
1.50	2.948±0.025	93±2	0.015	0.026±0.001	98±4
2.25	3.727±0.099	96±4	0.030	0.039±0.001	96±4
3.00	4.535±0.034	99±1	0.075	0.086±0.003	99±5
4.50	6.028±0.148	100±3	0.150	0.162±0.008	100±5

References

1. Daniels, J.S. and N. Pourmand, Label-free impedance biosensors: Opportunities and challenges. *Electroanalysis*, 2007. 19(12): p. 1239-1257.
2. Bard, A.J. and L.R. Faulkner, *Electrochemical Methods: Fundamentals and Applications*, 2nd Edition. 2000: John Wiley & Sons, Incorporated.
3. Krejci, J., et al., Effective Surface Area of Electrochemical Sensors. *Journal of The Electrochemical Society*, 2014. 161(6): p. B147.

VITAE

Name Miss Nur Indah Wardani

Student ID 5910230033

Education Attainment

Degree	Name of Institute	Year of Graduation
B.Sc. (Education)	Yogyakarta State University, Indonesia	2012
M.Sc. (Analytical Chemistry)	Sultan Idris Education University, Malaysia	2014

Scholarship Awards during Enrolment

1. The Thailand's Education Hub for southern Region of ASEAN Countries (TEH-AC 109/2016)
2. PSU Ph.D. Scholarship, Graduated school, Prince of Songkla University

List of Publications

Wardani, N. I., Kangkamano, T., Wannapob, R., Kanatharana, P., Thavarungkul, P., Limbut, W. 2023. Electrochemical sensor based on molecularly imprinted cryogel and multiwalled carbon nanotubes for direct insulin detection. *Talanta* 254, 124137.

Wardani, N. I., Kanatharana, P., Thavarungkul, P., Limbut, W. 2023. Molecularly imprinted polymer dual electrochemical sensor for the one-step determination of albuminuria to creatinine ratio (ACR). *Talanta* 265, 124769.

Poster Presentation

Wardani, N. I., Kangkamano, T., Wannapob, R., Kanatharana, P., Thavarungkul, P., Limbut, W. Electrochemical insulin sensor based on MWCNTs-molecularly

imprinted polymer cryogel. PERCH-CIC Congress X: 2018 International Congress for Innovation in Chemistry Contributing Expertise for Thailand 4.0. July 4-7, 2018. Jomtien Palm Beach Hotel & Resort, Pattaya, Chonburi, Thailand.

Wardani, N. I., Kangkamano, T., Wannapob, R., Kanatharana, P., Thavarungkul, P., Limbut, W. Molecularly imprinted polymer cryogel/MWCNTs electrochemical insulin sensor. Trace Analysis and Biosensor International Symposium 1 “Emerging Challenges and Opportunities”. 10-11 February 2020, Learning Resource Center Building, Room LRC1, 8th Floor, Prince of Songkla University, Hat Yai, Thailand.